Spectroscopic Studies On Some Biologically Important Systems

Thesis submitted for the degree of

Doctor of Philosophy (Science)

In

Physics (Experimental)

by

Sumana Pyne

Department of Physics
University of Calcutta

2023

Dedicated To

The Farmers

……who are the backbone of our society

Declaration

I hereby declare that the research works manifested in the thesis "*Spectroscopic Studies On Some Biologically Important Systems*" are original. All the experiments including sample preparations were carried out by me with the help of my lab-mates and my supervisor, Prof. Rajib Kumar Mitra. I further declare that these results have not been used elsewhere for the award of any degree/diploma from any university or institute.

Sumana Pyne

Date: 21 July, 2023

Sumana Pyne

(email: sumanapyne@gmail.com)

S N Bose National Centre for Basic Sciences

Block JD, Sec-III, Salt Lake, Kolkata-700106, India

The page is left blank intentionally

Abstract

Lipids are the building blocks of cell membrane which not only compartmentalize the cell but also do regulate many physico-chemical mechanisms (i.e., diffusion, active transport, energy conversion) in the cell. The lipid-water interface can be characterized by a network of H-bonds which sustains the liposome's structure and regulates the dynamics of both water and lipid molecules. The main aim of this thesis is to explore the roto-vibrational structure of H-bond network at the interface of liposomes/vesicles under different chemical environments by using state-of-the-art far-Fourier-transform infrared (THz) spectroscopy. This thesis consists of four articles: (a) The inner hydration in surfactant/cholesterol vesicles differs from the outer one: a spectroscopic investigation (b) Addition of cholesterol alters the hydration at the surface of model lipids: a spectroscopic investigation (c) The explicit role of interfacial hydration during polyethylene glycol induced lipid fusion and (d) Alteration of lipid hydration in alcoholic environment. In this thesis atomic force microscopy (AFM) and scanning electron microscopy have been used to monitor the structural modification and dynamic light scattering (DLS) measures the dimensions of thus modified liposomes. We investigate the solvation behaviour of micelles/vesicles and observe that when micelles are converted into vesicles inner solvation appears and the solvation nature of inner interface is surprisingly differing from the overall solvation which is strongly vesicle's charge dependent. We then investigate the hydration behaviour of two different charged phospholipids (DOPC and DOPG) in absence and in presence of cholesterol and observe that in presence of cholesterol, hydrogen bond network at lipid water interface becomes weaker and dynamics gets accelerated. We also investigate PEG-induced lipid fusion using three model phospholipids (DOPC, POPC and DPPC) and observe that liposomes follow some intermediate steps: bilayer aggregation, destabilization and finally lipid fusion. We find that such fusion process is associated with the dehydration of the membranes and fusion is associated with a substantial solvation entropic cost. In a subsequent work we investigate the structural modification of liposomes (POPC) in alcoholic environment and we found that the water at the lipid interface becomes stronger and more restricted in presence of both ethanol and TFE but the effect of TFE is more prominent.

List of Publications

Inside Thesis:

1. S. Pyne, P. Pyne, R. K. Mitra; The inner hydration in surfactant/cholesterol vesicles differs from the outer one: a spectroscopic investigation, ***ChemPhysChem*** *2022, e202200337*
2. S. Pyne, P. Pyne, R. K. Mitra; Addition of cholesterol alters the hydration at the surface of model lipids: a spectroscopic investigation, ***Phys. Chem. Chem. Phys.*** 2022, 24, 20381–20389.
3. S. Pyne, P. Pyne, R. K. Mitra; The explicit role of interfacial hydration during polyethylene glycol induced lipid fusion: a THz spectroscopic investigation, (***under review)***
4. S. Pyne, R. K. Mitra; Alteration of lipid hydration in alcoholic environment: THz Spectroscopic investigation, (***Manuscript under preparation)***

Outside Thesis:

1. S. Mondal, S. Pyne, P. Pyne, A. Patra, R K Mitra, S. Ghosh; Interfacial Structure and Electrostatics Related to Solute Activity in a Model Anionic-Surfactant/Polymer Self-Assembly, ***Langmuir*** 2023, 39, 2850-2858
2. P. Pyne, S. Pyne, R. K. Mitra; Sugar molecules inhibit Insulin aggregation: a decisive role being played by the protein solvation energetics, (**under review**)
3. S. I. Islam, S. Pyne, D. Das Mahanta, D. K. Palit, R. K. Mitra; Role of Micro-Heterogeneity in the H-bonded Network on the ESPT Mechanism of D-Luciferin (**To be submitted**)
4. R. Saha, I. Bhattacharya, S. Pyne, R. K. Mitra; Guanidinium thiocyanate ion induced protein fibrillation: insights role of protein hydration by THz study (**To be submitted**)

Acknowledgement

A journey becomes easier when we travel together. This is a five years journey which becomes more easier with the continuous support and encouragement of some people surrounding me. Without acknowledging them, this path cannot be finished.

First, I would like to acknowledge my supervisor, Prof. Rajib Kumar Mitra for his constant guidance and encouragement. He is always there to listen and to give me advice. His interactions were so friendly that it gave me opportunity to ask questions and express my ideas. He helped me to think several problems, from basic scientific concepts to research project. Discussing with him, I learned how to apply physics on biological systems and get a feel for biophysics which was beyond my knowledge. Apart from scientific discussions, he encouraged me to debate on general problems which helped me to develop my thinking skills. I feel I'm very lucky to get such an opportunity to work under his guidance.

I would like to thank my parents for always supporting me. My father is my first teacher who instills the value of education in me and my mother teaches me the subject of life. I am here only for their unconditional love, support, ideology and inspiration.

I express my deepest gratitude to my brother, Partha Pyne (dada) who is my teacher, friend and philosopher; ideology of my life. I learnt a lot of things from him. He is a magician with all the solutions in my problems. He encouraged me to develop my interest in physics. He is not only my brother, he is also my lab senior. We are working in same lab throughout 4.5 years. He taught me several things like Mathematica, plotting, data handling, analysis. He is my teacher who teaches me from class two to PhD final year. I feel I'm very lucky to get such a super cool brother.

I express my heartily gratitude to my lab mates, without them this journey would have been very difficult. I would like to thank all my past and present lab mates in "Biophotonics lab". A special thanks to Imadul da. He taught me very basic things like how to use a pipette, handling the liquid samples, and plotting the data in a software. Sometimes I discussed with Saikat da with basic physics/chemistry problems. Subhadip da is really a nice senior, his valuable suggestions and discussions always helped me to overcome some problems. My lab environment became empty without Ria, though she is my junior but she seems to be my guardian. I spent most of the time with Ria and dada. We have enjoyed a lot. Sometimes we were discussing sciences even outsides the lab, she helped me to learn the chemistry. Indrani di always encouraged me when I feel bored. I would like to special thanks to my two juniors: Shah Imtajul (Rahul) and Aritra. We are enjoying very much in the lab. I would like to thank Subhas da, Debashis da, Bivab da, Didhiti di, Sudip da, Anulekha di, Chaitrali di, Parama, Sudhanshu for their valuable discussions and suggestions. I am blessed that I get an opportunity to get such a friendly lab environments and it became my second home.

I would like to acknowledge some kind hearted persons whom I met in "THz lab". Among them my heartiest thanks to Dr. Animesh Patra (kakababu). He always discussed with some

scientific problems and motivated me for the research work. Another leading name is Dr. Nirnay Samanta, who helped me in thinking a real problem from a different perspective. He also taught me how to create different graphics in power point by using colour only. I spent some joyful times with Sonali di and Semanti di.

We (labmates) spent some enjoyable moments with sir and madam (Dr. Sukanya Chakrabarty) at their home where they were arranging some delicious foods. I would like to thank madam and sir for such enjoyable moments with delicious foods.

I express my heartily thanks to my friend cum sister-in-law, Paulomi di for always tolerate me. I would like to thanks all my family members: Kaku, Kaki, Ritwik (my brother), Grandmother for always caring and supporting me.

Without a good friend, life becomes terrific. I have no word to acknowledge them. A special thanks to Sreyashi who is always with me, her unconditional support always boost up my mental strength. I like to thank Mahi, Supravat, Silpayan and Chandana for staying with me in my ups and downs during my journey.

I would like to thank all the reviewers of different journals for their judicious evaluation and the members of my thesis committee. I thank all the academic and non-academic staffs at SNBNCBS for their kind help and cooperation. Special thanks to SNB mess and Canteen for arranging the delicious foods even at pandemic situations. I would like to acknowledge S N Bose National centre for Basic Sciences and DST for providing me the funding and research facilities.

I would like to express my deepest gratitude to my villagers who are the source of my mental strengths.

At last I convey my gratitude to the covid warriors whose selfless service has reborn the globe, and I am able to complete and summarize my thesis work.

Acronyms

AFM	Atomic Force Microscopy
Brij 30	Polyoxyethylene 4 laurylether
Cholesterol	3β-Hydroxy-5-cholestene,5-Cholesten-3β-ol
CTAB	Hexadecyltrimethylammonium bromide
DLS	Dynamic Light Scattering
DOPC	1,2-Dioleoyl-sn-glycero-3-phosphocholine
DOPG	1,2-Dioleoyl-sn-glycero-3-phospho-rac-(1-glycerol) sodium salt
DPPC	1,2-Dipalmitoyl-sn-glycero-3-phosphocholine
FTIR	Fourier Transform Infrared
HB	Hydrogen bond
Lib	Librational
PBS	Phosphate Buffer Saline
PCA	Principal Component Analysis
PEG	Polyethylene Glycol
POPC	2-Oleoyl-1-palmitoyl-sn-glycero-3-phosphocholine
SDS	Sodium dodecyl sulfate
SEM	Scanning Electron Microscope
SVD	Singular Value Decomposition
TFE	2,2,2-Trifluoroethanol
THz	Terahertz

Table of Contents

Chapter 1

Introduction

Human body is composed of ~ 63 trillion cells and every cell is a tightly package of countless membranes.[1] The American Heritage dictionary defines a membrane as "a thin pliable layer of plant or animal tissue covering or separating structures or organs".[1] Biological membranes act as a boundary which separate the inner environment of the cell from extracellular environment and also pass the essential nutrients, gases and solutes to keep the cells alive.[2] Eukaryotic cells consist of several such membranous organelle (scheme 1Ia) which are unique in structural configuration, composition and in functions.[1,2] Among them plasma membrane (PM) is the most dynamic and busiest membrane which mainly separates the cell contents from the rest of the world.[3] PM not only compartmentalizes the cell but also regulates a number of cellular functions, including membrane fusion, signal transduction and protein trafficking.[4–8] Membranes consist of several types of lipids, proteins, carbohydrate and sugar molecules;[9–11] the major component is lipid. The lipid composition of a membrane varies depending on the cell cycle, cell types and organisms.[3,12] The outer leaflet of mammalian plasma membrane is primarily composed of phosphatidylcholine (PC), sphingomyelin (SM) and gangliosides (GM), while the inner leaflets consist of phosphatidylethanolamine (PE), phosphatidylserine (PS) and other charged lipids (scheme 1Ib).[13] Lipids help membrane for budding, tubulation, fission and fusion and some characteristics that are essential for cell division and intracellular membrane trafficking.[3,12] There are basically three types of lipids: phospholipid, sphingomyelin and cholesterol, but the major structural lipid is the phospholipid.[3,14] Phospholipids are amphiphilic in nature, consist of both polar headgroup and nonpolar hydrophobic tail which consists of saturated or unsaturated fatty acyl chains with varying length.[15] The major sphingolipid in mammalian cell membrane is the sphingomyelin whose hydrophobic backbone is ceramide.[16] Again, the major sterol present in mammalian cell membrane is cholesterol which regulates the fluidity and rigidity of membrane.[17] In plasma membrane cholesterol content varies in between 20-30%, but in red blood cell it could rise up to 50%.[18,19] Non-bilayer lipids like cardiolipin can accommodate membrane proteins which regulate their activities.[20]

Biological membranes are quasi two-dimensional supramolecular assemblies which are anisotropic in nature.[21] Due to the complex nature of cellular membranes, artificial lipid

bilayers have been employed as a favourable model to investigate various physicochemical processes occurring in the membrane since the lipid bilayers closely mimic the bio-membranes in terms of their structures and physical properties.[22] Lipid bilayers provide a semifluid environment[23] for peptides and proteins and play a role on different biological phenomenon like lipid-protein interaction, ligand-membrane binding, ion transport, ion-membrane interaction etc.[24–28] An intriguing feature of lipids is that they are inherently dynamic; the interior hydrophobic region is isotropic in nature while the lipid interface is highly ordered.[29] Due to this complex organization of lipid membrane, the physical property like polarity, mobility or fluidity, as well as Hydrogen bonding (H-bonding) efficiency[30,31], vary across the membrane.[21,32]

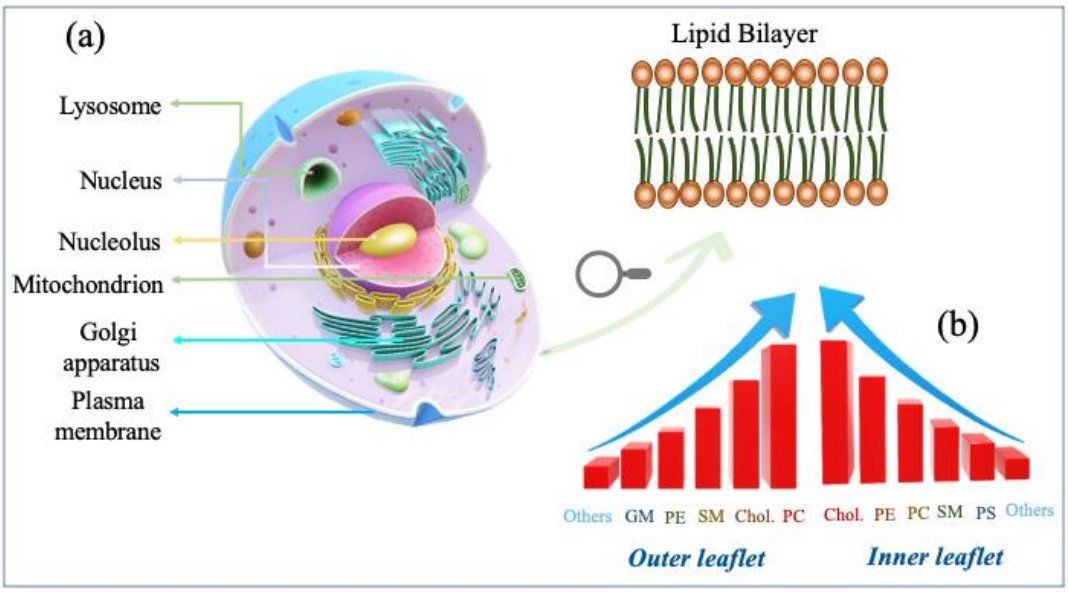

Scheme 1I: (a) Cartoon Picture of animal cell. (b) Lipid distribution in Plasma membrane

To understand the different physical properties as well as physicochemical processes occurring inside the membrane (more specifically inside the lipid), one of the most convenient ways is to use spectroscopy. Spectroscopy, defining the interaction between atoms/molecules and photons[33], has been a widely used technique to explore different inherent mechanism of biologically important systems like membrane dynamics, protein (un)folding, or protein-membrane interaction etc.[34,35] Equilibrium structural configuration as well as structural

fluctuations (dynamics) of those systems can directly be probed using various spectroscopic techniques e.g., vibrational[35–41] (infrared (IR) pump/probe spectroscopy, two-dimensional IR, sum frequency generation (SFG), Raman spectroscopy, Terahertz (THz) spectroscopy), rotational[42,43] (dielectric relaxation spectroscopy), electronic (absorption, fluorescence)[44,45] spectroscopy and also nuclear magnetic resonance spectroscopy[46,47] (provides the spin information of molecules). For the structural heterogeneity of membrane, dynamics span over a wide range of time scale from femtoseconds (for molecular vibrations) to a few hours (for trans-bilayer flipflops). In this time window, different kinds of motions of lipid in membrane such as shape fluctuation, membrane undulation, thickness fluctuations of bilayers, as well as the dynamics of individual lipids such as flip-flops between the leaflets, lateral diffusion within the monolayer, localized rotations and conformational and vibrational motion can occur (scheme 1IIa).[48–52]

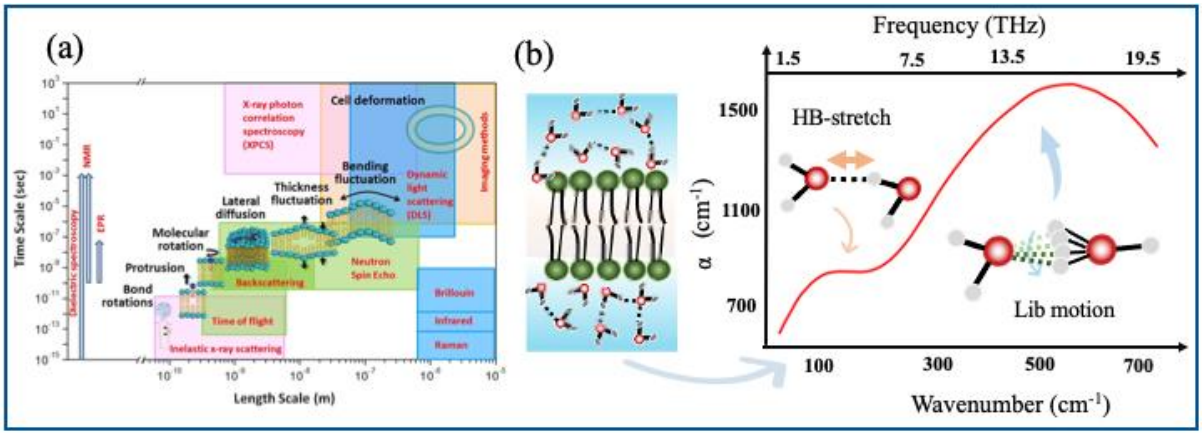

Scheme 1II: Schematic diagram of (a) different motion (dynamics) of lipid membrane over different length and time scale (Image source: Langmuir, 2020, 36, 15189-15211). (b) vibrational structure (HB-stretch & lib motion) of water at lipid-water interface.

The most integrated part of Lipid membrane is its interfacial region in terms of its physiochemical characteristics and function.[28,29] It offers unique dielectric characteristics, different from both bulk and hydrocarbon regions.[53] Interface plays a crucial role in membrane stability and cell viability.[54,55] Lipid-water interface can be characterized by a network of H-bonds which sustain the lipid structure and regulate the dynamics of both water and lipid molecules.[28,56] Water appears to be the essential solvent for life due to its many physical and

chemical properties and its ability to form H-bonds.[57,58] It has high melting and boiling points, as well as a wide temperature range over which it remains liquid, also a high dielectric constant, which is crucial to its solvent activity.[57,59] Due to such extreme environment, water has become a major matrix for life: most of the biological process occurs inside the water environments.[57,60] Water can influence the structure of bio-molecules such as membrane and it interacts with the membrane surface mostly through H-bonding,[61,62] a mainly local type of weak bonding among water molecules and between water and the polar or ionic group of biomolecules.[63] In liquid state, each water molecule can form slightly less than four H-bonds with its neighboring water molecules, two via the hydrogen donating OH-group and two via hydrogen accepting oxygen atom.[64] H-bond network is dynamic in nature and it fluctuates due to thermal motion; water exchanges its H-bond partners via breaking and reforming the H-bond over picosecond time scales.[65] Water molecules show different vibrational modes due to stretching, bending and rotating motion of H-bonds: hindered translational motion of H-bond or HB-stretch appears at ~200 cm^{-1} and hindered rotational motion (librational motion) at ~650 cm^{-1}.[42] H-bond bending motion appears at ~ 50 cm^{-1}.[66] Intramolecular OH stretching and bending vibrations of water molecules occur approximately within 10 and 20 fs.[58] Intermolecular H-bond stretching and bending vibration appears with a time scale of ~ 200 fs and 600-800 fs respectively.[67] Again water molecules librate within ten to hundreds of fs of time scale in its hydrogen bonded environment.[58] When lipid membrane is exposed to an aqueous environment, a new type of water network is formed: water at the immediate vicinity of the membrane, termed as "biological water" which offers structural and dynamical response different compared to bulk water.[58,68] Hydrogen bond network dynamics at lipid interface can be explored by using different experimental techniques. Incoherent elastic and quasi-elastic neutron scattering (EINS and QENS) techniques measure the displacement of individual hydrogen atom and provide information on translational and rotational dynamical motion of water molecules.[69,70] Femto-second (fs) resolved infrared pump-probe spectroscopy is a powerful technique, probes the reorientation dynamics of water molecules in lipid solutions. Nuclear magnetic resonance (NMR)[71,72], neutron scattering[73,74] and infrared spectroscopy[75,76] offer the dynamical response of individual water molecules. Small angle X-ray scattering and neutron scattering (SAX and SANS) can determine the radial distribution of counterion around biomolecules and can directly probe the hydration shell structure.[77] Some techniques including dielectric relaxation (DR)[78], optical Kerr-effect (OKE)[79] probe different "collective dynamics" of water molecules associated the biomolecules. Each of these spectroscopic techniques have their own advantages and limitations. Recently THz spectroscopy has come up with a unique feature of water in the

terahertz region (0.3 THz to 20 THz); the region between microwave and infrared in electromagnetic spectrum (1THz = 10^{12} Hz = $1ps^{-1}$). It measures the change in the collective dipole moment of water, more specifically the hydrogen bond network of water, thus the information of water associated with biomolecules (hydration water) can be extracted.[80,81] Another advantage of THz spectroscopy is that it is a label free, non-invasive experimental technique which can provide the subtle change in the dynamical orientation of water molecules.[82] THz frequency probes the dynamical and structural response as well as the amplitude of various collective water network motions, such as translational, rotational diffusion and librational motions.[40,83,84] These unique features make THz spectroscopy a powerful tool to explore the dynamical and structural fluctuation of water molecules at the hydration cell of lipid membrane (scheme 1IIb). In spite of having the detailed understanding about the structure and dynamics of lipid molecules, there has been a lack of in depth knowledge about the behavior of water buried inside the lipid molecule or the water within the hydration shell of lipid molecules.

The primary objective of this thesis is to explore the vibrational structure of water at the dynamical hydration shell of lipid molecules using terahertz spectroscopy and how this vibrational picture is perturbed under different chemical environments. We began the thesis work with vesicles, since vesicles can mimic the lipid cellular environment and then move on to liposomes. Vesicle is mainly an assembly of bilayer system consisting of three regions: the inner and outer regions are aqueous (polar) in nature with hydrophobic long chains forming the inner phase.[85,86] Some surfactant molecules can form vesicles in presence of cholesterol. When non-ionic surfactant molecules form vesicular structures, they are termed as Niosomes.[87,88] Lipid molecules can also form such bilayer structures, they are known as liposomes. Vesicles including liposomes offer a large number of applications in industrial field[89,90] and in pharmacology[91,92] to act as drug carrier agent[93,94], carrying genetic material, enzymes and others molecules into cell[89,91] in medicine industry[90,95] and also in food industry[96]. Depending on the preparation technique, vesicles are mainly classified into two wide categories: ULV (uni-lamellar vesicle consisting of a single bilayer) and MLV (multi-lamellar vesicle; made of more than one bilayer).[86] In this thesis we have tried to address four fundamental questions of liposomes/vesicles from the perspective of water.

- *How the solvation behaviour during the micelle to vesicle transformation is altered? Whether the water in the core region and outer to bulk region of vesicles possess similar*

physical properties or not and how these properties of water vary with the surfactant charge type?

- *Is the interfacial dynamics of lipid charge dependent? How the cholesterol molecules perturbed the interfacial dynamics of lipid caring the fact that cholesterol plays a key role in modifying the lipid's structure?*
- *How do the physical properties of the interfacial water in liposome changes during polyethene glycol (PEG) induced lipid fusion?*
- *How the hydration behaviour of lipid membrane alters in presence of alcohol (ethanol and TFE) knowing the fact that alcohol modulates the properties of lipid membrane?*

This thesis investigates the response (structure and dynamics) of surface water at different conformational states of vesicles and lipids: (a) The inner hydration in surfactant/cholesterol vesicles differs from the outer one: a spectroscopic investigation, (b) Addition of cholesterol alters the hydration at the surface of model lipids: a spectroscopic investigation (c) The explicit role of interfacial hydration during polyethylene glycol induced lipid fusion and (d) Alteration of lipid hydration in alcoholic environment. We have followed sonication technique to prepare the charged vesicles and injection technique to prepare the niosomes. We use film hydration extrusion technique to prepare liposomes. Dynamic light scattering technique is used to characterize the formation of vesicles and liposomes and also to estimate the size of such particles. We use atomic force microscopy to obtain the morphological picture of thus prepared vesicles and liposomes. Field emission scanning electron microscopic technique is used to monitor lipid fusion process. Finally, Far-FTIR (THz) spectroscopy is used to probe the hydration behavior at different conformation of vesicles/liposomes.

This thesis consists of following chapters as described briefly:

- ***Chapter 1*** deals with the general introduction of lipid membrane and their physiochemical response using different spectroscopy technique, especially the state of art THz spectroscopy as a label free technique, used to probe the hydration behavior of lipid cell membrane.
- ***Chapter 2*** consists of some basic theories, mathematical model and description of chemical used in this thesis. This chapter also deals with the working principal of the instrument which have been used to measure or extract the parameters in this thesis.
- ***Chapter 3*** consists of the formation of vesicles from micelle in presence of cholesterol and how the hydration behavior of micelles is altered when they are converted into the

vesicles. For that we have chosen three different charged surfactants: SDS (-ve), CTAB (+ve) and Brij 30 (neutral); cholesterol is used for the formation of vesicles. Here we have followed sonication and injection technique to prepare the charged and neutral vesicles. Dynamic Light Scattering (DLS) is used to monitor the size of the vesicles. Atomic force microscopy (AFM) gives the morphological picture of thus formed vesicles. Finally, FAR-IR (THz) spectroscopy is used to study the hydration behavior of vesicles. When micelles are converted into vesicles the water network alters which strongly depend on surfactant charge and cholesterol concentration.

- ***Chapter 4*** explores the interfacial water dynamics of two model phospholipid: negatively charged DOPG (1,2-Dioleoyl-*sn*-glycero-3-phospho-*rac*-(1-glycerol) sodium salt) and zwitterionic DOPC (1,2-Dioleoyl-*sn*-glycero-3-phosphocholine) in presence of cholesterol. We have followed film hydration sonication technique to prepare the liposomes in absence and in presence of cholesterol. DLS and AFM techniques affirm us the formation of liposomes. Our THz results conclude that cholesterol induces weaker hydrogen bond and faster hydrogen bond vibration/stretching dynamics at lipid interface.
- ***Chapter 5*** deals with the lipid fusion in presence of PEG. Here we have chosen three lipids (DOPC, POPC and DPPC) with different aliphatic tail as they undergo fusogenic transition in the presence of PEG (average molecular weight 4000). Dynamic light scattering and electron microscopic measurements confirm the formation of different intermediate steps of the liposomes during the fusion process: bilayer aggregation, destabilization and finally lipid fusion. Here we experimentally probe that PEG-induced membrane fusion is associated with the dehydration of the membrane(s). THz FTIR spectroscopy explore the explicit information on interfacial hydration of fused lipid membrane. Hydration measurements yield that stronger H bond is formed in the aggregated state of the lipid interface compared to that of the pristine liposome for all the liposomes irrespective of the constituting lipid molecules.
- ***Chapter 6*** explores the hydration behaviour of lipid in presence of two alcohols ethanol and 2,2,2-trifluoroethanol. Here POPC is chosen as a model lipid and we prepare the liposome by using film hydration technique. DLS and SEM is used to probe the structural perturbation of liposomes in presence of alcohols. THz FTIR results conclude that the water at the lipid interface becomes stronger and more restricted in presence of both ethanol and TFE but the effect of TFE is more prominent.

- ***Chapter 7*** summarizes the key finding of chapter 3, 4, 5 and 6. It also consists of some ideas of future research in this direction.

References:

(1) Stillwell, W. *An Introduction To Biological Membranes: From Bilayers to Rafts*; Elsevier.
(2) Nelson, D. L.; Cox, M. M. *Lehninger Principles of Biochemistry*, 7th ed.; W. H. Freeman and Company.
(3) Meer, G. V.; Voelker, D. R.; Feigenson, G. W. Membrane Lipids: Where They Are and How They Behave. *Nat. Rev. Mol. Cell Biol.* **2008**, *9*, 112–124.
(4) Okur, H. I.; Tarun, O. B.; Roke, S. Chemistry of Lipid Membranes from Models to Living Systems: A Perspective of Hydration, Surface Potential, Curvature, Confinement and Heterogeneity. *J. Am. Chem. Soc.* **2019**, *141*, 12168−12181.
(5) Grecco, H. E.; Schmick, M.; Bastiaens, P. I. H. Signaling from the Living Plasma Membrane. *Cell* **2011**, *144*, 897–909.
(6) Sunshine, H.; Iruela-Arispe, M. L. Membrane Lipids and Cell Signaling. *Curr. Opin. Lipidol.* **2017**, *28*, 408–413.
(7) Tauchi-Sato, K.; Ozeki, S.; Houjou, T.; Taguchi, R.; Fujimoto, T. The Surface of Lipid Droplets Is a Phospholipid Monolayer with a Unique Fatty Acid Composition. *J. Biol. Chem.* **2002**, *277*, 44507–44512.
(8) Walther, T. C.; Farese, R. V. Jr. Lipid Droplets and Cellular Lipid Metabolism. *Annu. Rev. Biochem.* **2012**, *81*, 687–714.
(9) Muller, M. P.; Jiang, T.; Sun, C.; Lihan, M.; Pant, S.; Mahinthichaichan, P.; Trifan, A.; Tajkhorshid, E. Characterization of Lipid-Protein Interactions and Lipid-Mediated Modulation of Membrane Protein Function through Molecular Simulation. *Chem. Rev.* **2019**, *119*, 6086–6161.
(10) Bao, G.; Suresh, S. Cell and Molecular Mechanics of Biological Materials. *Nat. Mater.* **2003**, *2*, 715–725.
(11) van Meer, G.; de Kroon, A. I. P. M. Lipid Map of the Mammalian Cell. *J Cell Sci.* **2011**, *124*, 5–8.
(12) Casares, D.; Escriba, P. V.; Rossello, C. A. Membrane Lipid Composition: Effect on Membrane and Organelle Structure, Function and Compartmentalization and Therapeutic Avenues. *Int. J. Mol. Sci.* **2019**, *20*, 2167.
(13) Ingoĺfsson, H. I.; Melo, M. N.; Eerden, F. J. V.; Arnarez, C.; Lopez, C. A.; Wassenaar, T. A.; Periole, X.; Vries, A. H. D.; Tieleman, D. P.; Marrink, S. J. Lipid Organization of the Plasma Membrane. *J. Am. Chem. Soc.* **2014**, *136*, 14554–14559.
(14) Klose, C.; Surma, M. A.; Simons, K. Organellar Lipidomics — Background and Perspectives. *Curr. Opin. Cell Biol.* **2013**, *25*, 1–8.
(15) Dresche, S.; Hoogevest, P. V. The Phospholipid Research Center: Current Research The Phospholipid Research Center: Current Research in Phospholipids and Their Use in Drug Delivery in Phospholipids and Their Use in Drug Delivery. *Pharmaceutics* **2020**, *12*, 1235.
(16) van Meer, G.; Lisman, Q. Sphingolipid Transport: Rafts and Translocators. *J. Biol. Chem.* **2002**, *277*, 25855–25858.
(17) Ikonen, E. Cellular Cholesterol Trafficking and Compartmentalization. *Nat. Rev* **2008**, *9*, 125–138.
(18) Mouritsen, O. G.; Zuckermann, M. J. What's So Special About Cholesterol? *Lipids* **2004**, *39*, 1101–1113.
(19) Lipowsky, R.; Sackmann, E. Structure and Dynamics of Membranes. **1995**, 1–64.
(20) Marsh, D. Lateral Pressure Profile, Spontaneous Curvature Frustration, and the Incorporation and Conformation of Proteins in Membranes. *Biophys. J.* **2007**, *93*, 3884–3899.
(21) Pal, S.; Chattopadhyay, A. What Is So Unique About Biomembrane Organization and Dynamics? In *Membrane Organization and Dynamics*; Springer; Vol. 1st cahpter.
(22) Sackmann, E. Supported Membranes:Scientific and Practical Applications. *Science* **1996**, *271*, 43–48.
(23) Singer, S. J.; Nicolson, G. L. The Fluid Mosaic Model of the Structure of Cell Membranes. *Science* **1972**, *175*, 720–731.
(24) Muller, M. P.; Jiang, T.; Sun, C.; Lihan, M.; Pant, S.; Mahinthichaichan, P.; Trifan, A.; Tajkhorshid, E. Characterization of Lipid-Protein Interactions and Lipid-Mediated Modulation of Membrane Protein Function through Molecular Simulation. *Chem. Rev.* **2019**, *119*, 6086–6161.
(25) Harayama, T.; Riezman, H. Understanding the Diversity of Membrane Lipid Compositio. *Nat Rev Mol Cell Biol.* **2018**, *19*, 281–296.
(26) Hénault, C. M.; Govaerts, C.; Spurny, R.; Brams, M.; Estrada- Mondragon, A.; Lynch, J.; Bertrand, D.; Pardon, E.; Evans, G. L.; Woods, K.; et al. A Lipid Site Shapes the Agonist Response of a Pentameric Ligand-Gated Ion Channel. *Nat. Chem. Biol.* **2019**, *15*, 1–9.

(27) Phillips, R.; Ursell, T.; Wiggins, P.; Sens, P. Emerging Roles for Lipids in Shaping Membrane-Protein Function. *Nature* **2009**, *459*, 379–385.
(28) Valentine, M. L.; Waterland, M. K.; Fathizadeh, A.; Elber, R.; Baiz, C. R. Interfacial Dynamics in Lipid Membranes: The Effects of Headgroup Structures. *J. Phys. Chem. B* **2021**, *125*, 1343–1350.
(29) Chattopadhyay, A. Exploring Membrane Organization and Dynamics by the Wavelength-Selective Fluorescence Approach. *Chem Phys Lipids* **2003**, *122*, 3–17.
(30) Skinner, J. L.; Peiniazek, P. A.; Gruenbaum, S. M. Vibrational Spectroscopy of Water at Interfaces. *Acc. Chem. Res.* **2011**, *45*, 93–100.
(31) Pullanchery, S.; Yang, T.; Cremer, P. S. Introduction of Positive Charges into Zwitterionic Phospholipid Monolayers Disrupts Water Structure Whereas Negative Charges Enhances It. *J. Phys. Chem. B* **2018**, *122*, 12260−12270.
(32) Chattopadhyay, A.; Mukherjee, S. Depth-Dependent Solvent Relaxation in Membranes: Wavelength-Selective Fluorescence as a Membrane Dipstick. *Langmuir* **1999**, *15*, 2142–2148.
(33) Demtroder, W. *Laser Spectroscopy*; 2014; Vol. 1.
(34) Nibali, V. C.; Havenith, M. New Insights into the Role of Water in Biological Function: Studying Solvated Iomolecules Using Terahertz Absorption Spectroscopy in Conjunction with Molecular Dynamics Simulations. *J. Am. Chem. Soc.* **2014**, *136*, 12800–12807.
(35) Laage, D.; Elsaesser, T.; Hynes, J. T. Water Dynamics in the Hydration Shells of Biomolecules. *Chem. Rev.* **2017**, *117*, 10694–10725.
(36) Otting, G.; Liepinsh, E.; Wuthrich, K. Protein Hydration in Aqueous Solution. *Science* **1991**, *254*, 974–980.
(37) Yamaguchi, S.; Tahara, T. Development of Electronic Sum Frequency Generation Spectroscopies and Their Application to Liquid Interfaces. *J. Phys. Chem. C* **2015**, *119*, 14815–14828.
(38) Khalil, M.; Demirdolven, N.; Tokmakoff, A. Coherent 2D IR Spectroscopy: Molecular Structure and Dynamics in Solution. *J. Phys. Chem. A* **2003**, *107*, 5258–5279.
(39) Dodo, K.; Fujita, K.; Sodeoka, M. Raman Spectroscopy for Chemical Biology Research. *J. Am. Chem. Soc.* **2022**, *144*, 19651–19667.
(40) Ebbinghaus, S.; Kim, S. J.; Heyden, M.; Yu, X.; Heugen, U.; Gruebele, M.; Leitner, D. M.; Havenith, M. An Extended Dynamical Hydration Shell around Proteins. *Proc. Natl. Acad. Sci. U.S.A.* **2007**, *104*, 20749–20752.
(41) Tielrooij, K. J.; Paparo, D.; Piatkowski, L.; Bakker, H. J.; Bonn, M. Dielectric Relaxation Dynamics of Water in Model Membranes Probed by Terahertz Spectroscopy. *Biophys. J.* **2009**, *97*, 2484–2492.
(42) Cametti, C.; Marchetti, S.; Gambi, C. M. C.; Onori, G. Dielectric Relaxation Spectroscopy of Lysozyme Aqueous Solutions: Analysis of the δ-Dispersion and the Contribution of the Hydration Water. *J. Phys. Chem. B* **2011**, *115*, 7144–7153.
(43) Fernandez, P.; Schrodle, S.; Buchner, R.; Kunz, W. Micelle and Solvent Relaxation in Aqueous Sodium Dodecylsulfate Solutions. *ChemPhysChem* **2003**, *4*, 1065–1072.
(44) Xu, J.; Toptygin, D.; Graver, K. J.; Albertini, R. A.; Savtchenko, R. S.; Meadow, N. D.; Roseman, S.; Callis, P. R.; Brand, L.; Knutson, J. R. Ultrafast Fluorescence Dynamics of Tryptophan in the Proteins Monellin and IIA. *J. Am. Chem. Soc.* **2006**, *128*, 1214–1221.
(45) Marguet, D.; Lenne, P. F.; Rigneault, H.; He, H. T. Dynamics in the Plasma Membrane: How to Combine Fluidity and Order. *EMBO J* **2006**, *25*, 3446–3457.
(46) Antonschmidt, L.; Matthes, D.; Dervişoğlu, R.; Frieg, B.; Dienemann, C.; Leonov, A.; Nimerovsky, E.; Sant, V.; Ryazanov, S.; Giese, A.; Schroder, G. F.; Becker, S.; Groot, B. L. d.; Griesinger, C.; Andreas, L. B. The Clinical Drug Candidate Anle138b Binds in a Cavity of Lipidic α-Synuclein Fibrils. *Nat. Commun.* **2022**, *13*, 5385.
(47) Lalli, D.; Idso, M. N.; Andreas, L. B.; Hussain, S.; Baxter, N.; Han, S.; Chmelka, B. F.; Pintacuda, G. Proton-Based Structural Analysis of a Heptahelical Transmembrane Protein in Lipid Bilayers. *J. Am. Chem. Soc.* **2017**, *139*, 13006–13012.
(48) Lipowsky, R.; Sackmann, E. *Structure and Dynamics of Membranes - From Cells to Vesicles*; Elesevier.
(49) Dufourc, E. J. Sterols and Membrane Dynamics. *J. Chem. Biol.* **2008**, *1*, 63–77.
(50) Sharma, V. K.; Mamontov, E.; Ohl, M.; Tyagi, M. Incorporation of Aspirin Modulates the Dynamical and Phase Behavior of the Phospholipid Membrane. *Phys. Chem. Chem. Phys.* **2017**, *19*, 2514–2524.
(51) Gupta, S.; De Mel, J. U. Dynamics of Liposomes in the Fluid Phase. *Curr. Opin. Colloid Interface Sci.* **2019**, *42*, 121–136.
(52) Qian, S.; Sharma, V. K.; Clifton, L. K. Understanding the Structure and Dynamics of Complex Biomembrane Interactions by Neutron Scattering Techniques. *Langmuir* **2020**, *36*, 15189–15211.
(53) Ashcroft, R. G.; Coster, H. G. L.; Smith, J. R. The Molecular Organization of Bimolecular Lipid Membranes: The Dielectric Structure of the Hydrophilic/Hydrophobic Interface. *Biochim Biophys Acta.* **1981**, *643*, 191–204.

(54) Chattopadhyay, M.; Krok, E.; Orlikowska, H.; Schwille, P.; Franquelim, H. G.; Piatkowski, L. Hydration Layer of Only a Few Molecules Controls Lipid Mobility in Biomimetic Membranes. *J. Am. Chem. Soc.* **2021**, *143*, 14551−14562.
(55) Flanagan, J. C.; Valentine, M. L.; Baiz, C. R. Ultrafast Dynamics at Lipid−Water Interfaces. *Acc. Chem. Res.* **2020**, *53*, 1860−1868.
(56) Kundu, A.; Verma, P. K.; Ha, J. H.; Cho, M. Studying Water Hydrogen-Bonding Network near the Lipid Multibilayer with Multiple IR Probes. *J. Phys. Chem. A* **2017**, *121*, 1435–1441.
(57) Rothschild, L. J.; Mancinelli, R. L. Life in Extreme Environments. *Nature* **2001**, *409*, 1092−1101.
(58) Laage, D.; Elsaesser, T.; Hynes, J. T. Water Dynamics in the Hydration Shells of Biomolecules. *Chem. Rev.* **2017**, *117*, 10694−10725.
(59) Yuan, R.; Yan, C.; Tamimi, A.; Fayer, M. D. Molecular Anion Hydrogen Bonding Dynamics in Aqueous Solution. **2015**, *119*, 13407–13415.
(60) Ball, P. Water As an Active Constituent in Cell Biology. *Chem. Rev.* **2002**, *108*, 74−108.
(61) Chattopadhyay, M.; Krok, E.; Orlikowska, H.; Schwille, P.; Franquelim, H. G.; Piatkowski, L. Hydration Layer of Only a Few Molecules Controls Lipid Mobility in Biomimetic Membranes. *J. Am. Chem. Soc.* **2021**, *143*, 14551–14562.
(62) Elola, M. D.; Rodriguez, J. Influence of Cholesterol on the Dynamics of Hydration in Phospholipid Bilayers. *J. Phys. Chem. B* **2018**, *122*, 5897–5907.
(63) Arunan, E.; Desiraju, G. R.; Klein, R. A.; Sadlej, J.; Scheiner, S.; Alkorta, I.; Clary, D. C.; Crabtree, R. H.; Dannenberg, J. J.; Hobza, P.; et al. Defining the Hydrogen Bond: An Account (IUPAC Technical Report). *Pure Appl. Chem.* **2011**, *83*, 1619−1636.
(64) Lagge, D.; Hynes, J. T. A Molecular Jump Mechanism of Water Reorientation. *Science* **2006**, *311*, 832–835.
(65) Steinel, T.; Asbury, J. B.; Zheng, J.; Fayer, M. D. Watching Hydrogen Bonds Break: A Transient Absorption Study of Water. *J. Phys. Chem. A* **2004**, *108*, 10957–10964.
(66) Walrafen, G. E. Raman Spectrum of Water: Transverse and Longitudinal Acoustic Modes below .Apprxeq.300 Cm-1 and Optic Modes above .Apprxeq.300 Cm-1. *J. Phys. Chem.* **1990**, *94*, 2237−2239.
(67) Fecko, C. J.; Eaves, J. D.; Loparo, J. J.; Tokmakoff, A.; Geissler, P. L. Ultrafast Hydrogen-Bond Dynamics in the Infrared Spectroscopy of Water. *Science* **2003**, *301*, 1698–1702.
(68) Pal, S. K.; Zewail, A. H. Dynamics of Water in Biological Recognition. *Chem. Rev.* **2004**, *104*, 2099–2123.
(69) Wood, K.; Plazanet, M.; Gabel, F.; Kessler, B.; Oesterhelt, D.; Tobias, D. J.; Zaccai, G.; Weik, M. Coupling of Protein and Hydration- Water Dynamics in Biological Membranes. *Proc. Natl. Acad. Sci. U. S. A.* **2007**, *104*, 18049−18054.
(70) Busch, S.; Smuda, C.; Pardo, L. C.; Unruh, T. Molecular Mechanism of Long-Range Diffusion in Phospholipid Membranes Studied by Quasielastic Neutron Scattering. *J. Am. Chem. Soc.* **2010**, *132*, 3232–3233.
(71) Kurze, V.; Steinbauer, B.; Huber, T.; Beyer, K. A (2)H NMR Study of Macroscopically Aligned Bilayer Membranes Containing Interfacial Hydroxyl Residues. *Biophys. J.* **2000**, *78*, 2441–2451.
(72) Hsieh, C. H.; Wu, W. G. Structure and Dynamics of Primary Hydration Shell of Phosphatidylcholine Bilayers at Subzero Temperatures. *Biophys. J. 71, 3278 (1996)* **1996**, *71*, 3278–3287.
(73) Fitter, J.; Lechner, R. E.; Dencher, N. A. Interactions of Hydration Water and Biological Membranes Studied by Neutron Scattering. *J. Phys. Chem. B* **1999**, *103*, 8036–8050.
(74) Foglia, F.; Lawrence, M. J.; Lorenz, C. D.; McLain, S. E. On the Hydration of the Phosphocholine Headgroup in Aqueous Solution. *J. Chem. Phys.* **2010**, *133*, 145103.
(75) Zhao, W.; Moilanen, D. E.; Fenn, E. E.; Fayer, M. D. Water at the Surfaces of Aligned Phospholipid Multibilayer Model Membranes Probed with Ultrafast Vibrational Spectroscopy. *J. Am. Chem. Soc.* **2008**, *130*, 13927–13937.
(76) Volkov, V. V.; Palmer, D. J.; Righini, R. Heterogeneity of Water at the Phospholipid Membrane Interface. *J. Phys. Chem. B* **2007**, *111*, 1377–1383.
(77) Angelov, B.; Angelova, A.; Garamus, V. M.; Lebas, G.; Lesieur, S.; Ollivon, M.; Funari, S. S.; Willumeit, R.; Couvreur, P. Small-Angle Neutron and X-Ray Scattering from Amphiphilic Stimuli-Responsive Diamond-Type Bicontinuous Cubic Phase. *J. Am. Chem. Soc.* **2007**, *129*, 13474–13479.
(78) Tielrooij, K. J.; Paparo, D.; Piatkowski, L.; Bakker, H. J.; Bonn, M. Dielectric Relaxation Dynamics of Water in Model Membranes Probed by Terahertz Spectroscopy. *BioPhys. J.* **2009**, *97*, 2484–2492.
(79) Zhong, Q.; Fourkas, J. T. Optical Kerr Effect Spectroscopy of Simple Liquids. *J. Phys. Chem. B* **2008**, *112*, 15529–15539.
(80) Charkhesht, A.; Regmi, C. K.; Mitchell-Koch, K. R.; Cheng, S.; Vinh, N. Q. High-Precision Megahertz-to-Terahert Dielectric Spectroscopy of Protein Collective Motions and Hydration Dynamics. *J. Phys. Chem. B* **2018**, *122*, 6341–6350.

(81) Wang, P.; Wang, X.; Liu, L.; Zhao, H.; Qi, W.; He, M. The Hydration Shell of Monomeric and Dimeric Insulin Studied by Terahertz Time-Domain Spectroscopy. *BioPhys. J.* **2019**, *117*, 533–541.
(82) Nibali, V. C.; Havenith, M. New Insights into the Role of Water in Biological Function: Studying Solvated Biomolecules Using Terahertz Absorption Spectroscopy in Conjunction with Molecular Dynamics Simulations. *J. Am. Chem. Soc.* **2014**, *136*, 12800−12807.
(83) Heyden, M.; Ebbinghaus, S.; Havenith, M. Terahertz Spectroscopy as a Tool to Study Hydration Dynamics. *Encycl. Anal. Chem.* **2010**. https://doi.org/10.1002/9780470027318.a9162.
(84) Heyden, M.; Sun, J.; Funkner, S.; Mathias, G.; Forbert, H.; Havenith, M.; Marx, D. Dissecting the THz Spectrum of Liquid Water from First Principles via Correlations in Time and Space. *Proc. Natl. Acad. Sci. U.S.A.* **2010**, *107*, 12068–12073.
(85) Huang, C.; Quinn, D.; Sadovsky, Y.; Suresh, S.; Hsia, K. J. Formation and Size Distribution of Self-Assembled Vesicles. *Proc Natl Acad Sci USA* **2017**, *114*, 2910–2915.
(86) Lasic, D. D. The Mechanism of Vesicle Formation. *Biochem J* **1988**, *256*, 1–11.
(87) Bhardwaj, P.; Tripathi, P.; Gupta, R.; Pandey, P. Niosomes: A Review on Niosomal Research in the Last Decade. *J Drug Deliv Sci Technol* **2020**, *50*, 101581.
(88) Chen, S.; Hanning, S.; Falconer, J.; Locke, M.; Wen, J. Recent Advances in Non-Ionic Surfactant Vesicles (Niosomes): Fabrication, Characterization, Pharmaceutical and Cosmetic Applications. *Eur J Pharm Biopharm* **2019**, *144*, 18–39.
(89) Pattni, B. S.; Chupin, V. V.; Torchilin, V. P. New Developments in Liposomal Drug Delivery. *Chem Rev* **2015**, *115*, 10938–10966.
(90) Betz, G.; Aeppli, A.; Menshutina, N.; Leuenberger, H. In Vivo Comparison of Various Liposome Formulations for Cosmetic Application. *Int J Pharm* **2005**, *296*, 44–54.
(91) Bozzuto, G.; Molinari, A. Liposomes as Nanomedical Devices. *Int J Nanomed* **2015**, *10*, 975–999.
(92) Moghassemi, S.; Hadjizadeh, A. Nano-Niosomes as Nanoscale Drug Delivery Systems: An Illustrated Review. *J Control Release* **2014**, *185*, 22–36.
(93) Uchegbu, I. F.; Vyas, S. P. Non-Ionic Surfactant Based Vesicles (Niosomes) in Drug Delivery. *Int J Pharm* **1998**, *172*, 33–70.
(94) Manconi, M.; Sinico, C.; Valenti, D.; Loy, G.; Fadda, A. M. Niosomes as Carriers for Tretinoin. I. Preparation and Properties. *Int J Pharm* **2002**, *234*, 237–248.
(95) Mu, L.; Sprando, R. L. Application of Nanotechnology in Cosmetics. *Pharm Res* **2010**, *27*, 1746–1749.
(96) Mozafari, M. R.; Johnson, C.; Hatziantoniou, S.; Demetzos, C. Nanoliposomes and Their Applications in Food Nanotechnology. *J Liposome Res* **2008**, *18*, 309–327.

Chapter 2

Theories, Techniques and Instruments

2.I. Theories:

2.I.a. Charge in vesicle surface from Zeta potential:

The most popular technique used to measure the charge at the vesicle surface is the zeta potential measurement.[1,2] Zeta potential can be defined as the potential at the slipping plane or the potential at the hydrodynamic shear boundary of colloidal systems.[2] The assumption for charge calculations from zeta potential for a bilayer system is as follows[3]:

1. Bilayer can be considered an infinite planar surface with bound charges uniformly smeared at x=0.
2. Dielectric constant of solution is constant at all x>0.
3. The ion of the solution can be treated as point charge.

Goey-chapman model is based on the Poisson-Boltzmann relationship which relates between surface potential and surface charge density of any colloidal systems like micelle/vesicles.

Poisson's equation[4] can be written as $\vec{\nabla}.\vec{E} = \frac{\rho}{\epsilon_0}$ (2.I.a1)

Where ρ is the volume charge density and ϵ_0 is the free space permittivity.

As $\vec{E} = -\vec{\nabla}\phi$ (ϕ is the electric potential),

Poisson's equation becomes as $\nabla^2\phi = -\frac{\rho}{\epsilon_0}$ (2.I.a2)

Again, electrochemical potential of ion is related to the electric potential as,

$$\vec{\nabla}\mu_i = -Z_i e\vec{\nabla}\phi \quad \text{(2.I.a3)}$$

Where μ_i is the chemical potential and Z_i is the valency of i-th ion.

For one dimensional systems, $\frac{d\mu_i}{dx} = -Z_i e\frac{d\phi}{dx}$

Boltzmann distribution of ion's can be written as $n_i = n_0 e^{-\frac{Z_i e\phi}{kT}}$ (2.I.a4)

Again, volume charge density $\rho = \sum_i e n_i Z_i e^{-\frac{Z_i e\phi}{kT}}$

Now, Poisson's Boltzmann equation becomes $\nabla^2\phi = -\frac{1}{\epsilon_0}\sum_i e n_i Z_i e^{-\frac{Z_i e\phi}{kT}}$ (2.I.a5)

For one-dimensional conducting plane surface,

$$\frac{d^2\phi}{dx^2} = -\frac{1}{\epsilon_0}\sum_i e n_i Z_i e^{-\frac{Z_i e\phi}{kT}} \quad \text{(2.I.a6)}$$

Debye-Huckel Approximation:

ϕ is small in everywhere in double layer

i.e. $Z_i e\phi \ll kT$ then $e^{-\frac{Z_i e\phi}{kT}} \simeq 1 - \frac{Z_i e\phi}{kT}$

Equation 2.I.a6 becomes as $\frac{d^2\phi}{dx^2} = -\frac{1}{\epsilon_0}\sum_i e n_i Z_i (1 - \frac{Z_i e\phi}{kT})$ (2.I.a7)

For electroneutrality in bulk electrolyte 1st term in equation 2.I.a7 is zero. So,

$$\frac{d^2\phi}{dx^2} = \frac{\sum_i e^2 n_i^0 Z_i^2 \phi}{\epsilon kT}$$

$$\frac{d^2\phi}{dx^2} = \kappa^2\phi \text{ where } \kappa = \sqrt{\frac{\sum_i e^2 n_i^0 Z_i^2}{\epsilon kT}}$$

Parameter κ depends on electrolyte concentration n_i^0, termed as Debye-Huckel parameter.

So, for the solution of equation 2.I.a6, we have performed the integration of equation 2.I.a6 and applied two boundary conditions that

1. In bulk where x=∞, $\frac{d\phi}{dx} = 0$ & $\phi = 0$
2. For most electrolytes as though they were symmetric with valency Z, equal to valency of counterions.

So, the solution of equation 2.I.a6 becomes as

$$\tanh\frac{Ze\phi(x)}{4kT} = \tanh\frac{Ze\phi_0}{4kT}e^{-\kappa x} \quad \text{(2.I.a8)}$$

At the shear plane, $\phi(x) = \zeta$; the potential is called the zeta potential (Scheme 2I).

$$\tanh\frac{Ze\zeta}{4kT} = \tanh\frac{Ze\phi_0}{4kT}e^{-\kappa x} \text{ where } \phi_0 \text{ is the surface potential.}$$

Surface charge density, $\sigma = -\in\left(\frac{d\phi}{dx}\right)_{x=0}$

$$\sigma = \sqrt{8n^0 \in kT}\ \sinh\left(\frac{Ze\phi_0}{2kT}\right) \qquad \text{(2.I.a9)}$$

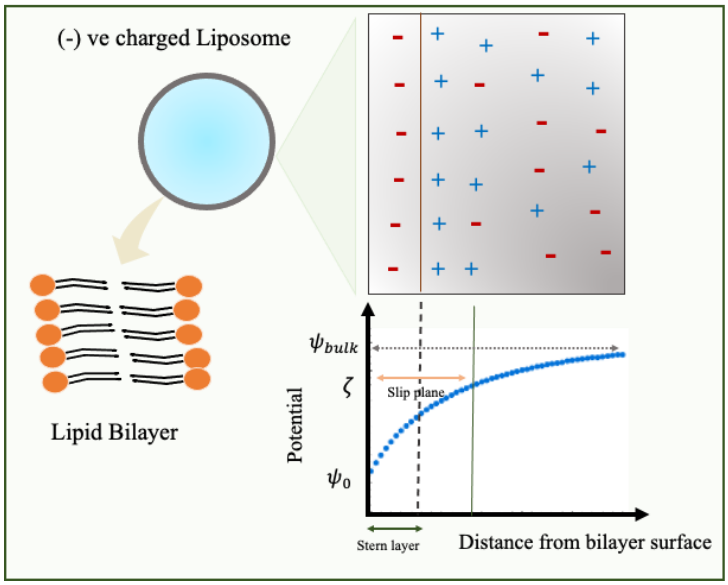

Scheme 2I: Schematic diagram of surface potential and zeta potential of a vesicle (-ve charged)

2.I.b. Principal Component Analysis (PCA):

Principal component analysis (PCA) is a very popular technique used to reduce the dimensionality of a dataset consisting a large number of variables.[5] We perform PCA using singular value decomposition method.[6–8] For PCA analysis, we construct a matrix A where change of absorption coefficient ($\Delta\alpha$) serves as the row vectors while Q as a column vector. Singular value decomposition provides three matrices, named as a score matrix (U), a singular matrix (S) and a loading matrix (V). They are related as:

$$A = USV^T \qquad \text{(2.I.b1)}$$

where V^T is the transpose of the matrix V. Principal components can be extracted from the following relation:

$$PC_i = s_i v_i \qquad \text{(2.I.b2)}$$

s_i are the diagonal elements of the S-matrix where v_i are the row vector of V.

2.I.c. Three Component Model:

Water is the major liquid for life and most of the biological phenomena occurs inside the cell in aqueous environment; there are mainly two types of water associated with the biomolecules; water in front of biomolecules, called the hydrated water and away from biomolecules, called the bulk water.[9–11] Interestingly this hydrated water can control the structure and stability of biomolecules and the structural and dynamical response of these two waters are completely different. Response of this hydrated water can be directly probed by using THz spectroscopy which measures the fluctuation of dipole moment of any solutions in terms of absorption coefficient.[12–15] Thus any change in dipole moment will reflect on the change in absorption coefficient of the solutions. For any biomolecules, absorption coefficient can be written as the average weight of absorption coefficient of solute molecule $\alpha_{solute}(\nu)$, hydration shell $\alpha_{sh}(\nu)$ and bulk water $\alpha_{bulk}(\nu)$ (scheme 2II).

$$\alpha_{total}(\nu) = \alpha_{solute}(\nu)\frac{V_{solute}}{V_{total}} + \alpha_{sh}(\nu)\frac{V_{sh}}{V_{total}} + \alpha_{bulk}(\nu)\frac{V_{bulk}}{V_{total}} \qquad (2.I.c1)$$

where V_{total}, V_{solute}, V_{sh}, and V_{bulk} are the total volume and volume occupied by solute molecule, volume occupied by dynamical hydration shell and volume of bulk water respectively.

Again equation (2.I.c1) can be written as

$$\alpha_{total}(\nu) = \alpha_{solute}(\nu)\phi_{solute} + \alpha_{sh}(\nu)\phi_{sh} + \alpha_{bulk}(\nu)\phi_{bulk} \qquad (2.I.c2)$$

$$[\ \phi_{solute} = \frac{V_{solute}}{V_{total}};\ \phi_{sh} = \frac{V_{sh}}{V_{total}};\ \phi_{bulk} = \frac{V_{bulk}}{V_{total}}\ ]$$

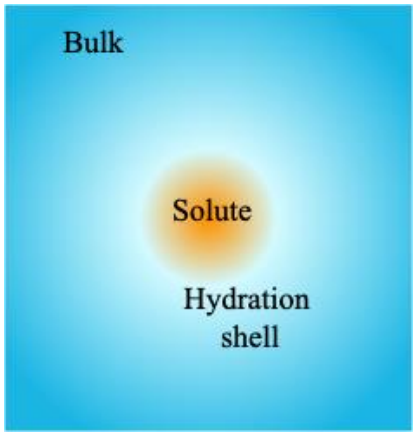

Scheme 2II: Schematic diagram of solute molecule with dynamical hydration shell in a solutions. Orange sphere defines the solute molecule and cyan shell is the dynamical hydration shell associated the solute molecules. Blue colour represents the bulk molecules.

2.I.d. Structural response of water at the hydration shell of biomolecules:

The bond between two atoms of a molecule behaves like a spring that has a certain intrinsic frequency and the molecule follows simple harmonic oscillator motion with a natural frequency.[16] When the molecules are in motion then the frictional force or damping come into play which is proportional to the velocity of molecular motion. If the light is applied to the damped motion of the particle i.e. driven by the light, then one dimensional equation of motion of atoms can be written as[17]

$$\frac{d^2y}{dx^2} + 2\gamma\frac{dy}{dx} + \omega_0^2 x = f\cos\omega t \qquad \text{(2.I.d1)}$$

where $\gamma = \frac{b}{2m}$; $\omega_0 = \sqrt{\frac{k}{m}}$; $f = \frac{eE}{m}$

solution of equation 2.I.d1 gives: $x(t) = f\frac{\cos(\omega t-\psi)}{\sqrt{(\omega_0^2-\omega^2)^2-4\gamma^2\omega^2}}$ where $\psi = \tan^{-1}(\frac{2\gamma\omega}{\omega_0^2-\omega^2})$

Absorption of radiation by the ions per unit time is:

$$P = -N < \vec{F}.\vec{v} > \qquad \text{(2.I.d2)}$$

Where $\vec{F} = -e\vec{E}\cos(\omega t)$ and $\vec{v} = \frac{d\vec{x}}{dt}$

Equation 2.I.d2 becomes as $P(\omega) = \frac{N(eE)^2\omega^2\gamma}{m\left[(\omega_0^2-\omega^2)^2+4\gamma^2\omega^2\right]}$ (2.I.d3)

Again, the absorption coefficient is related to dissipation as $P(\omega) = \frac{\alpha(\omega)c}{n}.\frac{1}{2} \in E^2$ (2.I.d4)

Where n is the refractive index and $\in$ is the dielectric constant of the medium and c is the velocity of light.

Putting equation 2.I.d3 into equation 2.I.d4 we get,

$$\alpha(\omega) = \frac{A\omega^2\gamma}{(\omega_0^2-\omega^2)^2+4\gamma^2\omega^2} \text{ where } A = 2\frac{n}{c}\frac{Ne^2}{m\in}$$

If molecule undergoes more than one underdamping motion then absorption coefficient can become as $\alpha(\omega) = \sum_i A_i \frac{\omega^2 \gamma_i}{\left(\omega_{0,i}^2 - \omega^2\right)^2 + 4\gamma_i^2 \omega^2}$ (2.I.d5)

2.I.e. Lifetime of Dipole moment autocorrelation function:

The motion of a dipole can be considered as a one-dimensional damped harmonic oscillator and the corresponding equation of motion can be written as

$$\frac{d^2x}{dt^2} + 2\gamma \frac{dx}{dt} + \omega_o^2 x = 0 \qquad (2.I.e1)$$

where γ and ω_o are the damping term and the natural frequency, respectively. When THz radiation is applied on a substance, it exerts a force $(-eEcos(\omega t))$ and correspondingly the power spectrum of the harmonic oscillator can be written as

$$I_x(\omega) = \frac{N\,(eE)^2 \omega^2\,\gamma}{m[\,(\omega_0^2 - \omega^2)^2 + 4\gamma^2\omega^2\,]} \qquad (2.I.e2)$$

with N, m being the number of oscillating dipoles per unit volume and mass of each dipole, respectively. The time correlation function of position can be expressed from power spectrum (using Wiener-Khintchine theorem) as[18]

$$C(t) = < x(0)x(t) > = \int_{-\infty}^{\infty} d\omega\, e^{i\omega t}\, I_x(\omega) \qquad (2.I.e3)$$

Combining 2.I.e2 and 2.I.e3 we get,

$$C_x(t) = \int_{-\infty}^{\infty} \frac{N\,(eE)^2 \omega^2\,\gamma}{m[\,(\omega_0^2 - \omega^2)^2 + 4\gamma^2\omega^2\,]} d\omega\, e^{i\omega t} \qquad (2.I.e4)$$

Since dipole moment correlation function $C_\mu(t)$ is proportional to the position correlation function, it can be estimated from equation (2.I.e3) in the following way[6]:

$$C_\mu(t) \propto \left(\cos\omega_1 t + \frac{1}{\tau\,\omega_1}\sin\omega_1 t\right) e^{-t/\tau} \qquad (2.I.e5)$$

where ω_1 represents the oscillation frequency of damped harmonic oscillator compared to natural frequency ω_0 with $\omega_1 = \sqrt{\omega_0^2 + \frac{\gamma^2}{4\pi^2}}$. The term, τ $(= \frac{1}{\gamma})$ stands for the lifetime of the autocorrelation function. Experimentally it can be estimated from the linewidth as $\tau_i = \frac{1}{\omega_i c}$; where ω_i are the fitted parameter of the i^{th} component.[6,19]

2.II. Experimental techniques:

2.II.a. Preparation of Bilayer Systems:

2.II.a.i. Vesicle Preparation:

The charged vesicles were prepared using sonication technique.[20,21] Concentration of both Sodium dodecyl sulfate (SDS) and hexadecyltrimethylammonium bromide (CTAB) surfactant was kept fixed at 20 mM, which is much higher than their corresponding critical micellar concentration (cmc) (~8 mM for SDS and ~ 1 mM for CTAB).[22] Dry cholesterol molecules were added to the micellar solutions followed by sonication up to 20 min in a bath sonicator (model no: UR1, 35 kHz, 2×240 W) at room temperature. Before the experiments, the solutions were kept in dark overnight for stabilization.

2.II.a.ii. Niosome Preparation:

Niosomes were prepared using chloroform injection technique.[23] Both Brij 30 and cholesterol in desired weight proportions were dissolved in chloroform and the solution was then injected in aqueous environment using a Hamilton syringe. This solution was then stirred in a magnetic stirrer for 30 min at a constant temperature of 40 ºC in order to evaporate chloroform. This homogeneous solution was also kept overnight before the experiments.

2.II.a.iii. Liposome preparation:

Film Hydration technique:

Liposomes were prepared using film hydration technique.[24,25] Briefly, lipid molecules were dissolved first in chloroform. A gentle stream of nitrogen was then passed through the solution to evaporate the chloroform. The lipid film was then placed in desiccator for 2 hrs. to ensure complete disappearance of any chloroform molecule. The dried lipid film was then hydrated with the phosphate buffer (50 mM, pH 7.4) solution. The lipid starts to swell and separate from glass vial and forms inhomogeneous cloudy solution which was then stirred with a magnetic stirrer to 30 min at a speed of 1100 rpm at 25 °C. The solution was kept at 4 ºC for complete swelling and again stirred for 30 min with 1100 rpm speed at 25 °C.

- *Sonication technique:* The solution was then sonicated for 30 min at room temperature. Finally, it was kept overnight at 4 ºC before the measurements. We also prepared liposomes using the same protocol in presence of cholesterol with varying $Q = \frac{[Cholesterol]}{[Lipid]}$.
- *Extrusion technique:* The solution was then extruded (scheme 2III) through a mini-extruder (Avanti polar lipid) with polycarbonate membrane filter (pore size 100 nm),

fitted with Hamiltonian syringes (model no 610017-1Ea). The samples were passed ~11 times through the filter to get uniform liposomes. Liposome solution was kept at 4 ºC overnight before experiment.

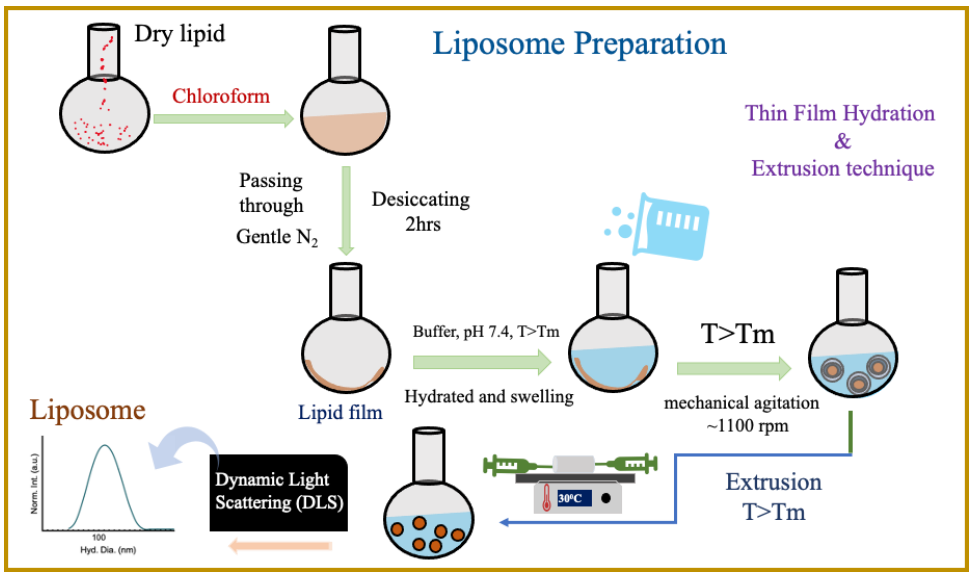

Scheme 2III. Preparation of liposomes by using film hydration based extrusion technique.

2.II.b. Analyses and Techniques:

2.II.b.i. Image collections & Analyses:

Atomic Force Microscopy:

The prepared samples were drop casted on freshly cleaved mica substrate and then kept for 30 min to ensure complete adsorption on the substrate. The excess solution was then washed by flowing milli Q water. Finally a gentle nitrogen flow was passed to vaporise the remaining water prior to the AFM measurements. Collected images of vesicles and liposomes are analysed by using *Image J* and *Gwyddion* software to extract the size and height of the particles.

Field Emission Scanning Electron Microscopy:

Firstly samples were drop casted on properly cleaned silicon wafer and kept it in desiccator overnight to ensure complete de-wetting of sample. Gold of thickness 1 nm was deposited on the sample prior to the imaging. Collected images of liposomes are analysed by using Image J and *Mathematica 13.0.1* software to extract the size of the particles.

2.II.b.ii. Measurements:

DLS Size measurements:

DLS measurements followed the light scattering technique. DLS experiment gives the intensity auto-correlation curve between time of measured data. By fitting this correlation curve with exponential function, the diffusion coefficient (D) can be extracted as diffusion coefficient is directly related to the lifetime of fitted data. Hydrodynamic diameter (d_H) of the particle is related to the diffusion coefficient of the solutions, can be calculated from the stoke-Einstein model[26]

$$d_H = \frac{k_B T}{3\pi\eta D}$$

Where k_B is the Boltzmann constant and η is the viscosity of the solutions.

Zeta Potential measurements:

Zeta potential measurements are based on the principles of light scattering. Here the sample is placed into a chamber which consists of two electrodes. When Electric field is applied into the electrodes then charged nanoparticles starts to migrate corresponding to the electrodes with a velocity proportional to zeta potential. The zeta potential is then calculated from the velocity or the electrophoretic mobility by using Henry equation[2,27]

$$U_e = \frac{2\epsilon\xi f(ka)}{3\eta}$$

where U_e is the electrophoretic mobility, ε the dielectric constsnt, ξ is the zeta potential, η is the viscosity of the medium and *"ka"* is the ratio between the particle diameter and the Debye length. For aqueous solutions a Smoluchowski's approximation is considered and the value of *f(ka)* is taken as 1.5.[1]

THz-FTIR measurements:

The Spectrometer is attached with an ATR (attenuated total reflection) sample compartment and all the measurements were performed in the ATR mode.[7] A diamond crystal with refractive index of 2.41 was used in the ATR attachment. The sample compartment was evacuated each time prior to the measurements using a vacuum pump. Each measurement was an average of 128 scans with resolution of 4 cm^{-1}. We measured three times of each sample and then averaged to get the final spectra to be analysed further. The spectral signature was obtained in ATR unit which was then converted into absorbance using following formula

$$\mathrm{Abs}(\nu) = \frac{\text{intensity in ATR unit}(\nu) \times 1000}{\text{Wavenumber } (\nu)}$$

Using Beer-Lambert law, the absorption coefficient was estimated as

$$\alpha(\nu) = \frac{1}{d_p}(\mathrm{Abs}_{\mathrm{reference}}(\nu) - \mathrm{Abs}_{\mathrm{sample}}(\nu))$$

where d_p is the penetration depth, obtained as[28]

$$d_p = \frac{\lambda}{2\,\pi\sqrt{(n_d \mathrm{Sin}\theta)^2 - n_s^2}}$$

where λ in the wavelength of the light, n_s and n_d are the refractive indices of the sample and diamond crystal respectively and θ is the incident angle (here $\theta = \frac{\pi}{4}$).

Change in the absorption coefficient was expressed as,

$$\Delta\alpha(\nu) = \alpha_{\mathrm{sample}}(\nu) - \alpha_{\mathrm{water}}(\nu)$$

2.II.c. Chemical used:

2.II.c.i. Lipids:

1,2-Dioleoyl-sn-glycero-3-phosphocholine (DOPC): DOPC is a zwitterionic phospholipid (scheme 2IVa), generally found in eukaryotic cells. Structurally, it consists two unsaturated long (18:1) oleic acids and colin as a headgroup. It has a transition temperature -16.5 ^{0}C, therefore exists in the fluid phase at room temperature.[29]

2-Oleoyl-1-palmitoyl-sn-glycero-3-phosphocholine (POPC): POPC is a zwitterionic phospholipid (scheme 2IVb), consists of two distinct tails: one is saturated long palmitic acid (16:0) and another is unsaturated oleic acid (18:1).[30] Molecular weight of POPC lipid is ~760.08 gm/mol.

1,2-Dipalmitoyl-sn-glycero-3-phosphocholine (DPPC): has phase transition temperature ~41 ^{0}C and remains in solid like gel state at room temperature.[31] Structurally, it consists two saturated long (16:0) palmitic acids and colin as a headgroup which is shown in scheme 2IVc.

1,2-Dioleoyl-sn-glycero-3-phospho-rac-(1-glycerol) sodium salt (DOPG):

DOPG is a negatively charged phospholipid, having molecular weight ~797.03 gm/mol. Structurally, it consists two unsaturated long (18:1) oleic acids and colin as a headgroup (scheme 2IVd). It has phase transition temperature -18^{0}C.[32]

3β-Hydroxy-5-cholestene,5-Cholesten-3β-ol (Cholesterol): has molecular weight ~386.65 gm/mol. Cholesterol is the major sterol, present in only mammalian cell membrane (scheme 2IVe). It does resides into phospholipid bilayer of membrane which regulates the fluidity and rigidity of membranes.[33] Cell membrane contains 20-30% cholesterol, whereas it could rise up to 50% in red blood cells.[34]

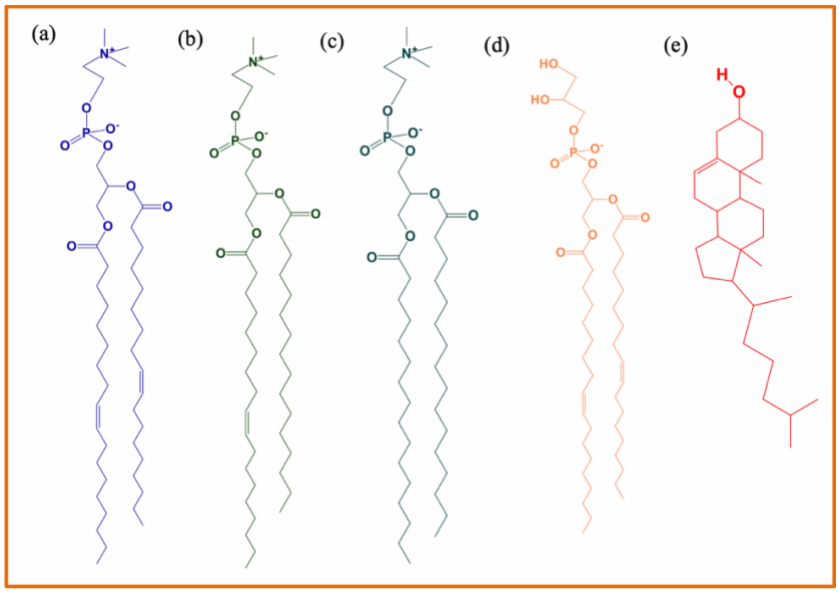

Scheme 2IV. Chemical structure of (a) DOPC (b) POPC (c) DPPC (d) DOPG and (e) cholesterol

---

2.II.c.ii. Surfactants:

Sodium dodecyl sulfate (SDS): is an anionic surfactant, having molecular weight ~288.38 gm/mol and the chemical structure of SDS in shown in scheme 2Va. It is amphiphilic in nature contains both hydrophilic headgroup and hydrophobic hydrocarbon tail parts. The critical micellar concentration (CMC) in water at 25^{0}C of SDS surfactant is ~8 mM and above the CMC value, it forms micelle in aqueous environments.[35] It is widely used as a cleaning and hygiene products and emulsifier in pharmaceutical field and in many industries.[36,37]

Hexadecyltrimethylammonium bromide (CTAB): is a cationic surfactant with molecular weight ~ 364.45 gm/mol and the chemical structure of CTAB in shown in scheme 2Vb. The critical

micellar concentration (cmc) of CTAB surfactant is ~1 mM.[38]As like most surfactants CTAB also forms micelle in aqueous environment. CTAB is an antiseptic agent against bacteria and fungi. It is used in synthesis of gold nanoparticles, mesoporous silica nanoparticles and sometimes in the extraction of DNA.[39,40]

Polyoxyethylene 4 laurylether (Brij 30): is a non-ionic surfactant (scheme 2Vc) with molecular weight gm/mol. It can form vesicle in presence of cholesterol, termed as a niosome.[41,42] Brij 30 is widely used as a emulsifying agent, penetration enhancer, and also as a solubilizing agents.[43] Recently, it is also used as a carrier vehicle of drug in drug industries.[44]

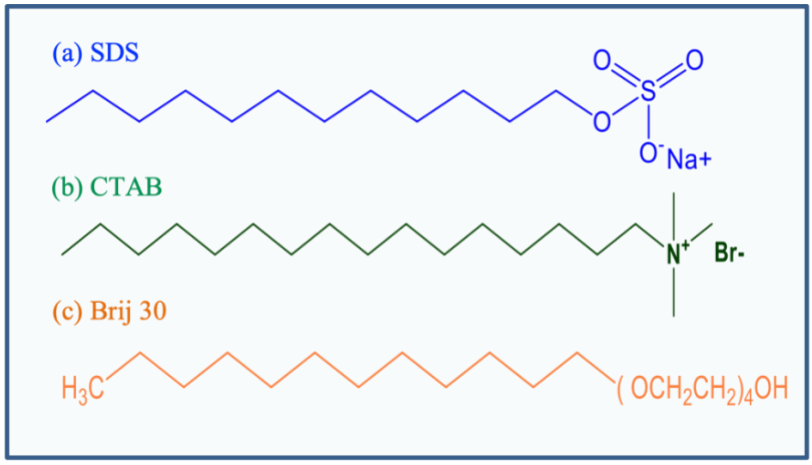

Scheme 2V. Chemical structure of (a) SDS (b) CTAB and (c) Brij 30 surfactants

2.II.c.iii. Co-Solvents:

Ethanol: Ethanol is a short chain alcohol, basically amphiphilic in nature (scheme 2VIa). Ethanol has a large application in medicine industry as a model anesthetic in food industry as food preservative.[45]When ethanol is introduced into lipid bilayer, primarily they are located at the lipid/water interface region, forms hydrogen bonds with lipid's headgroup.[46,47]

2,2,2-Trifluoroethanol (TFE): is an organic liquid and a cosolvent (scheme 2VIb) in cell biology which has a lot of applications to stabilize peptides and proteins.[48] It also alters the lipid's bilayer properties.[49]

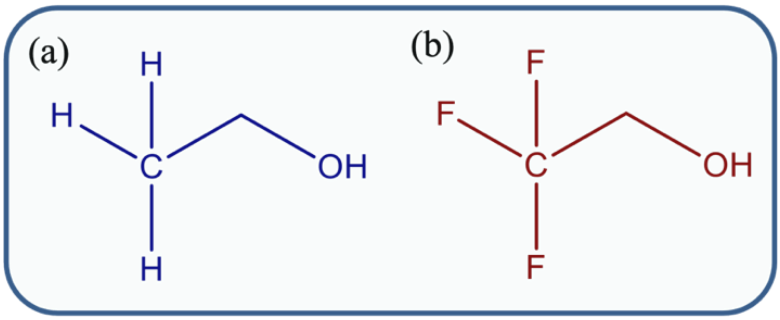

Scheme 2VI. Chemical structure of (a) Ethanol and (b) TFE

2.II.c.iv. Molecular Crowders:

Polyethylene Glycol 4000 (PEG 4000):

PEG is a water-soluble polymer (scheme 2VII), widely been used as a macromolecular agent[50,51] owning to its biocompatibility.[52] In lipid bilayers, PEG molecules alter the molecular order of the bilayer at the point of contact and produce volume exclusion induced aggregation followed by dehydration which eventually destabilizes the bilayer membranes.[53,54]

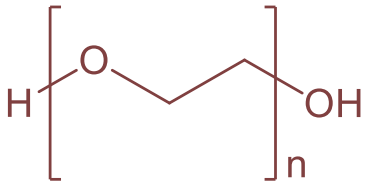

Scheme 2VII. Chemical structure of polyethylene glycol 4000

2.III. Instruments:

2.III.a. Dynamic Light Scattering (DLS):

Dynamic Light Scattering (DLS) (which is sometimes called as Quasi-Elastic Light Scattering) is a technique used to measure the hydrodynamic diameter (d_H) of particles.[26,55] As the particles are in Brownian motion, the intensity of scattered light fluctuates over time. The velocity of this Brownian motion is directly related to the diffusion coefficient of the particles in solutions. DLS mainly monitors the Brownian motion of the particles suspended in a liquid. The correlation function of intensity can be defined as $< I(t)I(t + \delta t) >$

For nondispersive particle, correlation function is exponentially decaying:

$$G(t) = A[1 + Be^{-2\Gamma\tau}]$$

Where A and B are the baseline and intercept of corelation function and $\tau=Dq^2$

D is the translational diffusion coefficient and $q = \frac{4\pi n}{\lambda} Sin(\frac{\theta}{2})$

λ is the wavelength of laser; θ is the scattering angle and n is the refractive index of dispersion. For polydisperse sample the correlation function can be written as $G(t) = A[1 + Bg(t)^2]$; Where g(t) is the sum of all exponential decays.

Here we perform DLS experiments with Nano S Malvern instrument with He-Ne laser with lasing power 4 mW and wavelength 632.8 nm. All the scattered photons (here the Rayleigh scattering) are collected at 173° scattering angle. The block diagram of DLS is shown in scheme 2VIII. According to Stokes-Einstein model, d_H of the particle is directly related to the diffusion coefficient of the solutions: $d_H = \frac{k_B T}{3\pi\eta D}$ where k_B is the Boltzmann constant and η is the viscosity of the solution.

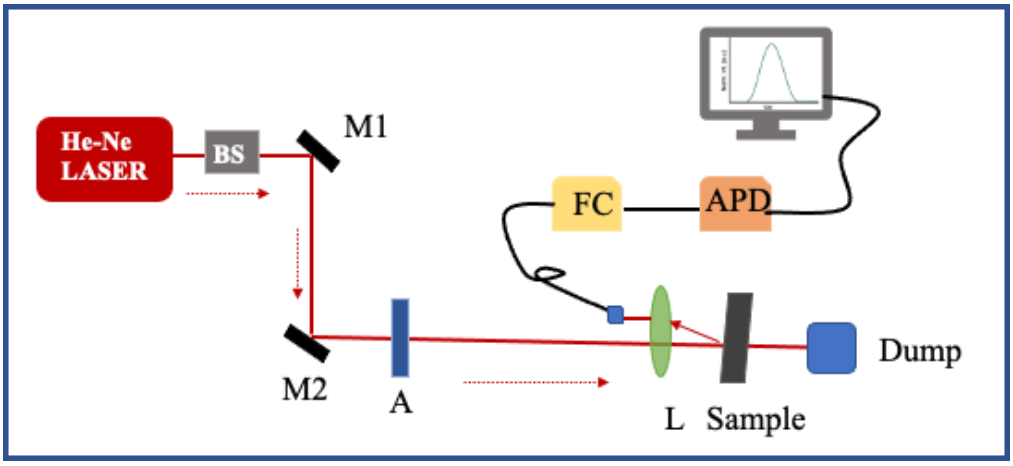

Scheme 2VIII. Block Diagram of Dynamic light scattering (DLS). BS, FC, APD, Dump stands for the beam sampler, fibre coupler, avalanche photodiode, beam dump respectively. M1 and M2 are the plane mirror, L is lens and A represents attenuator

2.III.b. FAR-FTIR (THz) Spectroscopy:

We perform the far-FTIR measurements by using Vertex 70V, Bruker, Germany. Here Globar is used as a IR source and DLaTGS (a complex material) as a detector. We collect the spectrum in between 50-450 cm^{-1} as a far-IR spectra. Measurements were carried out in ATR (attenuated total reflection) mode with a diamond crystal of refractive index 2.41. The sample compartment was evacuated using a vacuum pump every time prior to the experiments. FTIR follows the Michelson interferometer principal (schematic diagram is shown in scheme 2IX).[56] It is used to investigate the hydration behaviour of solute molecules which measures the change in the collective dipole moment fluctuations of water, more specifically the hydrogen bond network of water.[13,57] It directly probes the permanent and induced dipole moment of the systems in terms of absorption coefficient[12]:

$$\alpha(\omega) = \frac{1}{4\pi\varepsilon_0}\frac{2\pi\beta\omega^2}{3Vcn(\omega)}\int_{-\infty}^{+\infty} dt e^{i\omega t} < \vec{M}(0)\,\vec{M}(t) >$$

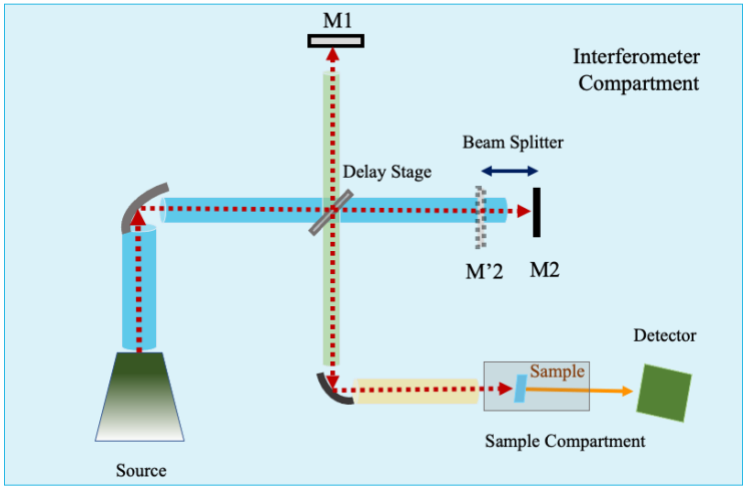

Scheme 2IX. Ray Diagram of Michelson interferogram. M1 represents the fixed mirror, M2 and M'2 represents the movable mirror respectively.

2.III.c. Atomic Force Microscopy (AFM):

Morphologies of vesicles and liposomes at different conformations are collected by using Atomic Force microscope (AFM; model no di INNOVA) technique.[58,59] Laser (of wavelength 600-700 nm) is used as a source and photodiode as a detector. It is a technique which is based on the detection of interaction force in between the microscopic tip and a sample surface.[60] The

term “Atomic” comes from the fact that the interaction between tip and sample surface involves some atoms. The most important part of AFM is the “AFM probe” (generally made by silicon or silicon nitride) which contains a cantilever with a sharp tip at one end (is shown in scheme 2X). The reflected and refracted laser beam illuminates the four quadrant photo-diode. When the tip is far away from the sample, i.e. in absence of any force, beam hit the middle of the photodiode and the signal provides from the upper and lower panel of the photodiode remains unchanged; so the signals provide by the operational amplifier (OP-AMP) is zero. But, when the tip is interacting with a sample surface with small force both the cantilever and reflected beam deflect resulting a non-zero output force from the OP-AMP. AFM probe raster scans on the sample surface and construct 3D-topography of images. It is widely used to collect the morphological picture of biological samples and from force-displacement curve one can easily probe the elasticity of the materials.

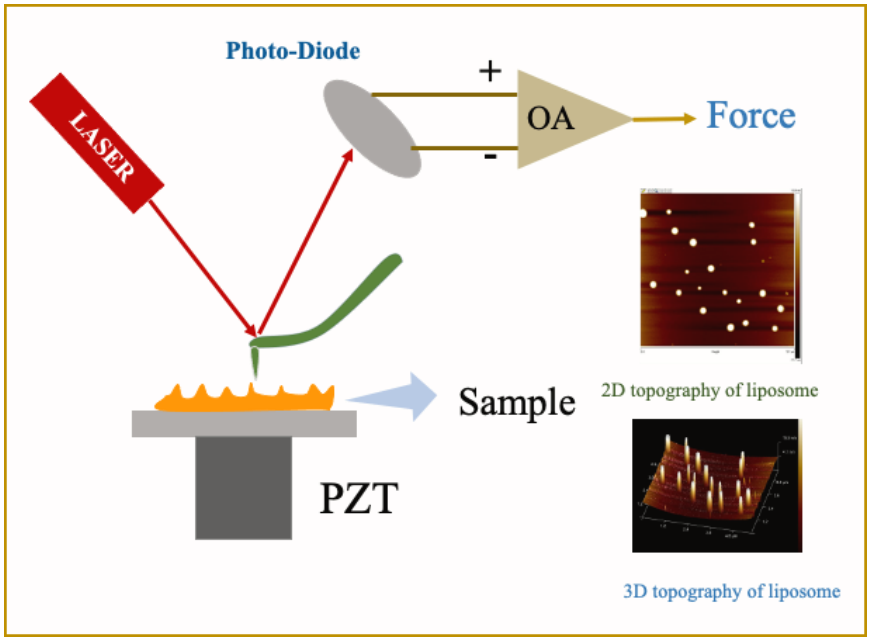

Scheme 2X. Block Diagram of AFM. OA stands for operational amplifier (OP-AMP) and PZT represents Piezoelectric scanner

2.III.d. Scanning Electron Microscope (SEM):

Scanning electron microscope is an electron microscope which is used to extract the surface chemistry and morphology with submicron resolution.[61,62] Here electron gun is used as a source which accelerates electrons through 1-30 kV accelerating voltages. Electromagnetic lenses are used to focus this electrons into a beam and scan the beam to the sample surface to generate the images. The SEM chamber is kept under a vacuumed with pressure $0.1\text{-}10^{-4}$ Pa to avoid the interaction of electrons with air. When high energy electron reaches to the sample surface several electron and X-ray signals are generated. The secondary electron comes from the few nanometre distance from the sample surface and they are very much sensitive to the sample surface and provides topographic information. Beside the topography, chemical composition of a material can be extracted from the SEM. To do this, X-ray spectra (also known as the EDX spot spectrum) are collected by focusing the electron beam on the sample and measuring the number of X-rays with various energies that hit the detector. By comparing the energy of the characteristic X-ray peaks to elemental standards, individual elements in the sample are identified. We image the liposome solution by using field-emission scanning electron microscope (FEI QUANTA FEG 250) (scheme 2XI).

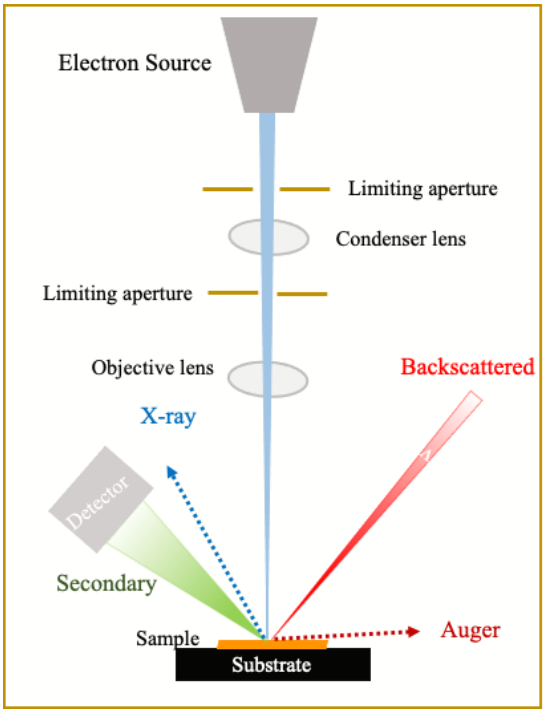

Scheme 2XI. Block Diagram of SEM

2.IV. References:

(1) Gilbile, D.; Docto, D.; Kingi, D. T.; Kurniawan, J.; Monahan, D.; Tang, A.; Kuhl, T. L. How Well Can You Tailor the Charge of Lipid Vesicles? *Langmuir* **2019**, *35*, 15960–15969.
(2) Smith, M. C.; Crist, R. M.; Clogston, J. D.; McNeil, S. E. Zeta Potential: A Case Study of Cationic, Anionic, and Neutral Liposomes. *Anal. Bioanal. Chem.* **2017**, *409*, 5779–5787.
(3) Hunter, R. J. *Zeta Potential in Colloid Science: Principles and Applications*; Academic Press.
(4) Griffiths, D. J. *Introducttion to Electrodynamics*, 4th ed.; PHI Learning Pvt. Ltd.
(5) Jolliffe, I. T. Principal Component Analysis; Springer.
(6) Schwaab, G.; Sebastiani, F.; Havenith, M. Ion Hydration and Ion Pairing as Probed by THz Spectroscopy. *Angew. Chem. Int. Ed.* **2019**, *58*, 3000–3013.
(7) Pyne, P.; Mitra, R. K. Excipients Do Regulate Phase Separation in Lysozyme and Thus Also Its Hydration. *J. Phys. Chem. Lett.* **2022**, *13*, 931−938.
(8) Sebastiani, F.; Ma, C. Y.; Funke, S.; Bäumer, A.; Decka, D.; Hoberg, C.; Esser, A.; Forbert, H.; Schwaab, G.; Marx, D.; Havenith, M. Probing Local Electrostatics of Glycine in Aqueous Solution by THz Spectroscopy. *Angew. Chem. Int. Ed.* **2021**, *60*, 3768–3772.
(9) Ball, P. Water as an Active Constituent in Cell Biology. *Chem. Rev.* **2008**, *108*, 74−108.
(10) Pal, S. K.; Zewail, A. H. Dynamics of Water in Biological Recognition. *Chem. Rev.* **2004**, *104*, 2099–2123.
(11) Laage, D.; Elsaesser, T.; Hynes, J. T. Water Dynamics in the Hydration Shells of Biomolecules. *Chem. Rev.* **2017**, *117*, 10694–10725.
(12) Nibali, V. C.; Havenith, M. New Insights into the Role of Water in Biological Function: Studying Solvated Biomolecules Using Terahertz Absorption Spectroscopy in Conjunction with Molecular Dynamics Simulations. *J. Am. Chem. Soc.* **2014**, *136*, 12800−12807.
(13) Ebbinghaus, S.; Kim, S. J.; Heyden, M.; Yu, X.; Heugen, U.; Gruebele, M.; Leitner, D. M.; Havenith, M. An Extended Dynamical Hydration Shell around Proteins. *Proc. Natl. Acad. Sci. U.S.A.* **2007**, *104*, 20749–20752.
(14) Heyden, M.; Bründermann, E.; Heugen, U.; Niehues, G.; Leitner, D. M.; Havenith, M. Long-Range Influence of Carbohydrates on the Solvation Dynamics of Waters-Answers from Terahertz Absorption Measurements and Molecular Modeling Simulations. *J. J. Am. Chem. Soc.* **2008**, *130*, 5773–5779.
(15) Sun, J.; Niehues, G.; Forbert, H.; Decka, D.; Schwaab, G.; Marx, D.; Havenith, M. Understanding THz Spectra of Aqueous Solutions: Glycine in Light and Heavy Water. *J. Am. Chem. Soc.* **2014**, *136*, 5031−5038.
(16) Banwell, C. N.; McCash, E. M. *Fundamentals of Molecular Spectroscopy*, 4th. ed.; McGraw-Hill Publishing Company.
(17) Dodo, T.; Sugawa, M.; Nonaka, E.; Honda, H.; Ikawa, S. Absorption of Farinfrared Radiation by Alkali Halide Aqueous Solutions. *J. Chem. Phys.* **1995**, *102*, 6208.
(18) Nitzan, A. *Chemical Dynamics in Condensed Phases*; Oxford university press, 2006.
(19) Sebastiani, F.; Bender, T. A.; Pezzotti, S.; Li, W. L.; Schwaab, G.; Bergman, R. G.; Raymond, K. N.; Toste, F. D.; Head-Gordon, T.; Havenith, M. An Isolated Water Droplet in the Aqueous Solution of a Supramolecular Tetrahedral Cage. *Proc. Natl. Acad. Sci. U.S.A.* **2020**, *117*, 32954–32961.
(20) Ghosh, S.; Roy, A.; Banik, D.; Kundu, N.; Kuchlyan, J.; Dhir, A.; Sarkar, N. How Does the Surface Charge of Ionic Surfactant and Cholesterol Forming Vesicles Control Rotational and Translational Motion of Rhodamine 6G Perchlorate (R6G ClO 4)? *Langmuir* **2015**, *31*, 2310–2320.
(21) Ferrer-Tasies, L.; Moreno-Calvo, E.; Cano-Sarabia, M.; Aguilella-Arzo, M.; Angelova, A.; Lesieur, S.; Ricart, S.; Faraudo, J.; Ventosa, N.; Veciana, J. Quatsomes: Vesicles Formed by Self-Assembly of Sterols and Quaternary Ammonium Surfactants. *Langmuir* **2013**, *29*, 6519–6528.
(22) Cui, X.; Mao, S.; Liu, M.; Yuan, H.; Du, Y. Mechanism of Surfactant Micelle Formation. *Langmuir* **2008**, *24*, 10771–10775.
(23) Kumar, G. P.; Rajeshwarrao, P. Nonionic Surfactant Vesicular Systems for Effective Drug Delivery — an Overview. *Acta Pharm Sin B* **2011**, *1*, 208–219.
(24) Lapinski, M. M.; Castro-Forero, A.; Greiner, A. J.; Ofoli, R. Y.; Blanchard, G. J. Comparison of Liposomes Formed by Sonication and Extrusion: Rotational and Translational Diffusion of an Embedded Chromophore. *Langmuir* **2007**, *23*, 11677–11683.
(25) Maulucci, G.; Spirito, M. D.; Arcovito, G.; Boffi, F.; Castellano, A. C.; Briganti, G. Particle Size Distribution in DMPC Vesicles Solutions Undergoing Different Sonication Times. *BioPhys. J.* **2005**, *88*, 3545–3550.

(26) Mitra, R. K.; Sinha, S. S.; Pal, S. K. Hydration in Protein Folding: Thermal Unfolding/Refolding of Human Serum Albumin. *Langmuir* **2007**, *23*, 10224–10229.
(27) Hunter, R. J. *Academic Press* **1981**.
(28) Milosevic, M. Internal Reflection and ATR Spectroscopy. *Appl. Spectrosc. Rev.* **2004**, *39*, 365–384.
(29) Ulrich, A. S.; Sami, M.; Watts, A. Hydration of DOPC Bilayers by Differential Scanning Calorimetry. *Biochim. Biophys. Acta* **1994**, *1191*, 225–230.
(30) Saito, H.; Morishita, T.; Mizukami, T.; Nishiyama, K.; Kawaguchi, K.; Nagao, H. Free Energy Profiles of Lipid Translocation across Pure POPC and POPC/CHOL Bilayer: All-Atom Molecular Dynamics Study. *J. Phys. Conf. Ser.* **2019**, *1290*, 012020.
(31) Biltonen, R.; Lichtenberg, D. The Use of Differential Scanning Calorimetry as a Tool to Characterize Liposome Preparations. *Chem. Phys. Lipids* **1993**, *64*, 129–142.
(32) Himeno, H.; Shimokawa, N.; Komura, S.; Andelman, D.; Hamada, T.; Takagi, M. Charge-Induced Phase Separation in Lipid Membranes. *Soft Matter* **2014**, *10*, 7959–7967.
(33) Ikonen, E. Cellular Cholesterol Trafficking and Compartmentalization. *Nat. Rev* **2008**, *9*, 125–138.
(34) Mouritsen, O. G.; Zuckermann, M. J. What's So Special About Cholesterol? *Lipids* **2004**, *39*, 1101–1113.
(35) Bruce, C. D.; Berkowitz, M. L.; Perera, L.; Forbes, M. D. E. Molecular Dynamics Simulation of Sodium Dodecyl Sulfate Micelle in Water: Micellar Structural Characteristics and Counterion Distribution. *J Phys Chem B* **2002**, *106*, 3788–3793.
(36) Hassan, R. R. A. Sodium Dodecyl Sulfate Micro-Emulsion as a Smart Cleaning Agent for Archeological Manuscripts: Surface Investigations. *Eur. Phys. J. Plus* **2021**, *136*, 1–18.
(37) Bondi, C. A. M.; Marks, J. L.; Wroblewski, L. B.; Raatikainen, H. S.; Lenox, S. R.; Gebhardt, K. E. Human and Environmental Toxicity of Sodium Lauryl Sulfate (SLS): Evidence for Safe Use in Household Cleaning Products. *Environ Health Insights.* **2015**, *9*, 27–32.
(38) Dorshow, R.; Briggs, J.; Bunton, C. A.; Nicoli, D. F. Dynamic Light Scattering from Cetyltrimethylammonium Bromide Micelles. Intermicellar Interactions at Low Ionic Strengths. *J Phys Chem* **1982**, *86*, 2388–2395.
(39) Elfeky, S. A.; Mahmoud, S. E.; Youssef, A. F. Applications of CTAB Modified Magnetic Nanoparticles for Removal of Chromium (VI) from Contaminated Water. *J Adv Res* **2017**, *8*, 435–443.
(40) Tamari, F.; Hinkley, C. S.; Ramprashad, N. A Comparison of DNA Extraction Methods Using Petunia Hybrida Tissues. *J Biomol Tech.* **2013**, 113–118.
(41) Manconi, M.; Valenti, D.; Sinico, C.; Lai, F.; Loy, G.; Fadda, A. M. Niosomes as Carriers for Tretinoin II. Influence of Vesicular Incorporation on Tretinoin Photostability. *Int J Pharm* **2003**, *260*, 261–272.
(42) Chen, S.; Hanning, S.; Falconer, J.; Locke, M.; Wen, J. Recent Advances in Non-Ionic Surfactant Vesicles (Niosomes): Fabrication, Characterization, Pharmaceutical and Cosmetic Applications. *Eur J Pharm Biopharm* **2019**, *144*, 18–39.
(43) Turos, E.; Garay-Jimenez, J. C.; Sona, A. J. An Evaluation of Non-Ionic Surfactants on the Cytotoxicity and Activity of Poly(Butyl Acrylate/Styrene) Nanoparticle Emulsions. *J Nanopart Res* **2019**, *21*, 165.
(44) Komaiko, J.; McClements, D. J. Optimization of Isothermal Low-Energy Nanoemulsion Formation: Hydrocarbon Oil, Non-Ionic Surfactant, and Water Systems. *J. Colloid Interface Sci.* **2014**, *425*, 59–66.
(45) Alzeer, J.; Hadeed, K. A. Ethanol and Its Halal Status in Food Industries. *Trends Food Sci Technol* **2016**, *58*, 14–20.
(46) Gurtovenko, A. A.; Anwar, J. Interaction of Ethanol with Biological Membranes: The Formation of Non Bilayer Structures within the Membrane Interior and Their Significance. *J. Phys. Chem. B* **2009**, *113*, 1983–1992.
(47) Patra, M.; Salonen, E.; Terama, E.; Vattulainen, I.; Faller, R.; Lee, B. W.; Holopainen, J.; Karttunen, M. Under the Influence of Alcohol: The Effect of Ethanol and Methanol on Lipid Bilayers. *BioPhys. J.* **2006**, *90*, 1121–1135.
(48) Buck, M. Trifluoroethanol and Colleagues: Cosolvents Come of Age. Recent Studies with Peptides and Proteins. *Q Rev Biophys.* **1998**, *31*, 297–355.
(49) Zhang, M.; Peyear, T.; Patmanidis, I.; Greathouse, D. V.; Marrink, S. J.; Andersen, O. S.; Ingolfsson, H. I. Fluorinated Alcohols' Effects on Lipid Bilayer Properties. *BioPhys. J.* **2018**, *115*, 679–689.
(50) Tyrrell, J.; Weeks, K. M.; Pielak, G. J. Challenge of Mimicking the Influences of the Cellular Environment on RNA Structure by PEG-Induced Macromolecular Crowding. *Biochem.* **2015**, *54*, 6447–6453.
(51) Deshwal, A.; Maiti, S. Macromolecular Crowding Effect on the Activity of Liposome-Bound Alkaline Phosphatase: A Paradoxical Inhibitory Action. *Langmuir* **2021**, *37*, 7273−7284.
(52) Liu, G.; Li, Y.; Yang, L.; Wei, Y.; Wang, X.; Wang, Z.; Tao, L. Cytotoxicity Study of Polyethylene Glycol Derivatives. *RSC Adv.* **2017**, *7*, 18252–18259.
(53) Lentz, B. R. PEG as a Tool to Gain Insight into Membrane Fusion. *Eur. Biophys. J.* **2007**, *36*, 315–326.

(54) Lentz, B. R.; Lee, J. Poly(Ethylene Glycol) (PEG)-Mediated Fusion between Pure Lipid Bilayers: A Mechanism in Common with Viral Fusion and Secretory Vesicle Release? *Mol. Membr. Biol.* **1999**, *16*, 279–296.
(55) Hoo, C. M.; Starostin, N.; West, P.; Mecartney, M. L. A Comparison of Atomic Force Microscopy (AFM) and Dynamic Light Scattering (DLS) Methods to Characterize Nanoparticle Size Distributions. *J Nanopart Res* **2008**, *10*, 89–96.
(56) Saptari, V. *Fourier-Transform Spectroscopy Instrumentation Engineering*; SPIE Optical Engineering Press.
(57) Heyden, M.; Ebbinghaus, S.; Havenith, M. Terahertz Spectroscopy as a Tool to Study Hydration Dynamics. *Encycl. Anal. Chem.* **2010**. https://doi.org/10.1002/9780470027318.a9162.
(58) Thomson, N. H.; Collin, I.; Davies, M. C.; Palin, K.; Parkins, D.; Roberts, C. J.; Tendler, S. J. B.; Williams, P. M. Atomic Force Microscopy of Cationic Liposomes. *Langmuir* **2000**, *16*, 4813–4818.
(59) Takechi-Haraya, Y.; Goda, Y.; Sakai-Kato, K. Atomic Force Microscopy Study on the Stiffness of Nanosized Liposomes Containing Charged Lipids. *Langmuir* **2018**, *34*, 7805−7812.
(60) Binnig, G.; Quate, C. F.; Gerber, C. Atomic Force Microscope. *Phys. Rev. Lett.* **1986**, *56*, 930–933.
(61) Inkson, B. J. Scanning Electron Microscopy (SEM) and Transmission Electron Microscopy (TEM) for Materials Characterization. In *Materials Characterization Using Nondestructive Evaluation (NDE) Methods*; Woodhead Publishing, 2016; pp 17–43.
(62) Reimschuessel, A. C. Scanning Electron Microscopy-Part I. *J. Chem. Educ.* **1972**, *49*, A413–A419.

Chapter 3

The Inner Hydration in Surfactant/Cholesterol Vesicles Differs from the Outer One: A Spectroscopic Investigation:

Vesicles contain two aqueous regions: *inner core* and *outer-to-bulk*. It has remained an open question whether hydration behaviour in the inner core differs from the outer-to-bulk region, mostly owning to the inability of the conventional spectroscopic techniques to deconvolute the contribution from these two regions. We, using THz-FTIR spectroscopy (1.5-13.5 THz) experimentally probe the *inner* hydration of three differently charged surfactant/cholesterol vesicles composed of SDS, CTAB and Brij 30. Both dynamic light scattering (DLS) and atomic force microscopy (AFM) measurements affirm the transition from micelles to vesicles as cholesterol is added into surfactant solutions. FTIR measurements show that hydration behaviour changes significantly as micelles are converted into vesicles, the change been exclusively caused due to the formation of an *inner core*. Our measurements on the hydrogen bond stretch and librational motion of the *inner hydration* show distinct features compared to the overall hydration, which in turn is found to be surfactant type and cholesterol concentration dependent.

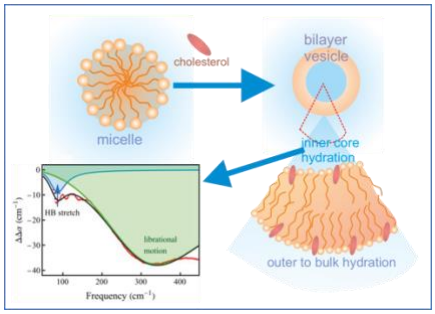

3I. Introduction:

Vesicles are bilayer amphiphile assemblies consisting of three distinct regions separated by two interfaces: "*inner"* and "*outer"* solvent exposed to hydrophilic regions of amphiphiles (*inner* and *outer-to-bulk*) and hydrophobic phase consisting of carbon chains of amphiphiles, respectively.[1,2] Apart from mimicking cell membranes[3] vesicles can offer a large number of applications in industry[4,5] and in pharmacology[6,7] acting as drug carrier agents[8,9] carrying genetic material, enzymes and others molecules into cells,[4,7] in medicine industry[5,10]and also in food industry.[11] Surfactant molecules are often used in preparing vesicles.[12–14] Earlier reports conclude that dialkyldimethylammonium bromide salts with varying chain length can form vesicles above their respective critical micellar concentration (cmc) values when sonicated in aqueous millieu.[15,16] Surfactant-based vesicles have earned much attention in recent times owning to their stability and easy preparation procedure.[12] However, the challenges remain in the fact that not all surfactants can form vesicles by themselves. Surfactants with single carbon

tail, above their *cmc* values, can, however, form vesicles in presence of cholesterol if sufficient external mechanical energy is supplied.[13,17] Cholesterol being a lipid molecule, is insoluble in water and hence only resides at the hydrophobic region of the thus formed vesicles.[18] Non-ionic surfactants (e.g. Tween 20, Span 30, Brij 30 etc.) can form vesicles, usually termed as *niosomes*,[19,20] depending upon their hydrophilic-lipophilic balance (HLB).[21,22] Previous studies suggest that surfactants with HLB value in the range of 14-17 are not suitable to prepare niosomes with, while those with the value of ~ 8.6 do form niosomes with high entrapment efficiency.[19,21] Certain other non-ionic surfactants with HLB > 6, produce niosomes only when combined with cholesterol.[23] Better stability and longer shelf life make niosomes efficient drug-delivery agents over liposomes.[24] As niosomes do not essentially carry any charge, they are less toxic, more compatible in nature and offer wide application in anti-cancer research.[25,26] In-spite of considerable efforts on studying the structure, stability and applications of vesicles, relatively less attention has been paid to investigate their hydration behaviour.[27] Dey et al.[28] have used femtosecond (fs) up-conversion spectroscopy to observe the solvation behaviour of vesicles composed of dodecyl-trimethyl-ammonium bromide (DTAB) and sodium dodecyl sulfate (SDS) surfactants and reported two different time scales: the slower time scale was attributed to the confined water inside the micelles/vesicles, whereas the ultrafast time scale (<0.3 ps) was associated with the water at the exposed/surface region of the micelles/vesicles. In a later study Mandal et al.,[29] using time resolved fluorescence study, have reported that both solvation and rotational relaxation time of coumarin 153 (C153) gradually increases with cholesterol content in 1-hexadecyl3-methylimidazolium chloride ([C_{16min}]Cl)/cholesterol and benzyldimethylhexadecylammonium chloride (BHDC)/cholesterol vesicles, implying a change in the water behaviour around C153 during micelle to vesicle transformation. Ghosh et al.[13] have carried out time-resolved fluorescence anisotropy, and fluorescence correlation spectroscopy measurements of SDS/cholesterol and CTAB/cholesterol vesicles and they concluded that hydrophobicity of vesicle bilayer increases as micelles are converted into vesicles. In-spite of these experimental efforts, understanding of the solvation behaviour during micelle to vesicle transformation and its alteration in presence of cholesterol still remains elusive. Additionally, it is also not evident whether the physical properties of water molecules in the *inner core* region and those in the *outer-to-bulk* region offer similar physical properties, and if not, up to what extent they differ from that of the bulk water. Also, it is interesting to investigate how these properties vary with surfactant charge type and cholesterol content. Such information could be of interest for specific solubilization and/or subsequent release of drugs/ligands in/from the inner core of vesicles when used as carriers. Conventional

spectroscopic techniques are not very useful to explicitly probe the inner hydration as they are mostly external probe dependent and such probes are solubilized in both the water region, and it remains difficult to deconvolute the subtle difference in their behaviour in these two regions. This makes the question remained unanswered. A plausible solution could be obtained using THz spectroscopy measurements which has emerged as a powerful technique to detect the collective hydrogen bond dynamics of water[30–32] in the solvation layer of bio-molecules[33–35] lipids[36,37] and others complex molecules.[38,39] The unique advantage of this technique lies on the fact that it is a label free tool as it directly probes the fluctuations of collective dipole moments of water; such fluctuations correlate in the form of strong absorbance of water in the THz frequency window.[31] Thus, any solute-induced change in the absorption coefficient of a solution manifests changes in the associated solvation of the solute (herein vesicles). We investigate the solvation nature of three differently charged vesicles using Fourier transform infrared (FTIR) spectroscopy in the terahertz (THz) frequency region (50-450 cm^{-1}, 1.5-13.5 THz). We prepare and characterize surfactant-based (CTAB, SDS and Brij-30) vesicles containing cholesterol molecules of varying concentrations; we define a parameter Λ ($= \frac{[\text{Cholesterol}]}{[\text{Surfactant}]}$) accordingly. We use dynamic light scattering (DLS) and atomic force microscopy (AFM) measurements to estimate the dimensions of the vesicles. We estimate the surface charge density of the charged vesicles using zeta potential measurements and verify how the introduction of cholesterol molecules perturb the charge distribution. We measure the change in solvation around the vesicles using THz-FTIR spectroscopy. We identify that solvation is noticeably altered as micelles are transformed into vesicles. Moreover, our study unambiguously addresses the concern to conclude that hydration at the *"inner core"* of the vesicles remarkably differs from that of the *"outer to bulk"* hydration, the difference being dependent on the surfactant charge type.

3II. Materials and Methods:

Sodium dodecyl sulfate (SDS), hexadecyltrimethylammonium bromide (CTAB), polyoxyethylene 4 laurylether (Brij 30), Cholesterol (3β-Hydroxy-5-cholestene,5-Cholesten-3β-ol) and chloroform were purchased from Sigma Aldrich with the highest available purity and were used without any further purification. Details of all the chemicals are described in sec 2II.c.ii. All the vesicles were prepared in aqueous medium using ultrapure milli Q water which is described in 2II.a.i. The details of all the used instruments are described in 2.III.

3III. Results and Discussions:

Structure of Vesicles: DLS measurements were carried out to measure the hydrodynamic diameter (d_H) of the vesicles. DLS profiles of SDS micelles (Λ=0.0) and cholesterol containing vesicles at different Λ values are shown in figure 3Aa. Similar profiles for CTAB micelles and vesicles are shown in figure 3Ab. DLS profiles indicate that the hydrodynamic diameter (d_H) of SDS and CTAB micelles at 20 mM concentration are ~2.8 and ~1 nm respectively.[40,41] Upon the addition of cholesterol to both the micelles, larger aggregates start forming. It was previously reported that at low cholesterol concentrations micelles, mixed micelles and vesicles co-exist.[13,42] However, with the increase in cholesterol concentration micelles and mixed micelles start disappearing and only vesicles predominate. At low cholesterol content (Λ=0.1), d_H of SDS-vesicle becomes as high as ~91 nm and it only increases to 106 nm at Λ=1.0;[13] similarly diameter of CTAB vesicles (Λ=0.1) is ~80 nm and it increases up to ~164 nm at Λ=1.0 (figure 3Ad).[13,42] DLS profiles of Brij 30/cholesterol niosomes are shown in figure 3Ac. We observe the coexistence of two types of particles with diameters ~ 78 and ~ 396 nm (figure 3Ad) for 10 mM Brij 30 aqueous solutions (Λ=0.0). Ghosh et al. has previously reported the formation of cholesterol mediated Tx-100 vesicles with two size distributions of ~150 and ~ 1300 nm.[43] As cholesterol is added to the Brij-30/water system, we observe a non-linear increase in the d_H (figure 3Ad). The particle size does not change appreciably up to Λ=0.2; as Λ increases to 0.25 the d_H shows a noticeable increase to 255 and 955 nm, respectively and remains unaltered up to Λ=0.4. Interestingly, beyond this mole fraction, we obtain the signature of the larger particles (~ 1 μm) only, the diameter of which increases regularly with increasing Λ (figure 3Ac and 3Ad).

AFM measurements: AFM images of two charged vesicular systems are shown in figure 3A(e-f). AFM images clearly identify the appearance of spherical particles with average diameter ~ 72 ±14 nm for SDS (figure 3Ae) and ~ 76± 24 nm for CTAB vesicles (figure 3Af) at Λ=0.5. For Brij 30 solutions we observe the signature of spherical particles with an average diameter of 160±8 nm (figure $3Ag_1$). The diameter of the particles does not change appreciably (average diameter: 146±20 nm) when small amount of cholesterol is added (Λ=0.2) (figure $3Ag_2$). At higher cholesterol concentration (Λ=0.5) the size increases to 430±70 nm (figure $3Ag_3$) along with a noticeable increase in the height of the particles compared to that at low cholesterol concentration suggesting the formation of larger aggregates at higher Λ, as also has been evidenced from the DLS measurements.

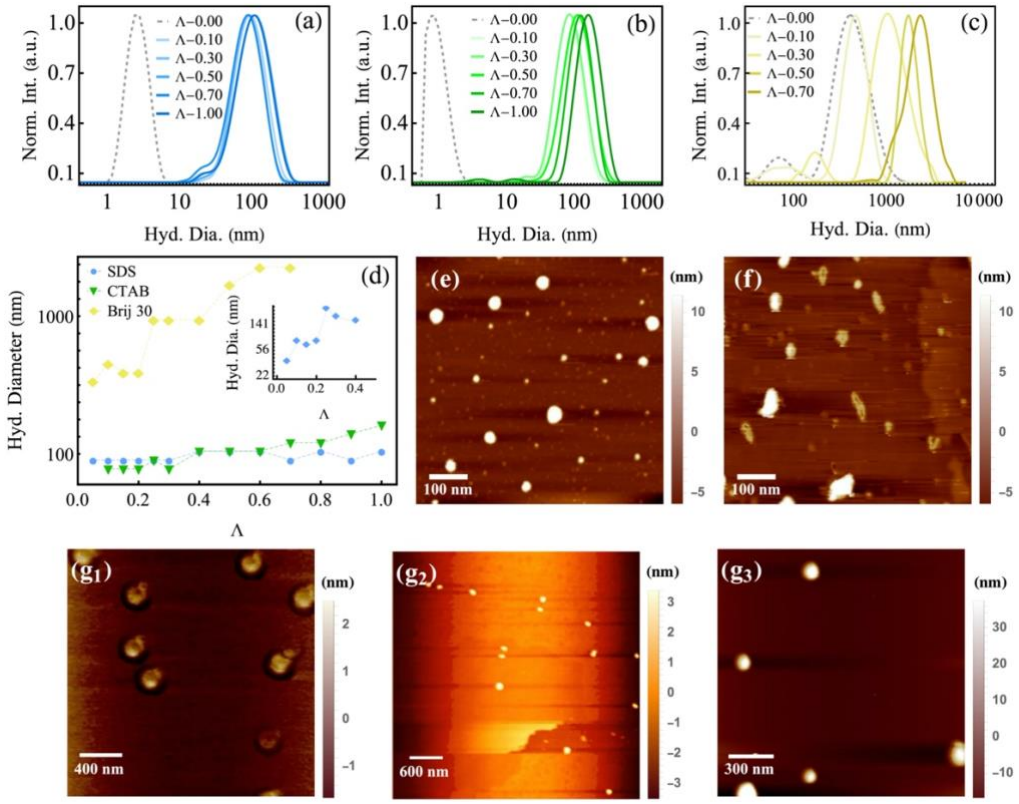

Figure 3A. Representative dynamic light scattering profile of (a) SDS (b) CTAB and (c) Brij 30 vesicles (in presence of cholesterol) at different Λ. The concentration of SDS and Brij 30 is kept at 20 and 10 mM, respectively. The grey broken lines represent surfactant solutions in absence of any cholesterol. (d) Hydrodynamic diameter of three different vesicular systems as a function of Λ; the inset shows hydrodynamic diameter of the smaller particles of Brij 30 solutions. (e-f) AFM images of (d) SDS, (e) CTAB Λ=0.5. (g_1-g_3) AFM images of Brij 30 vesicles at Λ=0.0, 0.2 and 0.5 respectively.

Charge at the surface of Vesicles: We perform zeta potential measurements to determine the charge at the vesicle surfaces (figure 3B and Table 3a). Zeta potential value for SDS micellar system is estimated to be -47.9±5.9 mV.[13,44] For vesicles with Λ=0.1 it increases to -79.1±3.9 mV (Table 3a). Upon further addition of cholesterol, it decreases mildly and at Λ=1.0 the value becomes -61.5 ± 1.7 mV (figure 3Ba and Table 3a). For CTAB micelles, zeta potential value is +48.7±6.9 mV;[13] as small amount of cholesterol is added (Λ=0.1) and vesicles are formed, it increases to +66.5±2.7 mV. The value reaches a maximum at Λ=0.2, and beyond that it increases mildly (figure 3Ba and Table 3a). These results corroborate well with the results obtained by Ghosh et al. for similar systems.[13] While Zeta potential quantifies the charge at the diffuse layer or the slip plane of micelles/vesicles, which monitors the stability of colloidal system, one also needs to calculate the surface charge density as it gives a clearer insight about

the charge distribution of micelles/vesicles at the surface. In self assembled systems (such as micelles, vesicles) counter-ions are strongly bound to the surfactant head-groups and therefore, the Stern layer thickness could be assumed to be the size of the hydrated counter-ions.[45] We assume the Stern layer thickness of SDS and CTAB to be as 5Å and 3Å, respectively as those of the sizes of hydrated Na^+ and Br^- counterions.[46,47] We calculate the surface charge density of vesicles form the Zeta potential data following a Goey Chapman model (in section 2.A.a). Surface charge density of vesicles are found to be higher than that of the micelles (figure 3Bb and table 3a). Cholesterol being a neutral molecule, carries no net charge. Addition of cholesterol into the micelles minimizes the electrostatic repulsion between the head group of surfactants inducing more surfactant molecules to be densely packed at the interface. As a result the surface charge density increases significantly compared to that of the micelles.[13] However, it suffers nominal change with the increase of cholesterol concentration in both the vesicles.

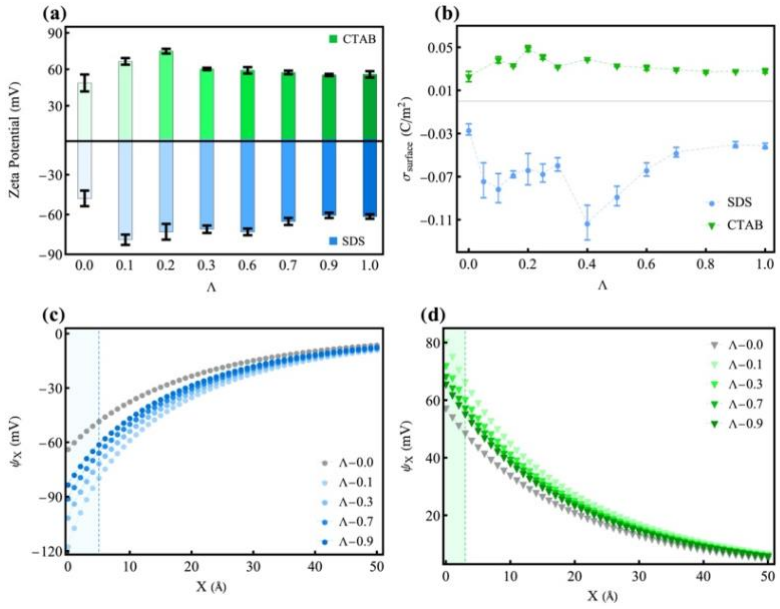

Figure 3B. (a) Zeta potential of CTAB (upper panel) and SDS (lower panel) vesicles as a function of Λ. (b) Surface charge density as a function of Λ for CTAB and SDS vesicles. (c-d) Electrostatic potential profile as a function of distance from the surface to bulk for (c) SDS and (d) CTAB vesicle solutions. The shaded region of each figure represents the corresponding stern layers.

Hydration at the surface of vesicles: We now focus on the hydration behaviour of the vesicles as estimated from the frequency dependent absorption coefficient α(ν) in the THz frequency window. The α(ν) profile for pure water can be deconvoluted (figure 3Cb) into two intense

peaks: one at ~ 130 cm^{-1} emanating from the hindered translational motion of water network (hydrogen bond stretching vibration) and another one at ~ 495 cm^{-1}, associated with the hindered rotational motion of water molecules (librational motion) (figure 3Cb).[48] We measure FTIR in the ATR (attenuated total reflection) mode, thus a decrease in the peak frequency (red shift) compared to the conventional transmission mode is observed.[49,50] This spectral feature of pure water undergoes substantial modification in micelles and in vesicle interfaces. Some representative α(ν) profiles of pure water, SDS micelles and SDS vesicle (Λ=0.5) are depicted in figure 3Ca. It is important to note here that both surfactant(s) and cholesterol do not show any noticeable absorption behaviour in this frequency window, and therefore, any change observed in the α(ν) profile is due solely to the modification in the associated solvation behaviour.

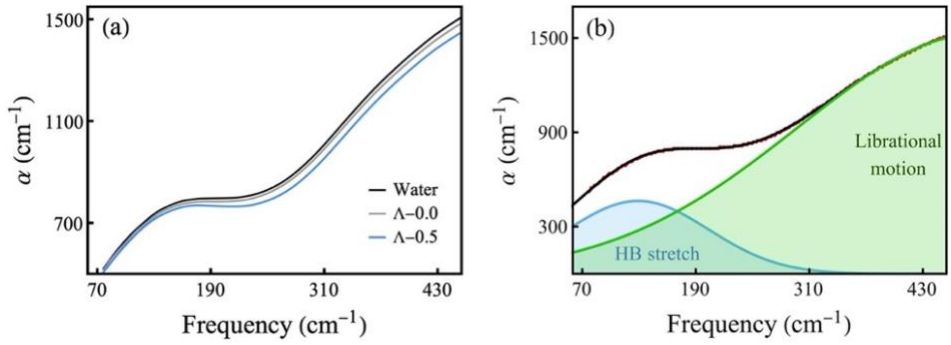

Figure 3C. (a) Frequency dependent absorption coefficient of pure water (black), SDS micelle (Λ=0.0, grey) and SDS/cholesterol vesicles (Λ=0.5, blue). (b) Deconvoluted (using gaussian equation) α(ν) profile of pure water.

We observe that micelles and vesicles offer decreased α(ν) profiles compared to pure water; such suppression in α(ν) with the addition of small molecules in water has been reported previously.[51–53] In order to obtain explicit information on micellar solvation, we calculate the difference, $\Delta\alpha(\nu)$ $(= \alpha_{\text{solution}}(\nu) - \alpha_{\text{water}}(\nu))$. $\Delta\alpha(\nu)$ profile of SDS micelles and of SDS/cholesterol vesicles at different Λ values are depicted in figure 3Da. Similar profiles for CTAB/cholesterol and Brij 30/cholesterol vesicles are shown in figure 3Ea and 3Eb, respectively. In order to identify the various vibrational modes of water in the solvation shell, we fit the $\Delta\alpha(\nu)$ profiles using a damped harmonic oscillator model:[54,55]

$$\Delta\alpha(\nu) = \sum_{i=1}^{2} \frac{a_i \omega_i \nu^2}{\nu^2 \omega_i^2 + \pi^2 \left(\nu_i^2 + \frac{\omega_i^2}{4\pi^2} - \nu^2 \right)^2} \qquad (3.1)$$

where a_i, ω_i, ν_i are the amplitude, width and the centre frequency of the i^{th} resonance. The unperturbed centre frequency is given as

$$\nu_{0,i} = \sqrt{\nu_i^2 + \frac{\omega_i^2}{4\pi^2}}$$

A representative fit of SDS micellar system is shown in figure 3Db in which we obtain two peaks, one at $\nu_1 \sim 160$ cm^{-1} and another at $\nu_2 \sim 452$ cm^{-1}. The observed blue shift in the H-bond stretch (table 3b) manifests the formation of higher number of and/or stronger H-bond,[56,57] while the red shift in the librational mode indicates a less hindered rotation of water molecules[49] at micellar interface compared to that in bulk water. We then investigate how interfacial solvation changes as micelles are converted into vesicles. We fit the $\Delta\alpha(\nu)$ curves for the vesicular systems and plot the peak frequencies ν_1 and ν_2 as a function of Λ (figure 3Dc and table 3b).

Note that $\Delta\alpha(\nu)$ provides information on the total hydration of micelles and vesicles (see equation 3.3 and 3.5) and does not differentiate between the *outer-to-bulk* and *inner* hydration. We, therefore, discuss these parameters in the ambit of *overall hydration*. In SDS micelles, ν_1^{SDS} appears at ~160 cm^{-1} while in vesicles, at low cholesterol content (Λ=0.1), it suffers a distinct ~62 cm^{-1} red shift. With further addition of cholesterol, $\nu_1^{SDS}(\Lambda)$ does not change appreciably (figure 3Dc and table 3b). For CTAB vesicles we observe a somewhat non-monotonous Λ dependent behaviour. In micelles, $\nu_1^{CTAB}(\Lambda=0.0)$ appears at ~136 cm^{-1}; with the addition of cholesterol $\nu_1^{CTAB}(\Lambda)$ shows an initial blue shift of ~12 cm^{-1} beyond which the frequency starts to decrease up to Λ_{CTAB} =0.6 and at Λ_{CTAB}> 0.7 it changes only subtly (figure 3Dc). In Brij 30 solution (Λ=0.0) $\nu_1^{Brij\ 30}$ appears at ~158 cm^{-1}, which decreases marginally up to Λ = 0.25, beyond which it decreases regularly with Λ, an eventual red shift of ~58 cm^{-1} is observed at high cholesterol content (Λ =0.7). We also observe changes in the peak frequency ν_2 during the micelle to vesicle structural transition (figure 3Dc, lower panel). ν_2 decreases more-or-less regularly with the increase in Λ for all the surfactant systems. A better interpretation of hydration modification could be obtained by comparing the absorption coefficient (α) values at the corresponding peak frequencies. It could be emphasized here that

α(ν) roughly corresponds to the population of water molecules collectively vibrating at that particular frequency.

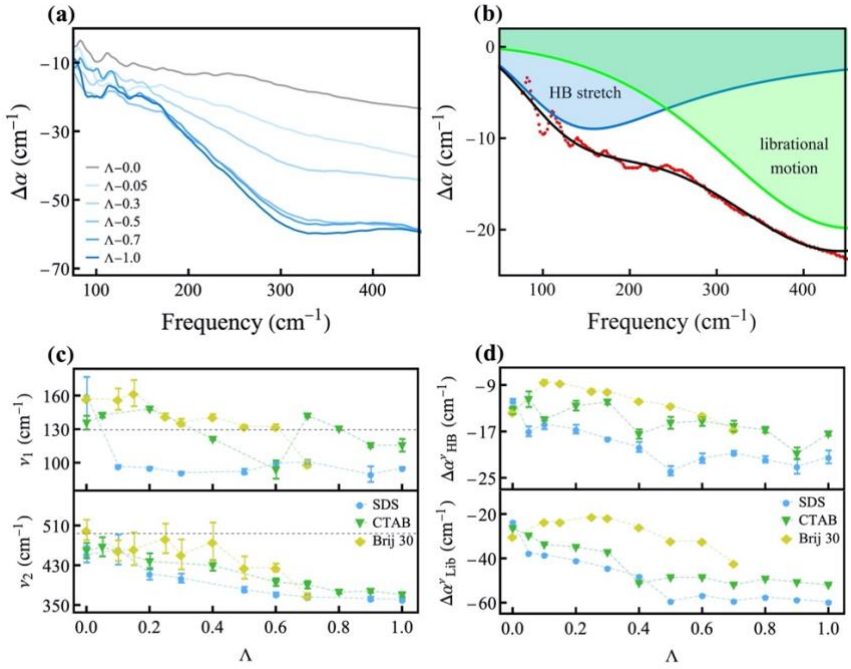

Figure 3D. (a) Representative change in absorption coefficient, $\Delta\alpha(\nu)$ (=α_{sample}- α_{water}) for SDS vesicles at different Λ. (b) Representative fitting of $\Delta\alpha(\nu)$ for SDS micelles (Λ = 0.0) using a damped harmonic oscillator model (equation 3.1). The red broken curve represents the raw data and the black solid line stands for the overall fitting. The 1st peak with frequency ν_1 (blue line) represents the hydrogen bond stretching of water molecules, the 2nd peak with frequency ν_2 (green line) represents the librational motion of water molecules. (c) Peak frequency (HB stretch and librational mode) of three vesicular systems as a function of Λ. The broken lines are guide to the eyes. The black dotted lines indicate the corresponding frequencies in bulk water. (d) $\Delta\alpha$, measured at peak frequency, as a function of Λ for HB stretching (upper panel) and librational mode (lower panel) of water. The dotted lines are guide to the eyes.

As pure water exhibits peaks at 130 and 495 cm^{-1} we plot the Δα values obtained at these two frequencies in the vesicles (figure 3Fa). As expected, all the Δα values are negative exhibiting a *THz deficit*[36,37], which correlates the decrease in α as water is replaced with low absorbing surfactants, where ϕ stands for the corresponding volume fraction(s). $\alpha_{micelle}$ is very small and could be neglected and $\Delta\alpha(\nu)$ is expressed as:

$$\Delta\alpha_{micelle}(\nu) = (\phi_{bulk} - 1)\alpha_{bulk}(\nu) + \phi_{hyd}^{micelle}\alpha_{hyd}^{micelle}(\nu) \qquad (3.3)$$

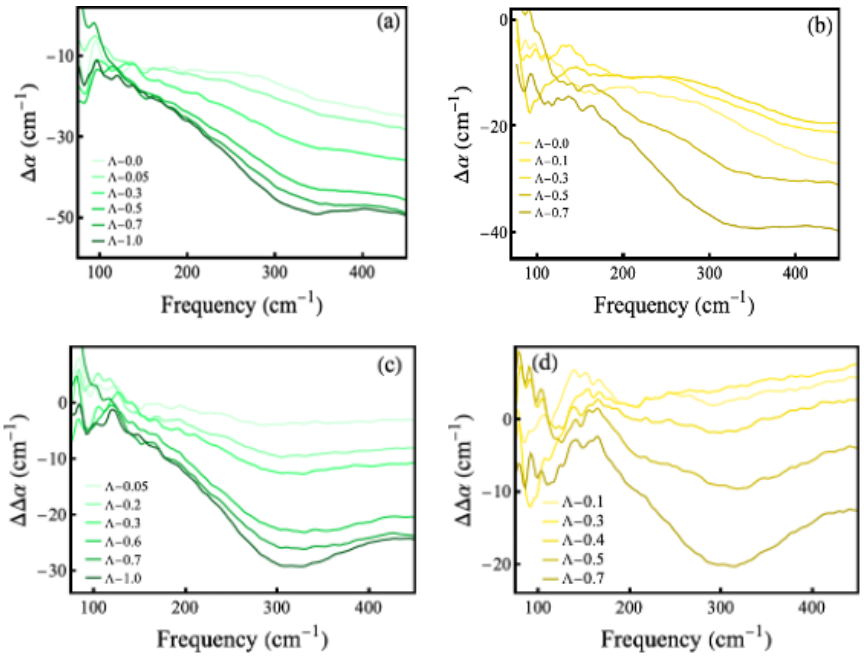

Figure 3E. Change in α as defined by Δα (=$\alpha_{micelle/vesicle}$- α_{water}) as a function of frequency for (a) CTAB and (b) Brij 30 vesicles at different Λ. Change in Δα (defined by, ΔΔα (=$\Delta\alpha_{vesicle}$- $\Delta\alpha_{micelle}$)) as a function of frequency of (a) CTAB and (b) Brij 30 vesicles.

It is evident from this equation that the value of $\phi_{hyd}^{micelle}\alpha_{hyd}^{micelle}(\nu)$ determines the sign and magnitude of $\Delta\alpha(\nu)$. Interesting to note here that further alteration in hydration is observed as vesicles are formed. To compare the hydration, we therefore plot the $\Delta\alpha_{micelle\rightarrow vesicle}$ values obtained at the HB and Lib frequencies of the corresponding micelles (figure 3Dd). We notice some interesting features in the parameter. For the ionic surfactants, THz absorbance decreases for both the vibrational modes as vesicles are formed, the effect being more prominent in SDS, especially in the low cholesterol content region. In Brij 30 systems, however, we observe a contrasting trend in which Δα shows an initial increase followed by a marginal decrease beyond Λ=0.4. Note that the thus obtained $\Delta\alpha_{micelle\rightarrow vesicle}$ values correspond to the change in hydration either due to the formation of a new interface and/or introduction of cholesterol molecules into the interface:

$$\alpha_{vesicle}^{total}(\nu) = \phi'_{bulk}\alpha_{bulk}(\nu) + \phi_{bilayer}\alpha_{bilayer}(\nu) + \phi_{hyd}^{out}\alpha_{hyd}^{out}(\nu) + \phi_{hyd}^{inner}\alpha_{hyd}^{inner}(\nu) \quad (3.4)$$

[also note that $\phi_{bulk} \neq \phi'_{bulk}$]. Since the bilayer is composed of surfactant and cholesterol molecules, $\alpha_{bilayer}(\nu)$ could be neglected owing to their very small values. It can be noted that two additional terms, which contain the absorption coefficients α_{hyd}^{out} and α_{hyd}^{inner} have been incorporated in equation (3.4). We can make another approximation here that the α_{hyd}^{out} term is more or less equivalent to $\alpha_{hyd}^{micelle}$. The difference in the α_{total} therefore mostly emanates from the term $\phi_{hyd}^{inner}\alpha_{hyd}^{inner}(\nu)$, which manifests the newly formed inner hydration core in the vesicles. If α_{hyd}^{inner} differs from α_{hyd}^{out}, the $\alpha_{vesicle}^{total}(\nu)$ value should be different from $\alpha_{micelle}^{total}(\nu)$. The $\Delta\alpha_{vesicle}$ can be expressed as:

$$\Delta\alpha_{vesicle} = (1 - \phi'_{bulk})\alpha_{bulk}(\nu) + \phi_{hyd}^{out}\alpha_{hyd}^{out}(\nu) + \phi_{hyd}^{inner}\alpha_{hyd}^{inner}(\nu) \qquad (3.5)$$

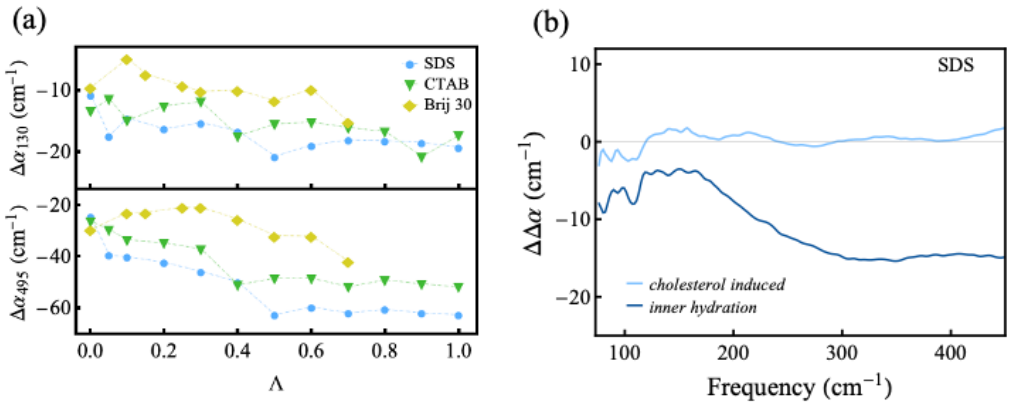

Figure 3F. (a) $\Delta\alpha$, measured at the peak frequency, as a function of Λ for hydrogen bond stretch (upper panel) and librational motion of water (lower panel). $\Delta\alpha_{130}$ and $\Delta\alpha_{495}$ signify the difference in absorption coefficient measured at 130 cm^{-1} and 495 cm^{-1} respectively. The broken lines are guide to the eyes. (b) ΔΔα(ν) profiles for SDS-cholesterol vesicles (inner hydration, dark blue) and Δα(ν) profile for SDS-cholesterol micellar system (sky blue).

Considering that micelles possess only a single surfactant/water interface, if we subtract $\alpha_{micelle}^{total}(\nu)$ from $\alpha_{vesicle}^{total}(\nu)$, we would obtain exclusive information on the *"inner-hydration"*, which otherwise is not an easily obtainable parameter. We measure $\Delta\Delta\alpha(\nu) = \Delta\alpha_{vesicle}(\nu) - \Delta\alpha_{micelle}(\nu)$ profiles for the three vesicle systems; representative profiles of ΔΔα(ν) at different Λ values for SDS/cholesterol vesicles are depicted in figure 3Ga. This can be expressed in terms of (from equations 3.2-3.5):

$$\Delta\Delta\alpha(\nu) = \left(\phi'_{bulk} - \phi_{bulk}\right)\alpha_{bulk}(\nu) + \phi_{hyd}^{out}\alpha_{hyd}^{out}(\nu) + \phi_{hyd}^{inner}\alpha_{hyd}^{inner}(\nu) - \phi_{hyd}^{micelle}\alpha_{hyd}^{micelle}(\nu)$$

$$\approx \left(\phi'_{bulk} - \phi_{bulk}\right)\alpha_{bulk}(\nu) + (\phi_{hyd}^{out} - \phi_{hyd}^{micelle})\alpha_{hyd}^{micelle}(\nu) + \phi_{hyd}^{inner}\alpha_{hyd}^{inner}(\nu) \qquad (3.6)$$

with the approximation that $\alpha_{bilayer} \sim \alpha_{micelle} \sim 0$ and $\alpha_{hyd}^{micelle} \sim \alpha_{hyd}^{out}$ (vide infra). It is now important to verify whether the thus obtained *"inner-hydration"* actually originates from the inner water/vesicle interface or the change is associated with cholesterol induced solvation or both. To verify this, we prepare an SDS micellar solution at a concentration just above its *cmc* (to ensure that no vesicles are formed) and into that solution we added cholesterol (Λ=0.1). This ensures that the thus formed mixed interface approximately mimics the outer surface of the vesicles; accordingly, the calculated $\Delta\alpha(\nu)$ profiles would reflect the modification of the SDS interface as a result of the inclusion of cholesterol at the SDS/water interface. We observe that $\Delta\alpha(\nu)$ changes only marginally (figure 3Fb), which unambiguously confirms that the observed change in $\Delta\Delta\alpha(\nu)$ (figure 3Ga) explicitly manifests the effect of the inner solvation, which eventually is governed by the term $\phi_{hyd}^{inner}\alpha_{hyd}^{inner}(\nu)$ (equation 3.6). $\Delta\Delta\alpha(\nu)$ profiles at different Λ values for CTAB/cholesterol and Brij 30/cholesterol vesicles are depicted in figure 3Ec and 3Ed, respectively. Note that any *non-zero* value of $\Delta\Delta\alpha(\nu)$ would indicate that α_{hyd}^{inner} differs from α_{hyd}^{out}. We indeed observe non-zero $\Delta\Delta\alpha(\nu)$ profiles for all the three vesicles (figure 3Ga) manifesting altered hydration of the inner core. To obtain a quantitative insight into the modified inner solvation shell we fit the $\Delta\Delta\alpha(\nu)$ profiles for all the systems using a damped harmonic oscillation model

$$\Delta\Delta\alpha(\nu') = \sum_{i=1}^{2} \frac{a'_i \omega'_i \nu'^2}{\nu'^2\omega'^2_i + \pi^2\left(\nu'^2_i + \frac{\omega'^2_i}{4\pi^2} - \nu'^2\right)^2} \qquad (3.7)$$

We use the primed symbols to denote values corresponding to the *inner hydration*. A representative fitting of $\Delta\Delta\alpha(\nu')$ profile for SDS vesicles (Λ=0.5) is shown in figure 3Gb. In SDS, two peaks are obtained, ν'^{SDS}_{HB} and ν'^{SDS}_{Lib} appearing at ~113 and ~360 cm^{-1}, respectively. Appearance of these peaks unambiguously suggests that the solvation layer in the inner core has finite difference than the outer interface, the effect seems to be more pronounced in the librational bands. We fit all the $\Delta\Delta\alpha(\nu)$ profiles and the results are depicted in figure 3Gc and table 3c. We observe that the inner core solvation nature varies with the surfactant type. For SDS, the change is significant at low cholesterol contents. For CTAB vesicles, interestingly,

we do not recover any signature of the H-bond stretch mode and the $\Delta\Delta\alpha(\nu)$ profiles are fitted with a single librational mode, $\nu_{Lib}^{\prime CTAB}$.

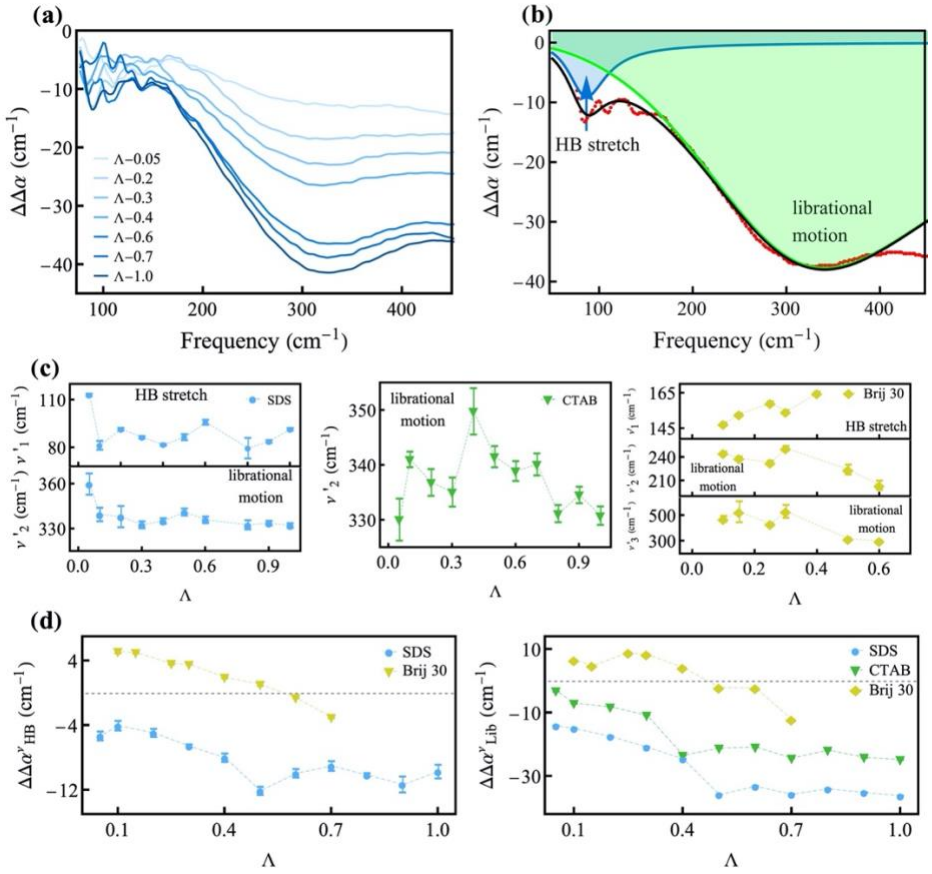

Figure 3G. (a) Representative figure showing change in $\Delta\alpha$ defined as $\Delta\Delta\alpha$ (=$\Delta\alpha_{vesicle}$- $\Delta\alpha_{micelle}$) as a function of frequency for SDS vesicles at different Λ. (b) Representative fitting of $\Delta\Delta\alpha$ for SDS Vesicle (Λ = 0.5) using a modified damped harmonic oscillator model (equation 3.7). The red curve represents the raw data and the black solid line shows the overall fitting. The 1st peak with frequency ν'_1 (blue line) represents the HB stretching while the 2nd peak with frequency ν'_2 (green line) presents the librational motion of water. (c) Peak frequencies of SDS, CTAB and Brij 30 vesicular systems as a function of Λ. The broken lines are guide to the eyes. (d) $\Delta\Delta\alpha$ (measured at the peak frequencies) as a function of Λ for different vesicles.

We observe a bell-shaped $\nu_{Lib}^{\prime CTAB}(\Lambda)$ profile with the maximum appearing at Λ_{CTAB}=0.4. For niosomes we observe interesting features; the $\Delta\Delta\alpha(\nu)$ values are found to be positive up to Λ=0.3. Moreover, for the best fit for the $\Delta\Delta\alpha(\nu)$ profiles (up to $\Lambda_{Brij\text{-}30}$=0.4) we need to consider

three bands[58] (table 3c). $\nu_{HB}^{'Brij\ 30}(\Lambda)$ increases with Λ (up to 0.4) regularly (figure 3Gc, right panel) indicating stronger and/or a higher number of H-bond in the *"inner-hydration"* water network. The librational bands do not change appreciably up to Λ=0.4, beyond which it decreases regularly (figure 3Gc). For a better understanding of how the formation of a new interface (during micelle to vesicle transition) influences hydration structure, we plot the peak frequencies of the *"overall"* (filled symbols) and *"inner"* (hollow symbols) hydration in figure 3H(a-c). We observe some distinct salient features of the *inner hydration*. In SDS vesicles (figure 3Ha): the $\Delta\Delta\alpha(\nu)$ profiles could be fitted with both H-bond vibration (ν_{HB}) and libration (ν_{Lib}) modes. ν_{HB} does not change noticeably, however, the libration band shows a distinct red shift (lower energy). Lowering of ν_{Lib} mode manifests that a significant reduction in the restricted rotation of water molecules within its tetrahedral network as the *inner core* develops, which leads to a-priori conclusion that the *inner core hydration* is more labile compared to the *outer* interface. We also check the change in THz absorption coefficient $\Delta\alpha_{HB}^{\nu}$ and $\Delta\alpha_{Lib}^{\nu}$ (for *overall hydration*) and $\Delta\Delta\alpha_{HB}^{\nu}$ and $\Delta\Delta\alpha_{HB}^{\nu}$ (for the *inner hydration*) at the peak frequency (figure 3Hd). The figure unambiguously points to the fact that the *inner hydration* suffers lesser *THz loss* compared to the *overall* hydration. Keeping in mind the fact that the total volume of the vesicles is very small (less than 5% of the total volume), the effect of volume fraction on the absorption coefficient could be neglected (equation 3.5 and 3.6). The difference in the values of Δα and ΔΔα therefore mostly emanates from the corresponding values of α_{hyd}^{inner}, which differs substantially from α_{hyd}^{out}. This observation, coupled with the fact that ν_{Lib} suffers a red shift, shows that the water molecules are less strongly bound to the *inner interface* compared to the overall hydration in SDS/cholesterol vesicles. Interestingly, this difference remains more or less independent of the cholesterol concentration. The *inner hydration* in CTAB vesicles does not offer any particular H-bond vibration mode; since ΔΔα is a difference spectrum, this could either be due to the fact that the mode is completely identical in *inner* and *outer* hydration, or the mode is sufficiently red shifted irrecoverable in the present frequency range. The libration band is, however, pronouncedly red shifted for the *inner hydration* (figure 3Hb). Weakening of the H-bond interaction is also supported from the fact the THz loss is less in the inner hydration (figure 3He). $\nu_{Lib}^{overall}$ shows a marked red shift (460 to 372 cm^{-1}) with increasing Λ, similar to that observed in SDS, however, ν_{Lib}^{inner} does not offer any such Λ dependency manifesting that hindered rotation of water molecules inside the CTAB vesicles does not depend on the addition of cholesterol. Interestingly, in Brij-30, the behaviour of the *inner hydration* is contrasting (figure 3Hc,f) than the charged vesicles. In addition to the usual

HB stretch and libration bands, an additional band appears in the frequency window of 200-250 cm^{-1}, the origin of which is not very clear. Appearance of such an intermediate band is often found in case of metal ions owing to the rattling motion.[30,59]

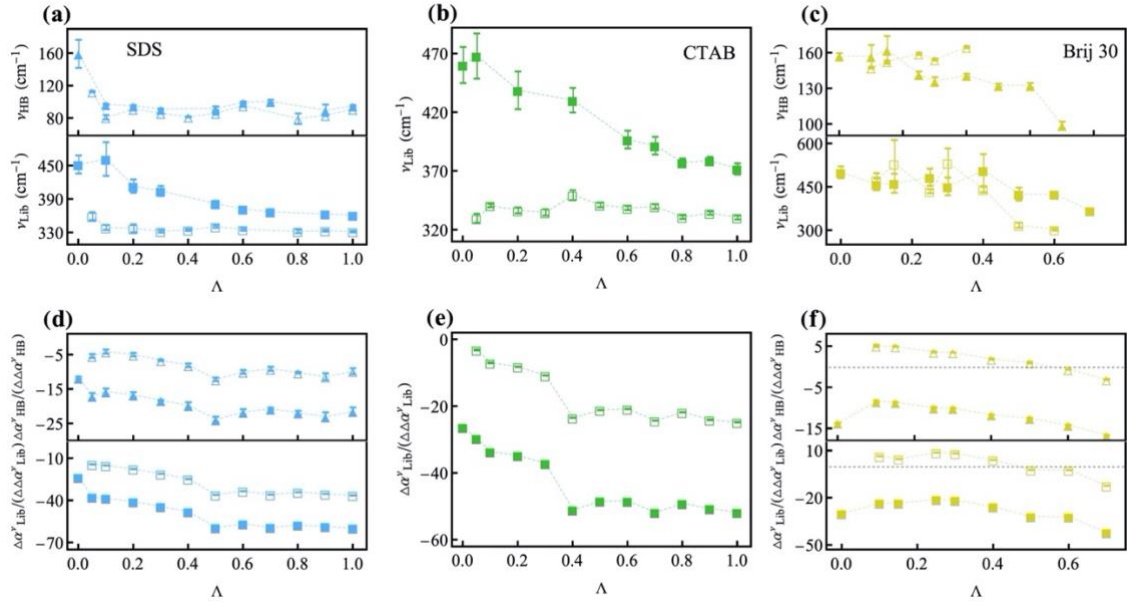

Figure 3H. Comparison of *overall* (solid symbols) and *inner* (hollow symbols) hydration of HB-stretch and librational mode for (a) SDS, (b) CTAB and (c) Brij 30 vesicles. $\Delta\alpha$ *or* $\Delta\Delta\alpha$ as a function of Λ for hydrogen bond stretch and librational motion of (d) SDS, (e) CTAB and (f) Brij 30 vesicles respectively. Units of $\Delta\alpha\ and/or\ \Delta\Delta\alpha$ are expressed in cm^{-1}.

Noticeably, the HB stretching and libration frequencies in the *inner hydration* are in tune with those in the *overall hydration*. The corresponding absorption co-efficient(s), however, show very unique features. In the low Λ values, we intriguingly observe a *THz excess* in the *inner hydration* as ΔΔα offers positive values for both the bands (figure 3Hf, hollow symbols). Note that $\Delta\alpha^{\nu}$ (which is a difference value with respect to that of bulk water) is always negative for all the systems (figure 3Hf, filled symbols), which, according to equation 3.3 and 3.5, reveals that the positive contribution from the $\phi_{hyd}^{micelle}\alpha_{hyd}^{micelle}(\nu)$ or $(\phi_{hyd}^{out}\alpha_{hyd}^{out}(\nu) + \phi_{hyd}^{inner}\alpha_{hyd}^{inner}(\nu))$ term(s) does not overwhelm the negative contribution emanating from the water replacement term, $(\phi_{bulk} - 1)\alpha_{bulk}(\nu)$. $\Delta\Delta\alpha^{\nu}$, on the other hand, is a difference of difference terms (equation 3.6). A negative value of this parameter, as observed in SDS and CTAB vesicles (hollow symbols, figures 3Hd, e), ascertains that the *inner hydration* contribution does not supress the THz loss arising from the first two terms. On the other hand,

positive values of $\Delta\Delta\alpha^{\nu}$ for Brij system (up to Λ=0.4) emphasizes an overwhelming positive contribution from the $\phi_{hyd}^{inner}\alpha_{hyd}^{inner}(\nu)$ term.

Overall Comprehension: ***In summary,*** as micelles are converted into vesicles, a new core of *inner hydration* develops. We have aimed to investigate how this inner hydration differs from the outer hydration. THz measurements lead us to deconvolute the *overall hydration* and investigate this *inner hydration* explicitly (equation 3.6). Such explicit identification of the difference in the hydration behavior of the two different regions has not been reported earlier. Our study unambiguously concludes that the *inner hydration* does differ markedly from the *overall hydration*, and the extent of such difference is surfactant charge dependent. In SDS and CTAB micelles the inner hydration offers a more labile binding with the interface than that in the outer surface. In non-ionic Brij-30 vesicles it offers strikingly different behaviour and shows stronger hydrogen binding of water with the inner surface. Our findings on the *inner hydration* of vesicles could contribute in fundamental as well as applied research toward developing vesicles as a delivery agent. While the results are immensely striking, a molecular level understanding on the origin of such differences is still illusive, and a detailed simulation study is strongly demanding.

Table 3a. Measured zeta potential and calculated surface charge density values for SDS/cholesterol and CTAB/cholesterol for different Λ-values.

Λ	**Zeta potential (mV)**	**Surface charge density (C m^{-2})**	**Λ**	**Zeta potential (mV)**	**Surface charge density (C m^{-2})**
SDS			**CTAB**		
0	-47.9 $\pm$ 5.8	-0.026 $\pm$ 0.005	0	48.8 $\pm$ 7	0.023 $\pm$ 0.005
0.1	-79.1 $\pm$ 3.9	-0.081 $\pm$ 0.014	0.1	66.5 $\pm$ 2.7	0.038 $\pm$ 0.003
0.2	-73.1 $\pm$ 5.9	-0.063 $\pm$ 0.015	0.2	74.9 $\pm$ 2	0.049 $\pm$ 0.003
0.3	-71.1 $\pm$ 2.8	-0.059 $\pm$ 0.006	0.3	60.3 $\pm$ 1	0.032 $\pm$ 0.001
0.4	-86.1 $\pm$ 2.9	-0.113$\pm$ 0.016	0.4	67.2 $\pm$ 1	0.039$\pm$ 0.001
0.5	-80.24 $\pm$ 1.4	-0.088 $\pm$ 0.009	0.5	61.3 $\pm$ 1.1	0.033 $\pm$ 0.001
0.6	-73.1 $\pm$ 2.5	-0.063 $\pm$ 0.006	0.6	59.1 $\pm$ 2.6	0.031 $\pm$ 0.002

0.7	-65.3 ± 2.6	-0.047 ± 0.004	0.7	57.4 ± 1.5	0.029 ± 0.001
0.9	-60.7 ± 2	-0.04 ± 0.003	0.8	54.7 ± 1.7	0.027 ± 0.001
1.0	-61.5 ± 1.7	-0.041 ± 0.002	0.9	55.3 ± 0.9	0.028± 0.001
			1.0	55.8 ± 2.6	0.028 ± 0.002

Table 3b. Peak frequency of *overall hydration* for three vesicles. Data are fitted by using damped harmonic oscillator equation:

SDS			**CTAB**			**Brij 30**		
Λ	$\boldsymbol{\nu_1(cm^{-1})}$	$\boldsymbol{\nu_2(cm^{-1})}$	**Λ**	$\boldsymbol{\nu_1(cm^{-1})}$	$\boldsymbol{\nu_2(cm^{-1})}$	**Λ**	$\boldsymbol{\nu_1(cm^{-1})}$	$\boldsymbol{\nu_2(cm^{-1})}$
0	159.9±17.3	452.9±16.2	0	136.3±6.1	460.7±15	0.0	157.8±2.2	502.2±20
0.1	97.3±0.9	462.7±30.2	0.05	143.1±2.1	468.3±19	0.1	157.3±9.5	460.7±20
0.2	95.9±0.7	414.1±11.9	0.2	148.8±1.2	439.1±16	0.15	162.8±11.7	464.2±32
0.3	91.6±0.7	405.3±9.0	0.4	121.7±1	430.7±10.5	0.25	142.3±2.4	485.3±29.7
0.5	92.7±2.3	382.5±5.2	0.6	94.4±8.1	397±7.5	0.3	136.5±3.3	453±30
0.6	100±0.9	373.1±3.4	0.7	142.7±1.5	377.6±3.5	0.4	141.4±1.3	508.5±56
0.7	101.3±1.8	367.8±4.8	0.8	130.9±1.3	377.6±3.5	0.5	132.9±1.2	426.5±22.5
0.9	90.3±6.9	364.3±3.7	0.9	116.2±1.9	379.2±3.2	0.6	132.9±1.9	426.5±8.2
1.0	95.9±0.8	362.1±2.7	1.0	116.1±5.6	372.2±4.8	0.7	99.3±3.1	369.6±5.5

Table 3c. Peak frequency of *inner hydration* for three vesicles. Data are fitted by using damped harmonic oscillator equation:

SDS			CTAB		Brij 30			
Λ	$\nu'_1(cm^{-1})$	$\nu'_2(cm^{-1})$	Λ	$\nu'_2(cm^{-1})$	Λ	$\nu'_1(cm^{-1})$	$\nu'_2(cm^{-1})$	$\nu'_3(cm^{-1})$
0.05	113.3±0.8	360±7.1	0.05	330.2±3.8	0.1	147.8±0.7	245.8±1.8	476.1±23
0.1	81.6±2.7	339.77±4.5	0.1	341.1±1.4	0.15	153.2±0.6	239.2±2.2	531.7±82
0.2	91.7±0.8	338.3±7.1	0.2	336.9±2.4	0.25	159.7±0.8	233.7±2.4	437.1±7
0.3	86.6±0.7	332.9±2.3	0.3	335.2±2.7	0.3	154.7±0.8	251.8±2.9	534.6±50
0.4	81.9±0.5	335.4±1.8	0.4	349.8±4.2	0.4	165.2±0.8	303.6±2.5	443.9±10
0.5	86.7±1.9	341.4±2.3	0.5	341.6±1.9	0.5		224.7±6.2	319.4±8.6
0.6	96.1±1.5	336.2±2.2	0.6	339±1.8	0.6		204.7±5.9	304.3±3.7
0.8	79.8±6.4	332.9±3.0	0.7	340.2±1.9				
0.9	84±0.8	333.9±1.6	0.8	331.2±1.6				
1.0	91.7±0.7	332.4±1.6	0.9	334.6±1.5				
			1.0	330.9±1.7				

3IV. References:

(1) Huang, C.; Quinn, D.; Sadovsky, Y.; Suresh, S.; Hsia, K. J. Formation and Size Distribution of Self-Assembled Vesicles. *Proc Natl Acad Sci USA* **2017**, *114*, 2910–2915.
(2) Lasic, D. D. The Mechanism of Vesicle Formation. *Biochem J* **1988**, *256*, 1–11.
(3) Le, Q. V.; Lee, J.; Lee, H.; Shim, G.; Oh, Y. K. Cell Membrane-Derived Vesicles for Delivery of Therapeutic Agents. *Acta Pharm Sin B* **2021**, *11*, 2096–2113.
(4) Pattni, B. S.; Chupin, V. V.; Torchilin, V. P. New Developments in Liposomal Drug Delivery. *Chem Rev* **2015**, *115*, 10938–10966.
(5) Betz, G.; Aeppli, A.; Menshutina, N.; Leuenberger, H. In Vivo Comparison of Various Liposome Formulations for Cosmetic Application. *Int J Pharm* **2005**, *296*, 44–54.
(6) Moghassemi, S.; Hadjizadeh, A. Nano-Niosomes as Nanoscale Drug Delivery Systems: An Illustrated Review. *J Control Release* **2014**, *185*, 22–36.
(7) Bozzuto, G.; Molinari, A. Liposomes as Nanomedical Devices. *Int J Nanomed* **2015**, *10*, 975–999.
(8) Uchegbu, I. F.; Vyas, S. P. Non-Ionic Surfactant Based Vesicles (Niosomes) in Drug Delivery. *Int J Pharm* **1998**, *172*, 33–70.
(9) Manconi, M.; Valenti, D.; Sinico, C.; Lai, F.; Loy, G.; Fadda, A. M. Niosomes as Carriers for Tretinoin II. Influence of Vesicular Incorporation on Tretinoin Photostability. *Int J Pharm* **2003**, *260*, 261–272.
(10) Mu, L.; Sprando, R. L. Application of Nanotechnology in Cosmetics. *Pharm Res* **2010**, *27*, 1746–1749.

(11) Mozafari, M. R.; Johnson, C.; Hatziantoniou, S.; Demetzos, C. Nanoliposomes and Their Applications in Food Nanotechnology. *J Liposome Res* **2008**, *18*, 309–327.
(12) Cano-Sarabia, M.; Angelova, A.; Ventosa, N.; Lesieur, S.; Veciana, J. Cholesterol Induced CTAB Micelle-to-Vesicle Phase Transitions. *J Colloid Interface Sci* **2010**, *350*, 10–15.
(13) Ghosh, S.; Roy, A.; Banik, D.; Kundu, N.; Kuchlyan, J.; Dhir, A.; Sarkar, N. How Does the Surface Charge of Ionic Surfactant and Cholesterol Forming Vesicles Control Rotational and Translational Motion of Rhodamine 6G Perchlorate (R6G ClO 4)? *Langmuir* **2015**, *31*, 2310–2320.
(14) Hao, J.; Liu, W.; Xu, G.; Zheng, L. Vesicles from Salt-Free Cationic and Anionic Surfactant Solutions. *Langmuir* **2003**, *19*, 10635–10640.
(15) Kondo, Y.; Abe, M.; Ogino, K.; Uchiyama, H.; Tucker, E. E.; scamchorn, J. F.; Christian, S. D. Stability of Surfactant Vesicles Formed from Cationic Didodecyldimethylammonium Bromide. *Colloids Surf B* **1993**, *1*, 51–56.
(16) Feitosa, E.; Jansson, J.; Lindman, B. The Effect of Chain Length on the Melting Temperature and Size of Dialkyldimethylammonium Bromide Vesicles. *Chem Phys Lipids* **2006**, *142*, 128–132.
(17) Woodbury, D. J.; Richardson, E. S.; Grigg, A. W.; Welling, R. D.; Knudson, B. H. Reducing Liposome Size with Ultrasound: Bimodal Size Distributions. *J Liposome Res* **2006**, *16*, 57–80.
(18) Andrade, L. D. O. Understanding the Role of Cholesterol in Cellular Biomechanics and Regulation of Vesicular Trafficking: The Power of Imaging. *Biomed Spectrosc Imaging* **2016**, *5*, S101–S117.
(19) Bhardwaj, P.; Tripathi, P.; Gupta, R.; Pandey, P. Niosomes: A Review on Niosomal Research in the Last Decade. *J Drug Deliv Sci Technol* **2020**, *50*.
(20) Chen, S.; Hanning, S.; Falconer, J.; Locke, M.; Wen, J. Recent Advances in Non-Ionic Surfactant Vesicles (Niosomes): Fabrication, Characterization, Pharmaceutical and Cosmetic Applications. *Eur J Pharm Biopharm* **2019**, *144*, 18–39.
(21) Manconi, M.; Sinico, C.; Valenti, D.; Loy, G.; Fadda, A. M. Niosomes as Carriers for Tretinoin. I. Preparation and Properties. *Int J Pharm* **2002**, *234*, 237–248.
(22) Kumar, G. P.; Rajeshwarrao, P. Nonionic Surfactant Vesicular Systems for Effective Drug Delivery — an Overview. *Acta Pharm Sin B* **2011**, *1*, 208–219.
(23) Manosroi, A.; Wongtrakul, P.; Manosroi, J.; Sakai, H.; Sugawara, F.; Yuasa, M.; Abe, M. Characterization of Vesicles Prepared with Various Non-Ionic Surfactants Mixed with Cholesterol. *Colloids Surf B* **2003**, *30*, 129–238.
(24) Mehta, S. K.; Jindal, N. Formulation of Tyloxapol Niosomes for Encapsulation, Stabilization and Dissolution of Anti-Tubercular Drugs. *Colloids SurfB* **2013**, *101*, 434–441.
(25) Zeng, W.; Li, Q.; Wan, T.; Liu, C.; Pan, W.; Wu, Z.; Zhang, G.; Pan, J.; Qin, M.; Lin, Y.; Wu, C.; Xu, Y. Hyaluronic Acid-Coated Niosomes Facilitate Tacrolimus Ocular Delivery: Mucoadhesion, Precorneal Retention, Aqueous Humor Pharmacokinetics, and Transcorneal Permeability. *Colloid Surf B* **2016**, *141*, 28–35.
(26) Puras, G.; Mashal, M.; Zárate, J.; Agirre, M.; Ojeda, E.; Grijalvo, S.; Eritja, R.; Diaz-Tahoces, A.; Martínez Navarrete, G.; Avilés-Trigueros, M.; Fernández, E.; Pedraz, J. L. A Novel Cationic Niosome Formulation for Gene Delivery to the Retina. *J Control Release* **2014**, *174*, 27–36.
(27) Kundu, N.; Banik, D.; Sarkar, N. Self-Assembly of Amphiphiles into Vesicles and Fibrils: Investigation of Structure and Dynamics Using Spectroscopy and Microscopy Techniques. *Langmuir* **2018**, *34*, 11637–11654.
(28) Dey, S.; Sasmal, D. K.; Das, D. K.; Bhattacharyya, K. A Femtosecond Study of Solvation Dynamics and Anisotropy Decay in a Catanionic Vesicle: Excitation- Wavelength Dependence. *Chem Phys Chem* **2008**, *9*, 2848–2855.
(29) Mandal, S.; Kuchlyan, J.; Ghosh, S.; Banerjee, C.; Kundu, N.; Banik, D.; Sarkar, N. Vesicles Formed in Aqueous Mixtures of Cholesterol and Imidazolium Surface Active Ionic Liquid: A Comparison with Common Cationic Surfactant by Water Dynamics. *J Phys Chem B* **2014**, *118*, 5913–5923.
(30) Schmidt, D. A.; Birer, O.; Funkner, S.; Born, B. P.; Gnanasekaran, R.; Schwaab, G. W.; Leitner, D. M.; Havenith, M. Rattling in the Cage: Ions as Probes of Sub-Picosecond Water Network Dynamics. *J Am Chem Soc* **2009**, *131*, 18512–18517.
(31) Heyden, M.; Sun, J.; Funkner, S.; Mathias, G.; Forbert, H.; Havenith, M.; Marx, D. Dissecting the THz Spectrum of Liquid Water from First Principles via Correlations in Time and Space. *Proc Natl Acad Sci USA* **2010**, *107*, 12068–12073.
(32) Falconer, R. J.; Markelz, A. G. Terahertz Spectroscopic Analysis of Peptides and Proteins. *J Infrared Millim Terahertz Waves* **2012**, *33*, 973–988.
(33) Ebbinghaus, S.; Kim, S. J.; Heyden, M.; Yu, X.; Heugen, U.; Gruebele, M.; Leitner, D. M.; Havenith, M. An Extended Dynamical Hydration Shell around Proteins. *Proc Natl Acad Sci USA* **2007**, *104*, 20749–20752.

(34) Born, B.; Kim, S. J.; Ebbinghaus, S.; Gruebele, M.; Havenith, M. The Terahertz Dance of Water with the Proteins: The Effect of Protein Flexibility on the Dynamical Hydration Shell of Ubiquitin. *Faraday Discuss* **2009**, *141*, 161–173.
(35) Samanta, N.; Das Mahanta, D.; Mitra, R. K. Collective Hydration Dynamics of Guanidinium Chloride Solutions and Its Possible Role in Protein Denaturation: A Terahertz Spectroscopic Study. *Phys Chem Chem Phys* **2014**, *16*, 23308–23315.
(36) Pal, S.; Samanta, N.; Das Mahanta, D.; Mitra, R. K.; Chattopadhyay, A. E Ff Ect of Phospholipid Headgroup Charge on the Structure and Dynamics of Water at the Membrane Interface: A Terahertz Spectroscopic Study. *J Phys Chem B* **2018**, *122*, 5066–5074.
(37) Kandomura, Y.; Yamamoto, N.; Tominaga, K. Broadband Dielectric Spectroscopy from Sub GHz to THz of Hydrated Lipid Bilayer of DMPC. *Eur Phys J E* **2019**, *42*, 139.
(38) Sebastiani, F.; Bender, T. A.; Pezzotti, S.; Li, W. L.; Schwaab, G.; Bergman, R. G.; Raymond, K. N.; Toste, F. D.; Gordon, T. H.; Havenith, M. An Isolated Water Droplet in the Aqueous Solution of a Supramolecular Tetrahedral Cage. *Proc Natl Acad Sci USA* **2020**, *117*, 32954–32961.
(39) Sebastiani, F.; Ma, C. Y.; Funke, S.; B ä umer, A.; Decka, D.; Hoberg, C.; Esser, A.; Forbert, H.; Schwaab, G.; Marx, D.; Havenith, M. Probing Local Electrostatics of Glycine in Aqueous Solution by THz Spectroscopy. *Angew Chem Int Ed* **2021**, *60*, 3768–3772.
(40) Bruce, C. D.; Berkowitz, M. L.; Perera, L.; Forbes, M. D. E. Molecular Dynamics Simulation of Sodium Dodecyl Sulfate Micelle in Water: Micellar Structural Characteristics and Counterion Distribution. *J Phys Chem B* **2002**, *106*, 3788–3793.
(41) Dorshow, R.; Briggs, J.; Bunton, C. A.; Nicoli, D. F. Dynamic Light Scattering from Cetyltrimethylammonium Bromide Micelles. Intermicellar Interactions at Low Ionic Strengths. *J Phys Chem* **1982**, *86*, 2388–2395.
(42) Ferrer-Tasies, L.; Moreno-Calvo, E.; Cano-Sarabia, M.; Aguilella-Arzo, M.; Angelova, A.; Lesieur, S.; Ricart, S.; Faraudo, J.; Ventosa, N.; Veciana, J. Quatsomes: Vesicles Formed by Self-Assembly of Sterols and Quaternary Ammonium Surfactants. *Langmuir* **2013**, *29*, 6519–6528.
(43) Ghosh, S.; Mandal, A. K.; Das, A. K.; Mondal, T.; Bhattacharyya, K. Diffusion of Organic Dyes in a Niosome Immobilized on a Glass Surface Using Fluorescence Correlation Spectroscopy. *Phys Chem Chem Phys* **2012**, *14*, 9749–9757.
(44) Loosli, F.; Stoll, S. Effect of Surfactants, PH and Water Hardness on the Surface Properties and Agglomeration Behavior of Engineered TiO2 Nanoparticles. *Env. Sci Nano* **2017**, *4*, 203.
(45) Gilbile, D.; Docto, D.; Kingi, D. T.; Kurniawan, J.; Monahan, D.; Tang, A.; Kuhl, T. L. How Well Can You Tailor the Charge of Lipid Vesicles? *Langmuir* **2019**, *35*, 15960–15969.
(46) Kielland, J. Individual Activity Coefficients of Ions in Aqueous Solutions. *J Am Chem Soc* **1937**, *9*, 1675–1678.
(47) Brown, M. A.; Goel, A.; Abbas, Z. Effect of Electrolyte Concentration on the Stern Layer Thickness at a Charged Interface. *Angew Chem Int Ed* **2016**, *55*, 3790–3794.
(48) Pyne, P.; Mitra, R. K. Excipients Do Regulate Phase Separation in Lysozyme and Thus Also Its Hydration. *J Phys Chem Lett* **2022**, *13*, 931–938.
(49) Ahlers, J.; Adams, E. M.; Bader, V.; Pezzotti, S.; Winklhofer, K. F.; Tatzelt, J.; Havenith, M. The Key Role of Solvent in Condensation: Mapping Water in Liquid-Liquid Phase-Separated FUS. *Biophys. J* **2021**, *120*, 1266–1275.
(50) Keshavarzi, Z.; Banadkoki, S. B.; Faizi, M.; Zolghadri, Y.; Shirazi, F. H. Comparison of Transmission FTIR and ATR Spectra for Discrimination between Beef and Chicken Meat and Quantification of Chicken in Beef Meat Mixture Using ATRFTIR Combined with Chemometrics. *J Food Sci Technol* **2020**, *57*, 1430–1438.
(51) Samanta, N.; Luong, T. Q.; Das Mahanta, D.; Mitra, R. K.; Havenith, M. Effect of Short Chain Poly(Ethylene Glycol)s on the Hydration Structure and Dynamics around Human Serum Albumin. *Langmuir* **2016**, *32*, 831–837.
(52) Heugen, U.; Schwaab, G.; Brundermann, E.; Heyden, M.; Yu, X.; Leitner, D. M.; Havenith, M. Solute-Induced Retardation of Water Dynamics Probed Directly by Terahertz Spectroscopy. *Proc Natl Acad Sci USA* **2006**, *103*, 12301–12306.
(53) Das, D. K.; Das Mahanta, D.; Mitra, R. K. Nonmonotonic Hydration Behavior of Bovine Serum Albumin in Alcohol/Water Binary Mixtures: A Terahertz Spectroscopic Investigation. *Chem Phys Chem* **2017**, *18*, 749–754.
(54) Dodo, T.; Sugawa, M.; Nonaka, E.; Honda, H.; Ikawa, S. Absorption of Farinfrared Radiation by Alkali Halide Aqueous Solutions. *J Chem Phys* **1995**, *102*, 6208–6211.
(55) Schwaab, G.; Sebastiani, F.; Havenith, M. Ion Hydration and Ion Pairing as Probed by THz Spectroscopy. *Angew Chem Int Ed* **2019**, *58*, 3000–3013.

(56) Li, X.; Liu, L.; Schlegel, H. B. On the Physical Origin of Blue-Shifted Hydrogen Bonds. *J Am Chem Soc* **2002**, *124*, 9639–9647.
(57) Conti Nibali, V.; Pezzotti, S.; Sebastiani, F.; Galimberti, D. R.; Schwaab, G.; Heyden, M.; Gaigeot, M. P.; Havenith, M. Wrapping Up Hydrophobic Hydration: Locality Matters. *J Phys Chem Lett* **2020**, *11*, 4809–4816.
(58) Mihrin, D.; Andersen, J.; Jakobsen, P. W.; Larsen, R. W. Highly Localized H_2O Librational Motion as a Far-Infrared Spectroscopic Probe for Microsolvation of Organic Molecules. *Phys Chem Chem Phys* **2019**, *21*, 1717–1723.
(59) Decka, D.; Schwaab, G.; Havenith, M. A THz/FTIR Fingerprint of the Solvated Proton: Evidence for Eigen Structure and Zundel Dynamics. *Phys Chem Chem Phys* **2015**, *17*, 11898–11907.

Chapter 4

Addition of cholesterol alters the hydration at the surface of model lipids: a spectroscopic investigation:

Cholesterol is known to modify the phase behavior of model lipid membranes as it makes phospholipid bilayer more structured. Simulation results have shown that addition of cholesterol allows more bulk like water to protrude into phospholipid interfaces. However, such claims have not so far been verified experimentally. We have investigated the alteration of hydrogen bond network structure of water at the surface of two model phospholipids DOPC and DOPG as cholesterol is added into those using ATR-FTIR spectroscopy in the FIR-THz region. Our measurements and analysis lead us to probe the collective H-bond network explicitly at the lipid surface. A detailed principal component analysis on the measured data concludes that the water-water H-bond vibration dynamics gets slower at the lipid surface as compared to bulk water, the effect being more prominent in case of the charged phospholipid, DOPG. However, as cholesterol is added and more bulk like water protrudes into the liposome interface, the H-bond vibration gets weaker and correspondingly the dynamics gets accelerated.

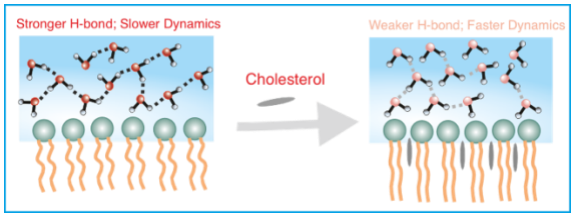

4I. Introduction:

Cell membrane acts not only as a barrier of permeability to compartmentalize cell but also provides a balance between hydrophilic-hydrophobic interactions to facilitate biomolecules to be functional.[1,2] Generally, plasma membrane contains more than thousands types of lipid molecules which can be divided broadly into three categories: phospholipid, sphingomyelin and sterol.[3–5] Phospholipids (the major structural lipid) are amphiphilic molecules having both hydrophilic and hydrophobic moieties.[6] In aqueous milieu phospholipids self-organize into bilayer structures, termed as liposomes, with their hydrophilic portion directly exposed to the aqueous environment and the non-polar hydrophobic residues construct the inner hydrophobic region. Liposomes have gained much attention as key agents in medicine and pharmacology as major chemicals and drugs interact with lipid inside body.[7,8] For clinical purposes, it is widely used as delivery agents of anti-cancer, anti-fungal, anti-inflammatory and anti-biotic

drugs, anesthetics and gene materials.[9] Cholesterol is the major sterol, present in mammalian cell membrane, which plays pivotal roles in membrane function, organization and dynamics by regulating the fluidity and rigidity of membranes.[10] Cell membranes generally contains 20-30 mol% cholesterol while in red blood cell the content could rise up-to 50 mol%.[11,12] Cholesterol contains a small hydrophilic hydroxyl group including a sterol ring attached with the hydrophobic tail. Such structure makes cholesterol to fit into lipid bilayer structures with the hydroxyl head group lying along the lipid head groups and the hydrophobic tail fitting inside the hydrophobic lipid bilayer.[13,14] Several experimental and theoretical studies have reported that incorporation of cholesterol modifies the structure and organization of phospholipid bilayers.[15,16] It usually increases the ordering of lipid acyl chains and enhances lipid packing in membranes by decreasing the area per head group of lipid molecules, the phenomenon commonly termed as the *condensing effect*.[15,17] Since hydration plays a key role in maintaining the structure and stability of biomolecules,[18,19] elucidating the hydration behavior of lipids is also an ever important aspect towards understanding lipid stability and functionality. Water at the lipid interface is expected to show slower dynamics than bulk water as they can interact to the lipid head groups. Several experimental and simulation studies also have rendered evidence towards this understanding. Recently, Flanagan et al.,[20] using two-dimensional infrared (2D-IR) and vibrational sum frequency generation (VSFG) techniques, reported a retarded water dynamics at lipid water interface. Yamamoto et al.,[21] using THz spectroscopy, have investigated the temperature dependent hydration behavior of DMPG and DMPC lipid bilayers both in gel and in crystalline phases and found that the lipids show distinct hydration behavior and different packing parameter in these two different phases. Our group has explored the interfacial water dynamics of negatively charged DOPG and zwitterionic DOPC lipid bilayers by using THz time domain spectroscopy and observed that the hydrogen bond network of water around lipid interface is dependent on lipid concentration as well as on the lipid head group polarity.[22] In a very recent study, using THz spectroscopy measurement, we have reported that the inner hydration of a cholesterol/surfactant vesicle is distinctly different compared to the outer hydration and the difference changes with the content of cholesterol as well as the charge type of the surfactant(s).[23]These studies have unambiguously established the altered water dynamics at the lipid interface, the extent of which in turn is lipid specific. While several attempts have been made towards understanding the hydration behavior of lipids, it has still not been extensively explored whether cholesterol plays any role in modifying lipid hydration specially/specifically considering the fact that addition of cholesterol does modify lipid structures. There have been a few simulation studies in this regard: Elola et

al.[24] using MD simulation has reported the abundance of more bulk like water at DPPC membrane interface in presence of cholesterol. They also reported that water molecules diffuse faster with shorter rotational relaxation time upon the insertion of cholesterol into DPPC lipids. In a more recent study Oh et al.[25] has made a detailed analysis on the hydrogen bond network of water in DPPC lipid membrane in presence of cholesterol. They found that with increasing cholesterol content the average number of DPPC-water hydrogen bond per DPPC molecule increases, which eventually also accelerates water relaxation dynamics. These simulation results provide insightful understanding on lipid hydration in presence of cholesterol, however, there has been no experimental validation of such claim. In this work, using far IR Fourier transform infrared spectroscopy in the terahertz (THz) frequency region (50-450 cm^{-1}; 1.5-13.5 THz), we explore the hydration behaviour of two differently charged lipid bilayers in presence of cholesterol. THz (far-IR) spectroscopy is a label free, non-invasive powerful technique to underline the collective hydrogen bond network of water molecule.[26–30] It can directly probe the permanent and induced dipole moments of water molecules present at the interface of biomolecules such as proteins,[31,32] lipids[21,22,33] etc. The total dipole moment is directly correlated with the absorption coefficient of the systems; thus any change in the absorption coefficient of a solution manifests alteration in the hydration behaviour of solute molecules.[34–36] Measurements of frequency dependent absorption coefficient therefore offers an elegant avenue to directly probe lipid hydration. We prepare DOPC, DOPG and DOPC/DOPG (1:1, mol/mol) liposomes in absence and in presence of cholesterol. Dynamic light scattering (DLS) and atomic force microscopy (AFM) was used to estimate the dimensions of the thus formed liposomes. As mentioned, hydration behavior in these liposomes was probed using FIR-FTIR measurements. Our study unambiguously concludes that cholesterol induces weaker hydrogen bond and faster hydrogen bond vibration/stretching dynamics at lipid interface, which establishes the validity of the earlier simulation results.

4II. Materials and Methods:

DOPC (1,2-Dioleoyl-sn-glycero-3-phosphocholine), DOPG (1,2-Dioleoyl-sn-glycero-3-phospho-rac-(1-glycerol) sodium salt), Cholesterol (3β-Hydroxy-5-cholestene,5-Cholesten-3β-ol) and chloroform were procured from Sigma Aldrich with their highest purity (>99%) and were used without any further purification. Details of all the lipids, using here, are described in section 2II.c.i. Freshly prepared 50 mM PBS (phosphate buffer saline) of pH 7.4 were used for preparing the liposomes and the liposomes preparation technique is described in section 2II.a.iii. All the used instruments are described in section 2.III.

4III. Results and Discussions:

Structures of liposomes: To ensure the formation of liposomes we measure the hydrodynamic diameter of three liposomes in presence of cholesterol. Representative DLS profiles of DOPC liposomes with different-Q are shown in figure 4Aa. Similar profiles for DOPG and DOPC/DOPG (1:1) liposomes are shown in figure 4Ab and figure 4Ac respectively. The hydrodynamic diameter of DOPC liposome is ~80 nm while that of DOPG liposome is ~50 nm. Interestingly, we notice that the diameter of DOPC/DOPG systems is reduced to ~38 nm. Diameter of all the liposomes increases upon the addition of cholesterol (figure 4Ad). Kotoucek et al.[37] has previously reported that in unsaturated lipids the size of liposome increases as the concentration of cholesterol increases, which corroborates our findings.

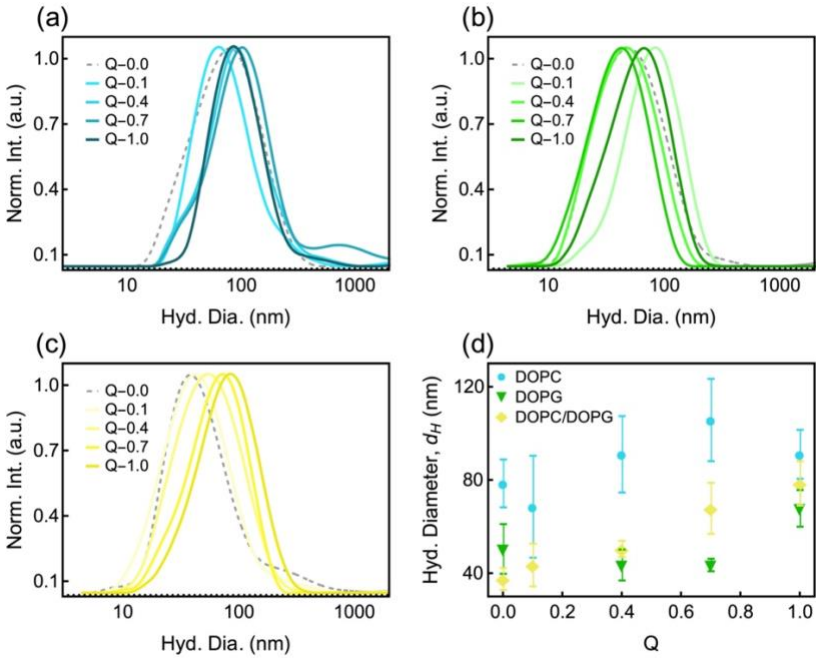

Figure 4A. DLS profile of (a) DOPC, (b) DOPG and (c) DOPC/DOPG liposomes in absence and in presence of cholesterol. (d) indicated hydrodynamic diameter as a function of Q for three liposomes respectively.

AFM measurements (figure 4B) also identify the appearance of spherical DOPC, DOPG and DOPC/DOPG liposomes with diameters of 49±12 nm, 55±21 nm and 48±25 nm, respectively at Q=0.4 corroborating the DLS results. Existence of spherical particle with a finite height

strongly supports the formation of liposomes and their structural modification in presence of cholesterol.

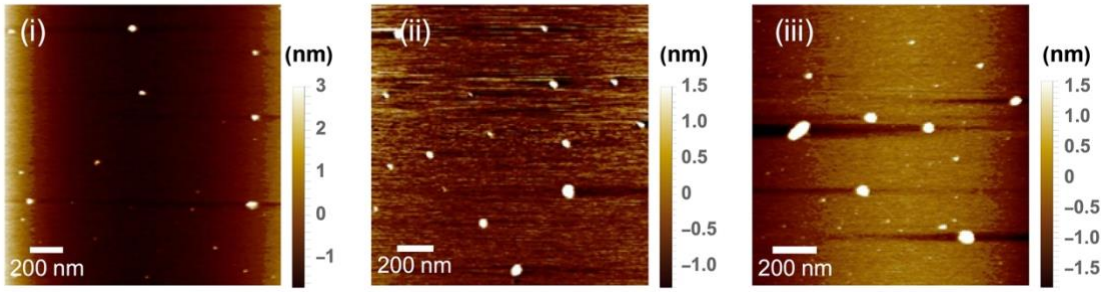

Figure 4B. AFM images of (i) DOPC, (ii) DOPG and (iii) DOPC/DOPG liposomes at Q=0.5 respectively.

Hydration Study: We now focus on the hydration behaviour of lipids in presence of cholesterol. We measure the frequency dependent absorption coefficient $\alpha(\nu)$ in liposome at different Q in the THz frequency window (1.5-13.5 THz; 50-450 cm^{-1}). Bulk water exhibits two intense bands in this frequency regime (figure 4Cb): ~136 cm^{-1} corresponding to the hindered translational motion (HB-stretch) and ~475 cm^{-1} due to the hindered rotational motion (librational motion) of water molecules.[29,34] $\alpha(\nu)$ of the lipid solution is found to be less than that of bulk water (figure 4Ca) which decreases even further upon the gradual insertion of cholesterol into the lipid bilayer.

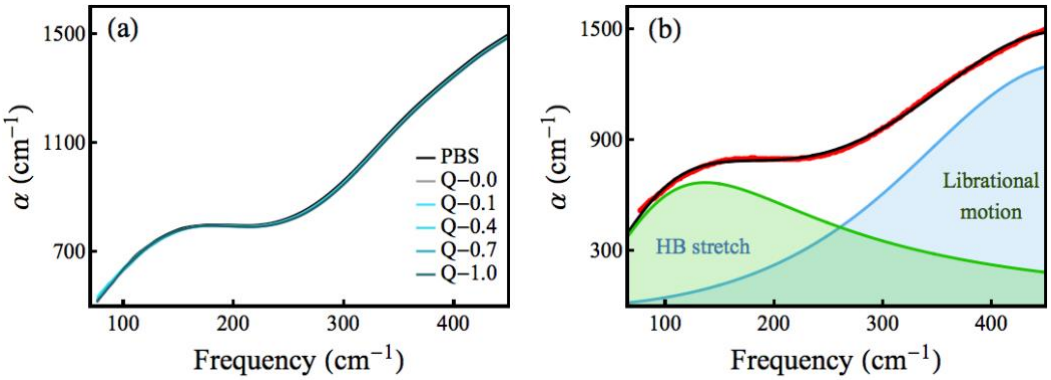

Figure 4C. (a) Absorption coefficient as a function of frequency for DOPC liposomes at different Q. (b) Representative fitted profile for water. Red curve shows the raw data of water, black line shows the

total fitted data. Blue curve indicated HB-stretch and green curve indicates libration motion of water molecule.

To get a clearer insight into the explicit hydration of the liposomes, we calculate the difference in absorption coefficient: $\Delta\alpha(\nu) = \alpha_{solution}(\nu) - \alpha_{buffer}(\nu)$. $\Delta\alpha(\nu)$ profiles for DOPC liposomes at different Q are shown in Figure 4Da. $\Delta\alpha(\nu)$ profiles for DOPG and DOPC/DOPG (1:1) liposomes are shown in figure 4Ea and 4Eb, respectively. $\Delta\alpha(\nu)$ profiles for both DOPG and DOPC/DOPG systems follow similar trend as that of the DOPC system. To separate the different vibrational modes appearing in the lipid hydration we fit the $\Delta\alpha(\nu)$ profile using a two-component damped harmonic oscillator model:

$$\Delta\alpha(\nu) = \sum_{i=1}^{2} \frac{a_i \omega_i \nu^2}{\nu^2\omega_i^2 + \pi^2\left(\nu_i^2 + \frac{\omega_i^2}{4\pi^2} - \nu^2\right)^2} \qquad (4.1)$$

where a_i, ω_i, ν_i are the amplitude, width and the centre frequency of the i^{th} resonance. The unperturbed centre frequency is given as

$$\nu_{0,i} = \sqrt{\nu_i^2 + \frac{\omega_i^2}{4\pi^2}}.$$

A representative fitting profile of DOPC (Q=0.4) with two distinct peaks has been shown in figure 4Db. Peak frequencies and the other fitting parameters are shown in figure 4Dc and table 4a. HB-stretch (ν_{HB}) in DOPC liposome (Q=0.0) appears at ~112 cm^{-1} which is 24 cm^{-1} red shifted compared to that in bulk water. On the other hand, ν_{HB} appears at ~189 cm^{-1} (~ 53 cm^{-1} blue shifted compared to bulk water) in negatively charged DOPG liposomes (Q=0.0). In mixed lipid ν_{HB} appears at ~117 cm^{-1} (19 cm^{-1} red shifted). A red (or blue) shift of HB-stretch manifests the formation of weaker (or stronger) hydrogen bond network in water.[38,39] The librational mode (ν_{Lib}) of interfacial water in these three liposomes appears at ~395 cm^{-1}, ~419 cm^{-1} and ~403 cm^{-1}, respectively (~80 cm^{-1}, 56 cm^{-1}, 72 cm^{-1} red shifted for compared to bulk water). A red (or blue) shift in the librational mode expresses a less (or more) restricted motion of water molecules at the lipid water interface.[32] These results thus a priori conclude that depending on the lipid charge, the water network around lipid bilayer interface gets modified; to put it more specifically, lipid-water hydrogen bonds act into play along with water-water hydrogen bonds. Earlier investigation also reveals that the behaviour of water around lipid interface differs from that of bulk water.[20,22]

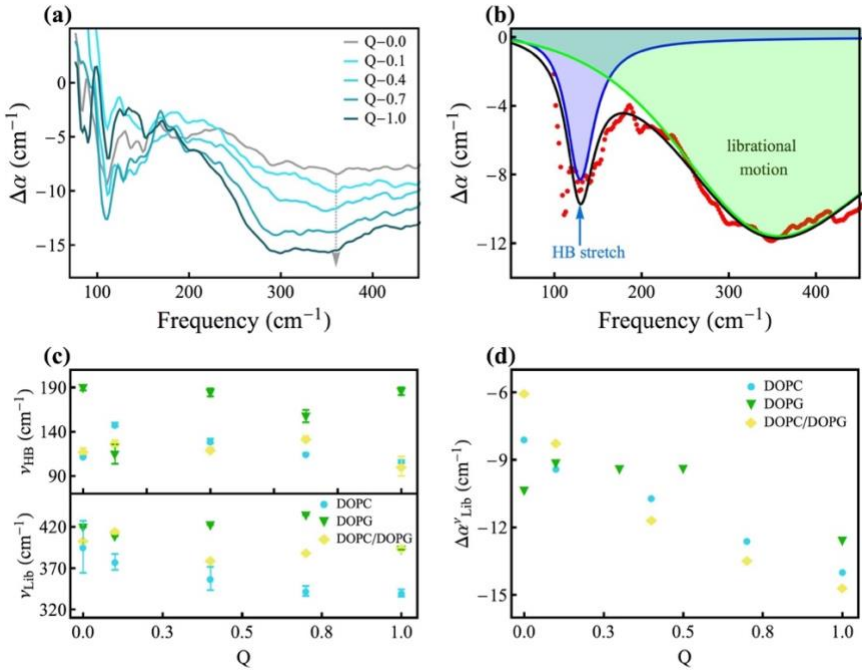

Figure 4D. (a) Change in absorption coefficient, $\Delta\alpha(\nu)$ (=α_{sample}- α_{water}) as a function of frequency for DOPC liposome at different Q. (b) Representative fitting of $\Delta\alpha(\nu)$ profiles for DOPC liposome (Q =0.4) using a damped harmonic oscillator model (equation 4.1). The red broken curve represents the raw data and the black solid line stands for the total fitting. The 1st peak with frequency ν_1 (blue line) represents the hydrogen bond stretching of water molecules, the 2nd peak with frequency ν_2 (green line) presents the librational motion of water molecules. (c) Peak frequency (HB stretch and librational mode) of different liposomes as a function of Q. (d) $\Delta\alpha(=\alpha_Q^\nu - \alpha_{water}^\nu)$, measured at the peak frequency, as a function of Q of liposomes for librational mode of water.

We then monitor how the lipid hydration gets further modified in presence of cholesterol. We fit the Δα(ν) profiles using equation 4.1 (figure 4Dc, table 4a). Before discussing the modification of water network in terms of the peak frequency, let us first discuss on the modification of a related parameter, Δα as it corresponds to the population of various water types around the lipids.[36,40] A representative profile for $\Delta\alpha^\nu_{Lib}$ against Q is shown in figure 4Dd. We observe a distinct increase in $|\Delta\alpha^\nu_{Lib}|$ (the negative sign suggests lower absorption compared to bulk water) for both DOPC and DOPC/DOPG liposome with increasing cholesterol, however the effect is mild in DOPG system (figure 4Dd). Considering a three-component model we express α(ν) of liposome solution as:

$$\alpha(\nu) = \alpha_{bulk}\phi_{bulk} + \alpha_{hyd}\phi_{hyd} + \alpha_{lipid}\phi_{lipid} \qquad (4.2)$$

where α_{bulk}, α_{lipid}, α_{hyd} are the absorption coefficients of pure water, pure lipid and water in the dynamical hydration shell of liposome, respectively and ϕ_i is the corresponding volume fraction with $\phi_{bulk} + \phi_{hyd} + \phi_{lipid} = 1$.

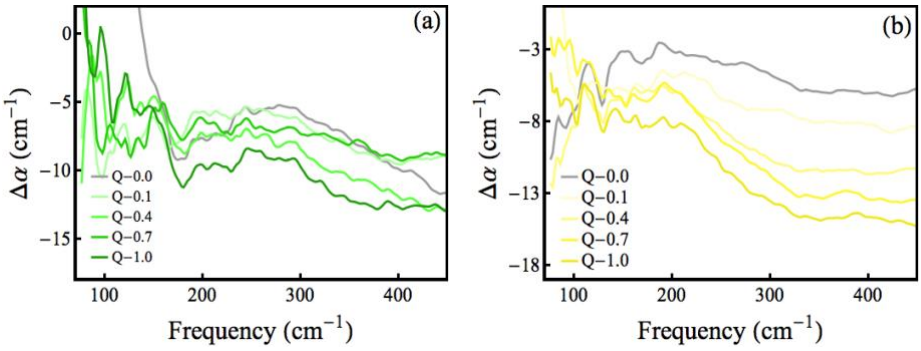

Figure 4E. $\Delta\alpha$ as a function of frequency at different Q-value for (a) DOPG and (b) DOPC/DOPG liposomes.

So, Δα in pristine liposomes can be written as:

$$\Delta\alpha(\nu) = \alpha_{bulk}(\nu)(\phi_{bulk} - 1) + \alpha_{hyd}(\nu)\phi_{hyd} + \alpha_{lipid}(\nu)\phi_{lipid} \tag{4.3}$$

In presence of cholesterol the modified $\Delta\alpha'$ is expressed as:

$$\Delta\alpha'(\nu) = \alpha_{bulk}(\nu)(\phi'_{bulk} - 1) + \alpha'_{hyd}(\nu)\phi'_{hyd} + \alpha_{lipid}(\nu)\phi'_{lipid} \tag{4.4}$$

α_{lipid} could be neglected as pure lipid offers negligible absorbance in this frequency window. Figure 4Dd clearly indicates to the fact that $\Delta\alpha'_{Lib} > \Delta\alpha_{Lib}$. This leads to the following inequality: $\alpha_{bulk}(\phi'_{bulk} - \phi_{bulk}) > \alpha_{hyd}\phi_{hyd} - \alpha'_{hyd}\phi'_{hyd}$. Solving this inequality exactly is a bit challenging since it contains terms which could not explicitly be measured; one needs to execute ab-initio simulation to solve this inequality. However, we can make some approximations to extract vital information from this inequality. DLS results show that the liposome size increases with the addition of cholesterol (figure 4Ad). This inevitably confirms: $\phi'_{bulk} < \phi_{bulk}$. So the left hand side of the inequality is negative, and subsequently, $\alpha_{hyd}\phi_{hyd} < \alpha'_{hyd}\phi'_{hyd}$. In our previous study we have observed that the addition of cholesterol does not perturb the hydration of surfactant interface.[23] This leads us to approximate that in the lipid interface also, cholesterol would not affect the interfacial hydration noticeably and we take $\alpha_{hyd} \approx \alpha'_{hyd}$, which finally concludes that $\phi'_{hyd} > \phi_{hyd}$. This inequality is a very useful information as it manifests that more water molecules are accommodated in the

hydration layer of lipids in presence of cholesterol compared to the unmodified liposomes. This observation is in line with previous result showing increased hydration around lipid head groups in presence of cholesterol.[41] Establishing the fact that water population is enhanced at lipid interfaces in presence of cholesterol, we now investigate how ν_{HB} and ν_{Lib} get modified when cholesterol is inserted into the lipid bilayer. Addition of small amount of cholesterol (Q=0.1) in DOPC liposome shifts ν_{HB} to a higher frequency (~147 cm^{-1}); however, with further addition of cholesterol ν_{HB} shifts successively towards lower frequencies (red shifted) and at high cholesterol concentration (Q=1.0) it again returns to its initial value (at Q=0.0). In DOPG liposome, we observe an oscillatory trend of HB-stretch in presence of cholesterol. $\nu_{HB}(Q)$ of the mixed liposome follows more or less a similar nature as that of DOPC liposomes. ν_{Lib} for DOPC liposomes

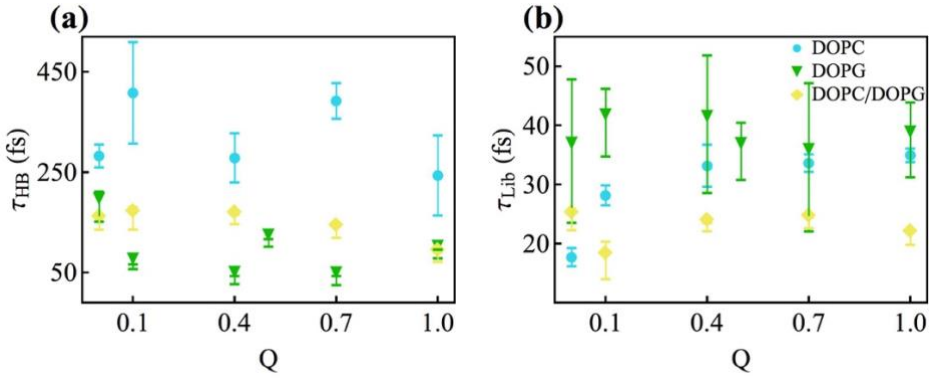

Figure 4F. Lifetime of oscillator's dipole moment autocorrelation function corresponding to (a) "HB-stretch" and (b) "librational motion" modes of water associated with DOPC, DOPG and DOPC/DOPG systems as a function of Q.

appears at 377 cm^{-1} at Q=0.1; a red shift of ~38 cm^{-1} is observed at Q=1.0 (figure 4Dc, lower panel). On the other hand, we notice an oscillatory trend in ν_{Lib} for DOPG liposome. For DOPC/DOPG liposome, ν_{Lib} suffers a ~11cm^{-1} blue shift in presence of small amount of cholesterol (Q=0.1); however, with further addition of cholesterol ν_{Lib} is gradually red shifted (~ 20 cm^{-1} at Q=1.0) (figure 4Dc, lower panel). Measurements of $\alpha(\nu)$ in the THz frequency region also lead us to estimate relaxation lifetime(s) (τ_i) of the corresponding modes (both HB-stretch & librational motion) (see section 2.I.e for details). τ_i in principal manifests the dynamical behavior of water wrapped in the lipid-water interface. We depict the calculated lifetime in figure 4F and table 4b. The lifetime corresponding to the intermolecular "HB

stretch" (τ_{HB}^{bulk}) of bulk water is ~44 fs while that for the librational mode (τ_{Lib}^{bulk}) is found to be ~ 22 fs.[26,42] τ_{HB} in the lipid interface is found to be much slower than that in bulk water. Slower H bond lifetime of water at lipid water interface has been reported earlier.[20] For DOPC liposome it appears to be ~282 fs, while for DOPG and DOPC/DOPG liposomes it is ~181fs and ~147 fs, respectively (figure 4Fa). τ_{Lib} is also found to increase in the three lipid-water interfaces compared to bulk water (figure 4Fb). We notice that both τ_{HB} and τ_{Lib} depends on the charge type of the liposomes. Upon the addition of cholesterol in all the three liposomes we observe a rather non-monotonous, more specifically an oscillatory trend of both τ_{HB} and τ_{Lib} (figure 4F, table 4b). While our experimental results unambiguously suggest a definite modification in the hydrogen bond network of lipid hydration in presence of cholesterol, from the observed non-regular trends in the $\Delta\nu$ and $\Delta\tau$ [change in both peak frequency and bond stretching] of interfacial water it seems difficult to reach at a cholesterol concentration independent definite conclusion on the extent of modification also on the charge type of the lipids. We therefore perform a principal component analysis (PCA) on $\Delta\alpha$ of each liposome in presence of cholesterol in order to reducing the datasets (see section 2.I.b for details of PCA).

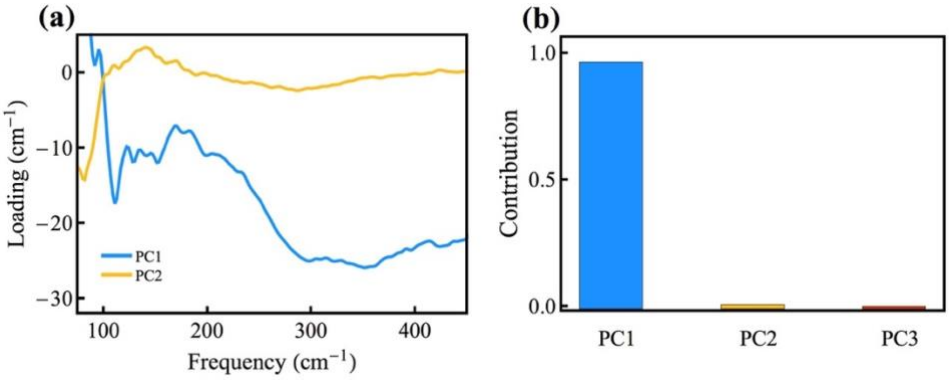

Figure 4G. (a) Representative principal components (PCs) of DOPC liposome ($Q \neq 0$). (b) Relative contribution of the first three components.

Representative first two principal components (PCs) and the contribution of the first three PCs for DOPC liposomes are shown in figure 4G. As the first PC offers a significantly high contribution (> 98%) for all the three liposomes, we consider only the first PC. For further analysis we fit the first PC of the three liposomes by using the same damping equation (equation 4.1) and the fitted parameters are summarized in table 4c.

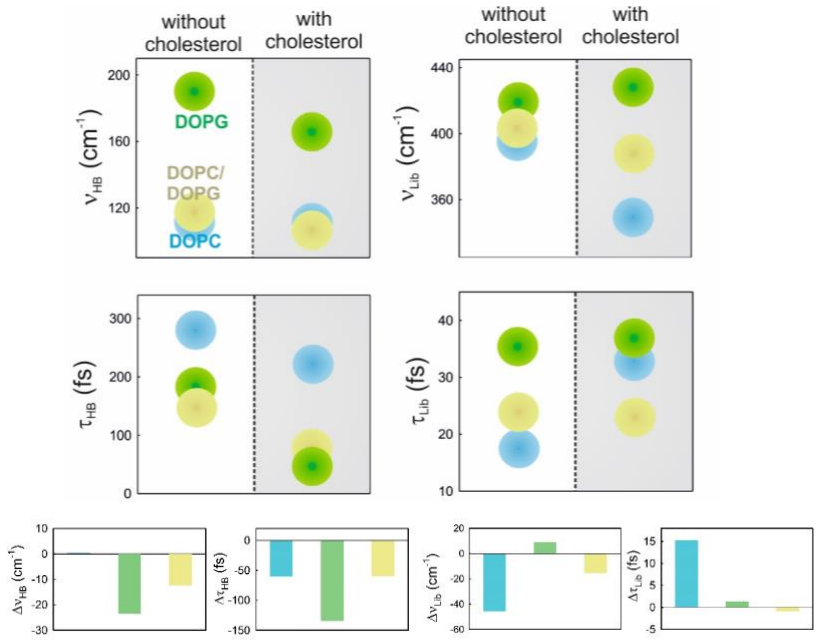

Figure 4H. Peak frequency (after performing PCA) corresponding to HB-stretch and librational mode and the lifetimes of these two modes of hydration layer of DOPC (blue), DOPG (green) and DOPC/DOPG (yellow) in absence (clear region) and in presence of cholesterol (shaded region). We also plot the difference in peak frequency ($\Delta\nu_i = \nu_i^{Q\neq0} - \nu_i^{Q=0}$) where *'i'* stands for HB and Lib, and the same way difference in lifetime in the lower panel.

The PC analysis provides a definite description of the water HB network structure and dynamics modification of the lipid membranes in presence of cholesterol. We plot the peak frequencies and the corresponding lifetimes in absence and in presence of cholesterol after performing the PCA (figure 4H). DOPG and DOPC/DOPG liposomes suffer distinct red shifts (~23 and ~13 cm^{-1} respectively; table 4d) in ν_{HB} indicating a weaker and/or smaller number of H-bond formation at the lipid interface in presence of cholesterol. The effect is rather subtle in DOPC. We found a contrasting feature in the ν_{Lib}; in DOPC liposomes ν_{Lib} is ~46 cm^{-1} red shifted while in DOPG it is ~9 cm^{-1} blue shifted (table 4d). In the mixed system the band gets 15 cm^{-1} red shifted. In all the three liposomes τ_{HB} gets faster in presence of cholesterol, the effect being more prominent in DOPG. In case of τ_{Lib} the changes are not straightforward; in DOPC it is slower while in the other two systems, the changes are marginal.

Overall Comprehencen: Cholesterol is known to alter the phase behaviour (more specifically the area per molecule and the ordering of the lipid molecules) by inserting itself within the lipid assembly.[15] Since the working temperature in the present study is higher than the T_m of the

concerned lipids,[43,44] both the lipids prefer to form a liquid disordered L_α phase in aqueous solutions. As cholesterol is added in these liposomes the acyl chains of the lipid molecules get more ordered and at a moderate cholesterol concentration both L_α and L_0 phases could coexist.[15,45] At an even higher cholesterol concentration the L_0 phase predominates. Our study is intended to explore whether such a phase change imparts any modification in the lipid hydration too. THz measurements enables us to explicitly determine the hydration at the interface as the calculation of $\Delta\alpha(\nu)$ subtracts the bulk contribution.[23] Thus the estimated peak frequencies and the lifetimes manifest the interfacial information only.

We focus our discussion based on the parameters obtained from the PCA analysis (figure 4H) as it helps to analyse the change explicitly. A quick look into the figure reveals that interfacial hydration is lipid charge dependent and addition of cholesterol does modify it. We first discuss the intermolecular H-bond stretch. ν_{HB} manifests the central frequency of the water-water intermolecular vibration mode and in bulk water it appears at 136 cm^{-1}. Note that this frequency lies in the far-IR region as this is intermolecular in nature and therefore correlates the collective motion of water network. Such vibrations suffer distinct perturbation water interacts with lipid structure. Interestingly, in uncharged DOPC it is slightly red shifted while in DOPG it suffers a large blue shift. Formation of strong H-bond with the charged DOPG interface shifts ν_{HB} towards higher frequency. The effect of this strong interaction seems not very prominent at the mixed interface. As cholesterol is added, the effect is found to be negligible in DOPC, while in DOPG and in the mixed interface it gets red shifted (figure 4H). Such red shift indicates weakening of the intermolecular H-bond at the interface in presence of cholesterol. A similar conclusion can also be drawn from the τ_{HB} estimation which unambiguously shows accelerated H-bond vibration of water at lipid surfaces in presence of cholesterol (figure 4H). Our experimental results matches excellently with previous simulation results. MD simulation by In Oh et al.[25] have predicted intrusion of bulk water into the lipid interface and a consequent rupture of the H-bond network, which clearly is reflected in the observed weakening and correspondingly red shift of the ν_{HB} peak (figure 4H, left panel). It has also been concluded that relaxation time scale of water decreases in presence of cholesterol[24] which we also have find in our experimental results. It is worth mentioning here that simulation estimates the H-bond relaxation dynamics in zwitterionic DPPC/water interface is to be 111 ps, which reduces to 56.6 ps at x_{chol}=0.5. While comparing these time constants with the experimental findings, one should be cautious about the particular mode responsible for the calculated time constant. Simulation study essentially probes H-bond making and

breaking process which is governed by diffusion and therefore the time is slow. Also, it involves single molecular motion, and therefore does not necessarily reciprocate the overall bulk hydration. The trend in experimental τ_{HB} with cholesterol is very distinct. Our analysis offers a τ_{HB} value of 282 fs in DOPC which reduces to 221 fs in presence of cholesterol (table 4c). This motion is relatively fast as it manifests the bond vibration and does not include any diffusive motion. Moreover, since THz measurements probe collective vibration, we obtain information on the global dynamics of water at the lipid interface, which indeed accelerates in presence of cholesterol. It is interesting to note that the dynamics gets substantially accelerated in case of charged lipid DOPG which indicates a larger water penetration in the lipid interface compared to the zwitterionic lipids. We also notice that in case of the mixed lipid interface, which can be used to mimic real cell membrane, the effect of cholesterol on the H-bond network mostly resembles that in case of DOPC rather than that in DOPG. While most of the simulation studies on the effect of cholesterol have so far been carried out using zwitterionic lipids, less attention has been paid on the charged lipids, wherein electrostatics could play a non-trivial role. Our results invoke further simulation studies using charged and mixed lipids. In a nutshell, our experimental study unambiguously establishes the fact that addition of cholesterol in model lipid membrane weakens the interfacial H-bond strength which eventually leads to a faster dynamic of the lipid membrane water. Our study could be found encouraging towards understanding lipid-lipid and lipid-protein interactions in a greater detail.

Table 4a. Peak frequency of *total hydration* for three liposomes. Data are fitted by using damped harmonic oscillator equation:

DOPC			**DOPG**			**DOPC/DOPG**		
Q	$\boldsymbol{\nu_{HB}(cm^{-1})}$	$\boldsymbol{\nu_{Lib}(cm^{-1})}$	**Q**	$\boldsymbol{\nu_{HB}(cm^{-1})}$	$\boldsymbol{\nu_{Lib}(cm^{-1})}$	**Q**	$\boldsymbol{\nu_{HB}(cm^{-1})}$	$\boldsymbol{\nu_{Lib}(cm^{-1})}$
0	112.2±1.1	395.8±3.1	0	189.7±3.1	419.6±0.03	0	117.9±3.4	403.7±0.007
0.1	147.9±2.3	377.6±9.5	0.1	114.6±10.1	408.8±0.02	0.1	126.9±3.4	415.2±0.02
0.4	129.4±2.5	357.5±1.4	0.4	184.4±4.4	422.5±0.14	0.4	119.8±1.9	379.8±0.003
0.7	114.8±0.9	342.4±6.1	0.7	157.5±6.9	434.4±0.26	0.7	132.2±2.6	389.4±0.001
1.0	106.4±1.5	339.9±4.4	1.0	185.7±4.3	392.7±0.02	1.0	100.9±10.9	394.8±0.02

Table 4b. Lifetime of oscillator's dipole moment autocorrelation function corresponding to "HB-stretch" and "librational motion" modes of water associated with DOPC, DOPG and DOPC/DOPG systems as a function of Q.

DOPC			**DOPG**			**DOPC/DOPG**		
Q	$\tau_{HB}(fs)$	$\tau_{Lib}(fs)$	**Q**	$\tau_{HB}(fs)$	$\tau_{Lib}(fs)$	**Q**	$\tau_{HB}(fs)$	$\tau_{Lib}(fs)$
0	282±22	17±2	0	181±29	35±12	0	147±12	24±2
0.1	407±101	28±2	0.1	61±4	40±5	0.1	157±22	17±3
0.4	278±49	33±3	0.4	34±8	40±11	0.4	155±9	22±0.7
0.7	391±35	33±1	0.7	33±9	34±12	0.7	129±11	23±0.9
1.0	243±79	34±1	1.0	86±8	37±6	1.0	80±9	20±1

Table 4c. Peak frequency and lifetime corresponding HB-stretch and librational mode of hydration layer of lipids in absence and in presence of cholesterol (after performing PCA).

	DOPC		DOPG		DOPC/DOPG	
	$Q = 0$	$Q \neq 0$	$Q = 0$	$Q \neq 0$	$Q = 0$	$Q \neq 0$
ν_{HB} (cm^{-1})	112.2	112.6	189.7	166.08	118	105.63
ν_{Lib} (cm^{-1})	395.8	349.9	419.7	428.8	403.7	388.4
τ_{HB} (fs)	282.06	221.7	181.08	46.62	147.2	87.8
τ_{Lib} (fs)	17.67	33	35.6	36.9	24.03	23.09

Table 4d. Peak frequency corresponding HB-stretch and librational mode of hydration layer of lipids and the corresponding peak shifts in absence and in presence of cholesterol (after performing PCA) (-ve sign indicates blue shift)

	DOPC			DOPG			DOPC/DOPG		
	$Q = 0$	$Q \neq 0$	Peak Shift (cm^{-1})	$Q = 0$	$Q \neq 0$	Peak Shift (cm^{-1})	$Q = 0$	$Q \neq 0$	Peak Shift (cm^{-1})
ν_{HB} (cm^{-1})	112.2±1.1	112.6±1.5	0.4	189.7±3.1	166.08±10.4	23.62	118±3.4	105.63±0.4	12.37

ν_{Lib} (cm^{-1})	395.8±3.1	349.9±3.8	45.9	419.7±0.03	428.8±9.6	-9.1	403.7±0.007	388.4±10.3	15.3

4IV. References:

(1) Albert, B.; Johnson, A.; Lewis, J.; Raff, M.; Roberts, K.; Walter, P. *Molecular Biology of the Cell*, 5th ed.; Garland Science, 2008.

(2) Okur, H. I.; Tarun, O. B.; Roke, S. Chemistry of Lipid Membranes from Models to Living Systems: A Perspective of Hydration, Surface Potential, Curvature, Confinement and Heterogeneity. *J. Am. Chem. Soc.* **2019**, *141*, 12168−12181.

(3) Meer, G. V.; Voelker, D. R.; Feigenson, G. W. Membrane Lipids: Where They Are and How They Behave. *Nat. Rev. Mol. Cell Biol.* **2008**, *9*, 112–124.

(4) Ingoĺfsson, H. I.; Melo, M. N.; Eerden, F. J. V.; Arnarez, C.; Lopez, C. A.; Wassenaar, T. A.; Periole, X.; Vries, A. H. D.; Tieleman, D. P.; Marrink, S. J. Lipid Organization of the Plasma Membrane. *J. Am. Chem. Soc.* **2014**, *136*, 14554–14559.

(5) Klose, C.; Surma, M. A.; Simons, K. Organellar Lipidomics — Background and Perspectives. *Curr. Opin. Cell Biol.* **2013**, *25*, 1–8.

(6) Dresche, S.; Hoogevest, P. V. The Phospholipid Research Center: Current Research The Phospholipid Research Center: Current Research in Phospholipids and Their Use in Drug Delivery in Phospholipids and Their Use in Drug Delivery. *Pharmaceutics* **2020**, *12*, 1235.

(7) Allen, T. M.; Cullis, P. R. Liposomal Drug Delivery Systems: From Concept to Clinical Applications. *Adv Drug Deliv Rev.* **2013**, *65*, 36–48.

(8) Torchilin, V. P. Recent Advances with Liposome as Pharmaceutical Carriers. *Nat. Rev.* **2005**, *4*, 145–160.

(9) Matos, C.; Lobao, P. Non-Steroidal Anti-Inflammatory Drugs Loaded Liposomes for Topical Treatment of Inflammatory and Degenerative Conditions. *Curr Med Chem.* **2020**, *27*, 3809–3829.

(10) Ikonen, E. Cellular Cholesterol Trafficking and Compartmentalization. *Nat. Rev* **2008**, *9*, 125–138.

(11) Mouritsen, O. G.; Zuckermann, M. J. What's So Special About Cholesterol? *Lipids* **2004**, *39*, 1101–1113.

(12) Lipowsky, R.; Sackmann, E. *Structure and Dynamics of Membranes*; Elsevier, 1995.

(13) Cheng, C. Y.; Olijve, L. L. C.; Kausik, R.; Han, S. Cholesterol Enhances Surface Water Diffusion of Phospholipid Bilayers. *J. Chem. Phys.* **2014**, *141*, 22D513.

(14) Mihailescu, M.; Soubias, O.; Worcester, D.; White, S. H.; Gawrisch, K. Structure and Dynamics of Cholesterol-Containing Polyunsaturated Lipid Membranes Studied by Neutron Diffraction and NMR. *J. Membr. Biol.* **2011**, *239*, 63–71.

(15) Meyer, F. D.; Smit, B. Effect of Cholesterol on the Structure of a Phospholipid Bilayer. *Proc. Natl. Acad. Sci. U.S.A.* **2009**, *106*, 3654–3658.

(16) Pandit, S. A.; Chiu, S. W.; Jakobsson, E.; Grama, A.; Scott, H. L. Cholesterol Packing around Lipids with Saturated and Unsaturated Chains. *Langmuir* **2008**, *24*, 6858–6865.

(17) Hung, W. C.; Lee, F. Y.; Huang, H. W. The Condensing Effect of Cholesterol in Lipid Bilayers. *Biophys. J.* **2007**, *92*, 3960–3967.

(18) Laage, D.; Elsaesser, T.; Hynes, J. T. Water Dynamics in the Hydration Shells of Biomolecules. *Chem. Rev.* **2017**, *117*, 10694−10725.

(19) Ball, P. Water as an Active Constituent in Cell Biology. *Chem. Rev.* **2008**, *108*, 74−108.

(20) Flanagan, J. C.; Valentine, M. L.; Baiz, C. R. Ultrafast Dynamics at Lipid−Water Interfaces. *Acc. Chem. Res.* **2020**, *53*, 1860−1868.

(21) Yamamoto, N.; Andachi, T.; Tamura, A.; Tominaga, K. Temperature and Hydration Dependence of Low-Frequency Spectra of Lipid Bilayers Studied by Terahertz Time-Domain Spectroscopy. *J. Phys. Chem. B* **2015**, *119*, 9359–9368.

(22) Pal, S.; Samanta, N.; Dasmahanta, D.; Mitra, R. K.; Chattyopadhya, A. Effect of Phospholipid Headgroup Charge on the Structure and Dynamics of Water at the Membrane Interface: A Terahertz Spectroscopic Study. *J. Phys. Chem. B* **2018**, *22*, 5066–5074.

(23) Pyne, S.; Pyne, P.; Mitra, R. K. The Inner Hydration in Surfactant/Cholesterol Vesicles Differs from the Outer One: A Spectroscopic Investigation. *ChemPhysChem*. https://doi.org/10.1002/cphc.202200337.

(24) Elola, M. D.; Rodriguez, J. Influence of Cholesterol on the Dynamics of Hydration in Phospholipid Bilayers. *J. Phys. Chem. B* **2018**, *122*, 5897–5907.

(25) Oh, M. I.; Oh, C. I.; Weaver, D. F. Effect of Cholesterol on the Structure of Networked Water at the Surface of a Model Lipid Membrane. *J. Phys. Chem. B* **2020**, *124*, 3686−3694.
(26) Sebastiani, F.; Bender, T. A.; Pezzotti, S.; Li, W. L.; Schwaab, G.; Bergman, R. G.; Raymond, K. N.; Toste, F. D.; Head-Gordon, T.; Havenith, M. An Isolated Water Droplet in the Aqueous Solution of a Supramolecular Tetrahedral Cage. *Proc. Natl. Acad. Sci. U.S.A.* **2020**, *117*, 32954–32961.
(27) Schwaab, G.; Sebastiani, F.; Havenith, M. Ion Hydration and Ion Pairing as Probed by THz Spectroscopy. *Angew. Chem. Int. Ed.* **2019**, *58*, 3000–3013.
(28) Pyne, P.; Mitra, R. K. Excipients Do Regulate Phase Separation in Lysozyme and Thus Also Its Hydration. *J. Phys. Chem. Lett.* **2022**, *13*, 931−938.
(29) Samanta, N.; Luong, T. Q.; Das Mahanta, D.; Mitra, R. K.; Havenith, M. Effect of Short Chain Poly(Ethylene Glycol)s on the Hydration Structure and Dynamics around Human Serum Albumin. *Langmuir* **2016**, *32*, 831−837.
(30) Schmidt, D. A.; Birer, O.; Funkner, S.; Born, B. P.; Gnanasekaran, R.; Schwaab, G. W.; Leitner, D. M.; Havenith, M. Rattling in the Cage: Ions as Probes of Sub-Picosecond Water Network Dynamics. *J. Am. Chem. Soc.* **2009**, *131*, 18512–18517.
(31) Born, B.; Kim, S. J.; Ebbinghaus, S.; Gruebele, M.; Havenith, M. The Terahertz Dance of Water with the Proteins: The Effect of Protein Flexibility on the Dynamical Hydration Shell of Ubiquitin. *Faraday Discuss.* **2009**, *141*, 161–173.
(32) Ahlers, J.; Adams, E. M.; Bader, V.; Pezzotti, S.; Winklhofer, K. F.; Tatzelt, J.; Havenith, M. The Key Role of Solvent in Condensation: Mapping Water in Liquid-Liquid Phase-Separated FUS. *Biophys. J.* **2021**, *120*, 1–10.
(33) Pal, S.; Chattopadhyay, A. Hydration Dynamics in Biological Membranes: Emerging Applications of Terahertz Spectroscopy. *J. Phys. Chem. Lett.* **2021**, *12*, 9697–9709.
(34) Heyden, M.; Sun, J.; Funkner, S.; Mathias, G.; Forbert, H.; Havenith, M.; Marx, D. Dissecting the THz Spectrum of Liquid Water from First Principles via Correlations in Time and Space. *Proc. Natl. Acad. Sci. U.S.A.* **2010**, *107*, 12068–12073.
(35) Nibali, V. C.; Havenith, M. New Insights into the Role of Water in Biological Function: Studying Solvated Biomolecules Using Terahertz Absorption Spectroscopy in Conjunction with Molecular Dynamics Simulations. *J. Am. Chem. Soc.* **2014**, *136*, 12800−12807.
(36) Ebbinghaus, S.; Kim, S. J.; Heyden, M.; Yu, X.; Heugen, U.; Gruebele, M.; Leitner, D. M.; Havenith, M. An Extended Dynamical Hydration Shell around Proteins. *Proc. Natl. Acad. Sci. U.S.A.* **2007**, *104*, 20749–20752.
(37) Kotoucek, J.; Hubatka, F.; Masek, J.; Kulich, P.; Velinska, K.; Bezdekova, J.; Fojtikova, M.; Tomeckova, A.; Straska, J.; Hrebik, D.; Macaulay, S.; Kratochvilova, I.; Raska, M.; Turanek, J. Preparation of Nanoliposomes by Microfluidic Mixing in Herring-Bone Channel and the Role of Membrane Fluidity in Liposomes Formation. *Sci. Rep* **2020**, *10*, 5595.
(38) Nibali, V. C.; Pezzotti, S.; Sebastiani, F.; Galimberti, D. R.; Schwaab, G.; Heyden, M.; Gaigeot, M. P.; Havenith, M. Wrapping Up Hydrophobic Hydration: Locality Matters. *J. Phys. Chem. Lett.* **2020**, *11*, 4809−4816.
(39) Li, X.; Liu, L.; Schlege, H. B. On the Physical Origin of Blue-Shifted Hydrogen Bonds. *J. Am. Chem. Soc.* **2002**, *124*, 9639–9647.
(40) Pyne, P.; Das Mahanta, D.; Gohil, H.; Prabhu, S. S.; Mitra, R. K. Correlating Solvation with Conformational Pathways of Proteins in Alcohol–Water Mixtures: A THz Spectroscopic Insight. *Phys. Chem. Chem. Phys.* **2021**, *23*, 17536–17544.
(41) Chen, C.; Tripp, C. P. An Infrared Spectroscopic Based Method to Measure Membrane Permeance in Liposomes. *Biochim. Biophys. Acta* **2008**, *1778*, 2266–2272.
(42) Huse, N.; Ashihara, S.; Nibbering, E. T. J.; Elsaesser, T. Ultrafast Vibrational Relaxation of O–H Bending and Librational Excitations in Liquid H2O. *Chem. Phys. Lett.* **2005**, *404*, 389–393.
(43) Himeno, H.; Shimokawa, N.; Komura, S.; Andelman, D.; Hamada, T.; Takagi, M. Charge-Induced Phase Separation in Lipid Membranes. *Soft Matter* **2014**, *10*, 7959–7967.
(44) Ulrich, A. S.; Sami, M.; Watts, A. Hydration of DOPC Bilayers by Differential Scanning Calorimetry. *Biochim. Biophys. Acta* **1994**, *1191*, 225–230.
(45) Subczynski, W. K.; Wisniewska, A.; Hyde, J. S.; Kusumi, A. Three-Dimensional Dynamic Structure of the Liquid-Ordered Domain in Lipid Membranes as Examined by Pulse-EPR Oxygen Probing. *BioPhys. J.* **2007**, *92*, 1573–1584.

Chapter 5

The explicit role of interfacial hydration during polyethylene glycol induced lipid fusion: a THz spectroscopic investigation

While the phenomenon of excipient mediated membrane fusion has been studied widely, the inherent role of interfacial hydration involved in the process has mostly remained unaddressed. Here we report experimental validation of the fact that PEG-induced membrane fusion is associated with the dehydration of the membrane(s). We explore the explicit hydration behavior at three different lipids (DOPC, POPC and DPPC) membranes with different aliphatic tails as they undergo fusogenic transition in the presence of PEG of average molecular weight of 4000 using THz-FTIR spectroscopy in the frequency window of 1.5-13.5 THz. Dynamic light scattering and electron microscopic measurements confirm the formation of different intermediate steps of the liposomes during the fusion process: bilayer aggregation, destabilization and finally lipid fusion. We observe that membrane hydration follows a systematic trend with the lipid specificity as the fusion process sets in.

5I. Introduction:

Membrane fusion is a key event in intracellular membrane trafficking e.g. egg fertilization, viral entry, intracellular transport, neurotransmission through cell etc.[1–4] Bilayer membrane fusion follows a complex mechanism involving several steps and proceeds through some intermediate structures called *'stalk'*.[5,6] To initiate the stalk stage the fusing membranes must overcome electrostatic and hydration barriers among them; this could be achieved by destabilizing the bilayer.[1,2] In living cells several proteins like SNAP Receptor (SNARE), SM protein, Rab protein etc. facilitate membranes to undergo intracellular fusion.[7–11] These proteins usually act as the source of energy for the intracellular fusion; for example, SNARE delivers ~40-140 k_BT energy to fuse membranes,[9,10] helical bundle of SNARE complex exerts force on the membrane anchor and provides an essential driving force to promote lipid fusion.[12]

Investigating membrane fusion in-vivo is often challenging owing to the fast, dynamic and complex nature of the membranes. Therefore, external molecules[13–15] are employed to fuse lipid membranes in-vitro condition to capture the intermediate states. Previous studies have shown that Ca^{2+} can fuse membranes in absence of proteins.[13] Such charge induced lipid fusion

proceeds through three successive processes: docking, aggregation and close contact; however, identifying and analyzing the kinetics of these intermediate steps remains mostly illusive.[16] Polyethylene glycols (PEG) are also a common class of molecules used to fuse membranes in absence of proteins.[15–18] PEG is a water-soluble polymer widely used as a macromolecular agent[19,20] as well as a molecular crowder owning to its biocompatibility.[21] In lipid bilayers PEG molecules have been found to alter the molecular order of the bilayer. Lipid membranes need to overcome hydration repulsion in order to fuse and to achieve this the hydration structure at the membrane must be perturbed.[17] Previous fluorescence studies have suggested that exclusion by PEG induces dehydration at the membrane interface which in turn destabilizes it and eventually induces them to aggregate.[16,17] While several experimental and simulation studies have been carried out to understand the mechanism of membrane fusion process in terms of mechanical strain and the corresponding energetics of the membranes [6,22–24] less attention has been paid on experimentally establishing the role of (de)hydration during membrane fusion. A key question remains elusive that how the interfacial water of lipid membrane behaves during the fusion process.

Membrane fusion process has mostly been experimented using probe-based spectroscopy/microscopy techniques, e.g., fluorescence, FRET etc.[25–29] While such techniques are useful in capturing the morphology and energetics of the intermediate steps, they cannot offer explicit information on interfacial hydration. In this context far-IR/THz spectroscopy offers a unique platform to label free determination of such hydration as it probes the fluctuations of the collective water dipole itself. THz spectroscopy has extensively been used to investigate biomolecular hydration in the recent past.[30–34] Our group has recently explored the hydrogen bond network structure and dynamics of water in negatively charged DOPG and zwitterionic DOPC membranes in absence and in presence of cholesterol; our study has concluded that H-bond dynamics gets accelerated in presence of cholesterol.[35] With the background that THz spectroscopy can divulge the explicit hydration structure and hydration at membrane interface, in the present study, we explore the hydration behavior of three lipids with different aliphatic tails: 1,2-dioleoyl-sn-glycero-3-phosphocholine (DOPC), 2-oleoyl-1-palmitoyl-sn-glycero-3-phosphocholine (POPC) and 1,2-dipalmitoyl-sn-glycero-3-phosphocholine (DPPC) as they undergo fusogenic transition in the presence of PEG (average molecular weight 4000). These phosphocholines differ in their hydrophobic tail parts with saturation level and tail length (scheme 2IV). We use dynamic light scattering and electron microscopy measurements to monitor the lipid fusion process and the results confirm the

formation of different intermediate steps of the liposomes during the fusion process. THz-FTIR results conclude that liposomes indeed get dehydrated in presence of PEG as the fusion process sets in.

5II. Materials and Methods:

DOPC (1,2-Dioleoyl-sn-glycero-3-phosphocholine), POPC (2-Oleoyl-1-palmitoyl-sn-glycero-3-phosphocholine) and DPPC (1,2-Dipalmitoyl-sn-glycero-3-phosphocholine) were procured from Avanti polar lipid with the highest purity (>99%) and were used without any further purification. PEG 4000 and chloroform were procured from Sigma Aldrich. Here we denote PEG 4000 as PEG. Milli-Q water was filtrated with a 0.2 μm filter before it was used to prepare the PBS buffer. 50 mM PBS (phosphate buffer saline) of pH 7.4 were used for preparing the liposomes. Liposomes preparation technique is described in section 2II.a.iii. All the used instruments are described in section 2.III.

5III. Results and Discussions:

Structure of liposomes in presence of PEG 4000: We measure the hydrodynamic diameter (d_H) of the three thus prepared liposomes (DOPC, POPC, DPPC) using dynamic light scattering (DLS) technique. Representative DLS profiles of POPC liposomes in presence of different concentrations of PEG are provided in figure 5A(a-c). For homogeneous pristine liposome we measure a diameter of ~ 100 nm.[36] As PEG concentration is increased (1%-25%) we observe the appearance of different structures of liposome, which could be identified with the various stages of aggregation of the liposomes (figure 5Ab). Interestingly, beyond 25% PEG concentration, we again observe a homogeneous size distribution of liposomes (figure 5Ac). These results thus reflect the PEG concentration dependent structural modification of POPC liposomes. Similar size alteration is also observed in the other two liposomes, however, with varying PEG concentration dependencies (figure 5Ba). For the concentration region PEG <1% the structure does not alter appreciably and we assign this structure as *Liposome Like State* (*LLS)*. For PEG > 1% (table 5a) we found that d_H increases sharply, reaches a maximum and then decreases (figure 5Ba, table 5b); we assign this state as the *aggregation state* (*AS)*. At an even higher PEG concentration, d_H does not change appreciably as a *fused state (FS)* is reached. To visualize the morphological structures of the various conformations of liposomes in presence of PEG, we image the three different regions using field emission scanning electron microscope (FESEM). In pristine POPC liposomes we observe spherical structures which are

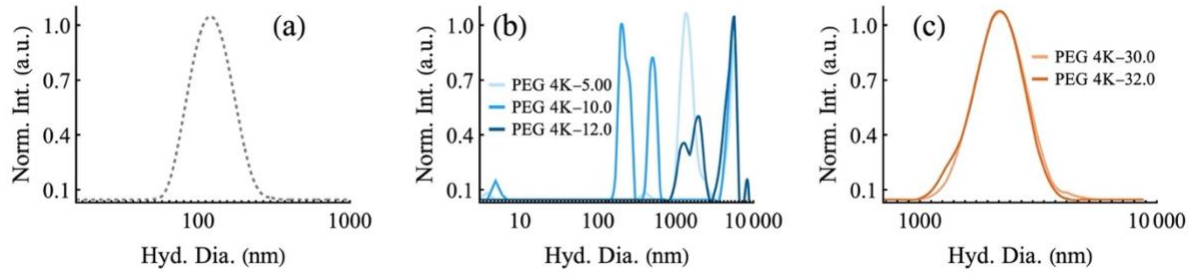

Figure 5A. DLS profiles of POPC liposome at different concentration of PEG (a) 0% PEG (b) aggregation state (AS) and (c) Fusion state (FS).

mostly in their monomeric states (figure 5Bbi). For POPC we identify the appearance of spherical particles of various sizes which are in the close vicinity of each other, perhaps this signifies the onset of aggregation (figure 5Bbii). In the FS region we observe the clear signature of the assimilation of liposomes (figure 5Bbiii) providing a direct evidence of lipid fusion.[37] We also make a detail analysis of the SEM images to obtain the statistical distribution of the

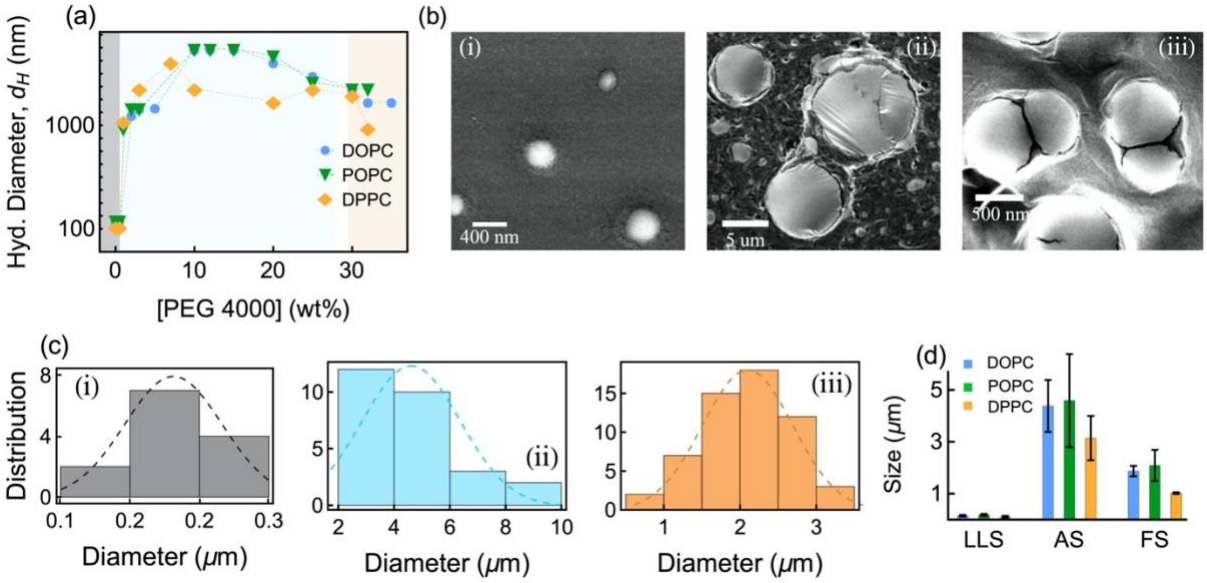

Figure 5B. (a) Hydrodynamic diameter as a function of PEG for three liposomes respectively. (b) SEM images of POPC liposome of three different states: (i) LLS, (ii) AS and (iii) FS. (c) Diameter distribution (from SEM images) of the three different states of POPC liposome. (d) Size comparison of three liposomes (DOPC, POPC, POPG)) of three different states.

size of the particles in these three states. In LLS, the average size of the particles is ~180±30 nm (figure 5Bci); large particle (aggregates) with average diameter of 4.58±1.5 μm is identified in the AS state (figure 5Bcii). In the FS, we observe the particles with diameter 2.09±0.59 μm (figure 5Bciii). We observe more or less similar size distribution in the other two liposomes also (figure 5Bd).

Hydration behaviour of liposomes at different state of fusion:

Upon establishing the appearance of the individual forms of liposome aggregation in presence of PEG, we now monitor the hydration behavior of those using THz-FTIR spectroscopy. We measure the absorption coefficient, $\alpha(\nu)$ of the liposome solutions in the 50-450 cm^{-1} window. In this frequency window the absorption profile of bulk water can be deconvoluted into two distinct curves (figure 5Cb) peaking at: ~136 cm^{-1} corresponding to the hindered translational motion (HB-stretch) and at ~475 cm^{-1} due to the hindered rotational motion (librational motion).[38,39] In pristine liposomes we observe that the α(ν) profiles have lower values than bulk water (figure 5Ca), which can be explained from the fact that high absorbing water molecules being replaced with lower absorbing liposomes, a phenomenon commonly termed as *"THz deficit"*.[31,35,40,41] It should be noted here that measured absorption coefficient of the liposome

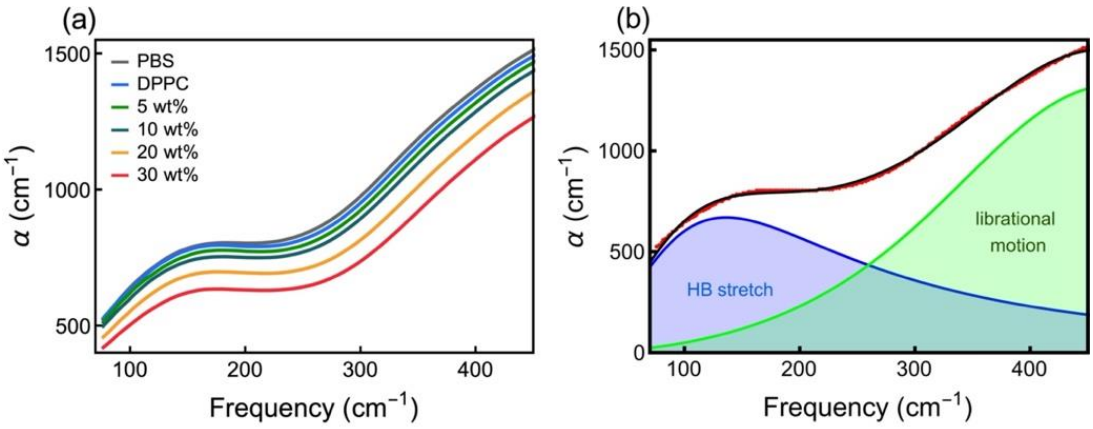

Figure 5C. absorption coefficient as a function of frequency for DPPC liposomes with different concentration of PEG 4000. (b) Representative fitted profile for water. Red curve shows the raw data of water, black line shows the total fitted data. Blue curve indicated HB-stretch and green curve indicates libration motion of water molecule.

solutions ($\alpha_{liposome}^{solution}(\nu)$) is a sum of contribution(s) received from bulk water ($\alpha_{water}(\nu)$), liposome ($\alpha_{liposome}(\nu)$) and liposome hydration ($\alpha_{liposome}^{hyd}(\nu)$). Considering the fact that the volume fraction of the liposomes is very small and liposomes themselves absorb nominally in this frequency window, the difference in the absorption coefficient could be estimated as: $\Delta\alpha(\nu) = \alpha_{liposome}(\nu) - \alpha_{water}(\nu)$; ideally its value should be zero unless ($\alpha_{water}(\nu) \neq \alpha_{liposome}^{hyd}(\nu)$). Interestingly we obtain non-zero $\Delta\alpha(\nu)$ profile(s) (figure 5Db) for all the systems which unambiguously establishes the fact that liposome possesses a hydration different than bulk water, similar to other biomolecules.[32,42–44]

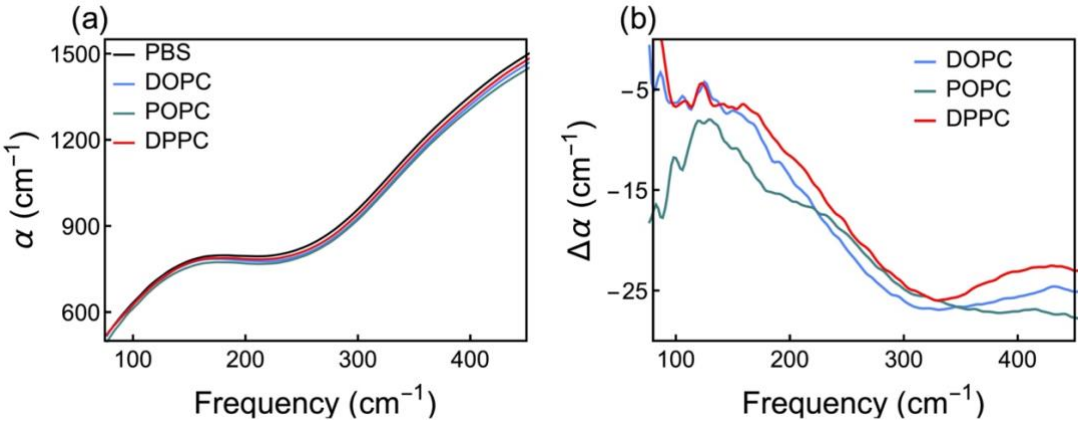

Figure 5D. (a) absorption coefficient and (b) $\Delta\alpha$ as a function of frequency for three liposomes respectively.

To quantify the difference we fit all the $\Delta\alpha(\nu)$ profiles using a two component damped harmonic oscillator model:[30]

$$\Delta\alpha(\nu) = \sum_{i=1}^{2} \frac{a_i \omega_i \nu^2}{\nu^2\omega_i^2 + \pi^2\left(\nu_i^2 + \frac{\omega_i^2}{4\pi^2} - \nu^2\right)^2} \tag{5.1}$$

where a_i, ω_i, ν_i are the amplitude, width and the centre frequency of the i^{th} resonance. The unperturbed centre frequency is given as

$$\nu_{0,i} = \sqrt{\nu_i^2 + \frac{\omega_i^2}{4\pi^2}}. \tag{5.2}$$

A representative fitting profile of POPC liposomes at PEG = 5% with two distinct deconvoluted modes is shown in figure 5Eb. We deconvolute all the $\Delta\alpha(\nu)$ profiles with this model and the fitted parameters are summarized in figure 5Ed and table 5c. Note that the fitting of the $\Delta\alpha(\nu)$ profiles and the obtained fiting parameters provide explicit information on the altered interfacial hydration of the liposomes as the contribution from bulk water has already been subtracted (equation 5.1). The peaks are found to be shifted from the bulk values, and this confirms a systematic alteration of hydration during membrane fusion. ν_{HB} for pristine DOPC liposome appears at ~96 cm^{-1} which is ~ 40 cm^{-1} red shifted compared to bulk water. For POPC and DPPC also the peak gets red shifted to appear at ~107 and ~104 cm^{-1}, respectively. ν_{lib} peak also suffers a red shift compared to bulk water. Such alteration in the ν_{HB} and ν_{lib} manifests the formation of weaker H bonds as compared to bulk water coupled with less hindered rotation of water around the pristine liposomes.[34,45] This result also corroborates with our recent report that lipid interfacial hydration is different from bulk water.[35]

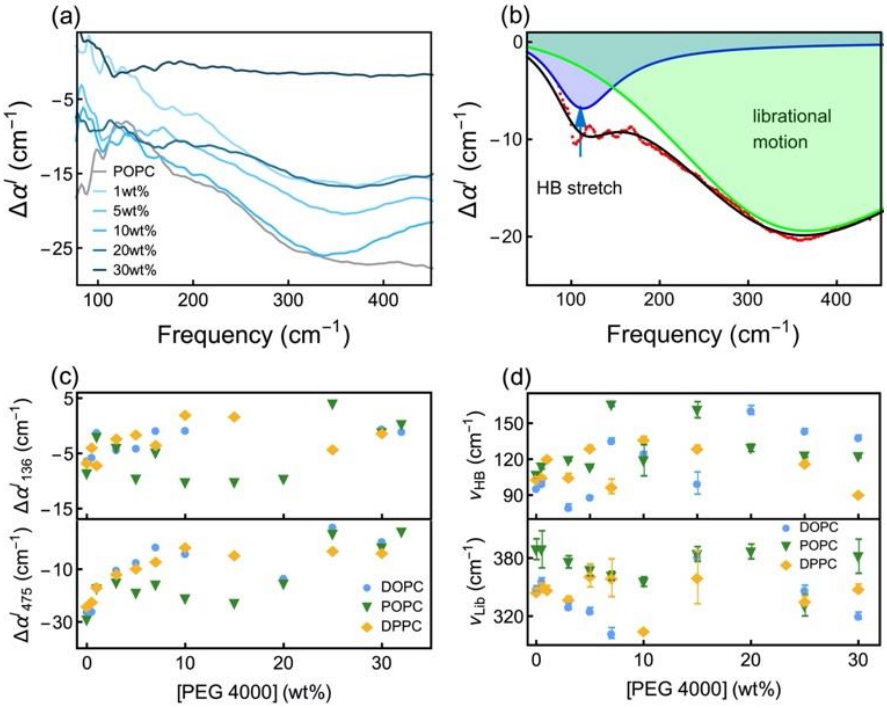

Figure 5E. (a) Representative profiles of change in absorption coefficient ($\Delta\alpha^l(\nu) = \alpha_{liposome}(\nu) - \alpha_{PEG}(\nu)$) as a function of frequency with increasing PEG concentration. (b) Representative fitting of $\Delta\alpha^l(\nu)$ profile for POPC liposome solution (in presence of [PEG]= 5 wt%) using a damped harmonic oscillator model (equation 5.1). The red broken curve represents the raw data and the black solid line

stands for the total fitting. The 1st peak with frequency ν_{HB} (blue line) represents the hydrogen bond stretch while the 2nd peak with frequency ν_{Lib} (green line) presents the librational motion of water molecules. (c) $\Delta\alpha^l$ measured at 136 and 475 cm^{-1} respectively as a function of [PEG] for both HB-stretch and librational mode of water. (d) Peak frequency (HB stretch and librational mode) of lipid hydration as a function of [PEG] for different liposomes.

We next investigate how such hydration gets further perturbed as PEG is added. We measure the absorption profiles of the lipid solutions in presence of PEG and observe a drastic decrease in the α(ν) profiles (figure 5Ca). To extract the explicit lipid hydration, we define a parameter: $\Delta\alpha^l(\nu)(=\alpha_{liposome}^{solution}(\nu)-\alpha_{PEG}^{solution}(\nu))$ (figure 5Ea, 5F(a-b)) which quantifies the altered hydration at liposome interface in presence of PEG. We monitor the change in $\Delta\alpha^l$ at two particular frequencies: 136 cm^{-1} (ν_{HB}) and 475 cm^{-1} (ν_{lib}). We observe that as the concentration of PEG increases both $|\Delta\alpha_{136}^l|$ and $|\Delta\alpha_{475}^l|$ decreases gradually (figure 5Ec), which signifies a dehydration at the interface. Since THz measurements probe the hydration at the liposome interface explicitly, the observed decrease flourishes a direct experimental evidence of membrane dehydration in presence of PEG as predicted earlier.[6,15]

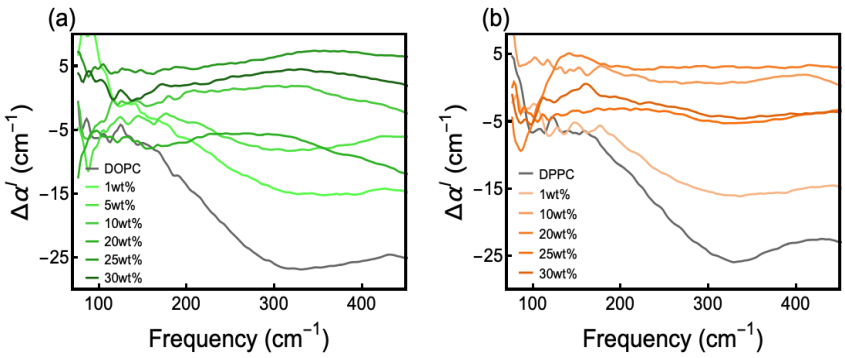

Figure 5F. $\Delta\alpha$ as a function of frequency at different concentration of PEG 4000 for (a) DOPC and (b) DPPC liposomes.

For a quantitative insight we fit all the $\Delta\alpha^l(\nu)$ profiles using the same two component damped harmonic oscillator model (equation 5.1). The results are depicted in figure 5Ed, table 5c. We found that upon the addition of small amount of PEG (0.5%) into DOPC, ν_{HB} suffers a marginal blue shift (~4 cm^{-1}) compared to the pristine liposomes. With further addition of PEG, ν_{HB} increases gradually up-to 20% PEG beyond which it decreases again. For POPC

liposomes, ν_{HB} suffers a marginal blue shift compared to the pristine POPC liposome (PEG=0.5%) and follows a trend similar as that of DOPC liposomes. For DPPC, ν_{HB} does not change appreciably upon the addition of small amount of PEG; however, it increases gradually up to 10% PEG and then decreases up to 30% (see table 5c). In DOPC at PEG=0.5% ν_{Lib} appears at ~357 cm^{-1} (8 cm^{-1} blue shifted compared to pristine liposomes) (figure 5Ed, lower panel). Upon further addition of PEG, we notice a rather non-monotonic change in ν_{Lib}. In POPC it decreases up to 10% (red shift) beyond which it remains almost constant with PEG concentration. Similar non-monotonous trend in ν_{Lib} is also observed in DPPC liposomes.

At this point it is very important to verify the extent to which bare PEG molecules alter the collective dynamics of bulk water. As a control we study the hydration behavior of PEG solutions at different concentrations. We measure the difference in absorption coefficient: $\Delta\alpha_{PEG}(\nu) = \alpha_{PEG}^{solution}(\nu) - \alpha_{water}(\nu)$. Representative $\Delta\alpha_{PEG}(\nu)$ profiles at different PEG concentrations are shown in Figure 5Ga. We fit the $\Delta\alpha_{PEG}(\nu)$ profiles using equation 5.1 and the fitted parameters are presented in table 5d. We observe a regular decrease in ν_{HB} with increasing PEG concentration up-to 7% beyond which it does not change appreciably (upper panel; figure 5Gd and table 5d). ν_{Lib} is found to remain mostly unchanged with PEG

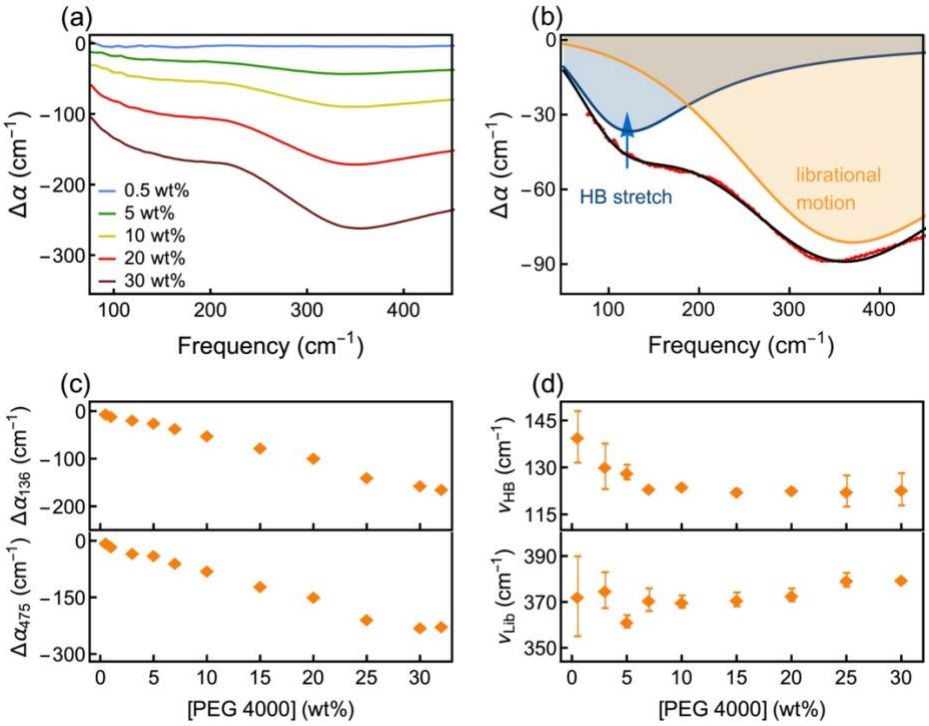

Figure 5G. (a) Change in absorption coefficient ($\Delta\alpha_{PEG}(\nu) = \alpha_{PEGsolution}(\nu) - \alpha_{water}(\nu)$) at different concentration of PEG. (b) Representative fitting of $\Delta\alpha_{PEG}(\nu)$ profiles for PEG solution (10 wt%) using the damped harmonic oscillator model (equation 5.1). The red broken curve represents the raw data and the black solid line stands for the total fitting. The 1st peak with frequency ν_1 (blue line) represents the hydrogen bond stretching of water molecules, the 2nd peak with frequency ν_2 (brown line) presents the librational motion of water molecules. (c) $\Delta\alpha$ measured at 136 and 475 cm^{-1} respectively as a function of [PEG] for both HB-stretch and librational mode of water. (d) Peak frequency (HB stretch and librational mode) of water as a function of PEG 4000.

concentration. PEG is known to alter water H-bond network as it forms a hydration layer around itself, thereby rupturing the tetrahedral bulk water network.[46] This makes the ν_{HB} to suffer the observed red shift. This control study thus confirms that PEG, by virtue of its modifying the water network structure, induces osmotic stress in the solution, which varies near-linearly with the PEG concentration as has previously been shown from thermodynamic considerations.[47] This study strongly confirms that PEG does influence water structure, however, in a near-linear manner, and therefore the observed non-linear behavior in the PEG-liposome solution is enrooted to the various bipartite interactions taken together.

While our results unambiguously identify a distinct modification of the lipid hydration, an initial look at figure 5Ed invokes a rather inconclusive insight on the systematic H-bond structure at different states of fusion (LLS, AS, FS). To reach at a statistically conclusive statement we perform a principal component analysis (PCA) of all the $\Delta\alpha^l(\nu)$ profiles for the three different states (see section 2.I.b for PCA analysis details).

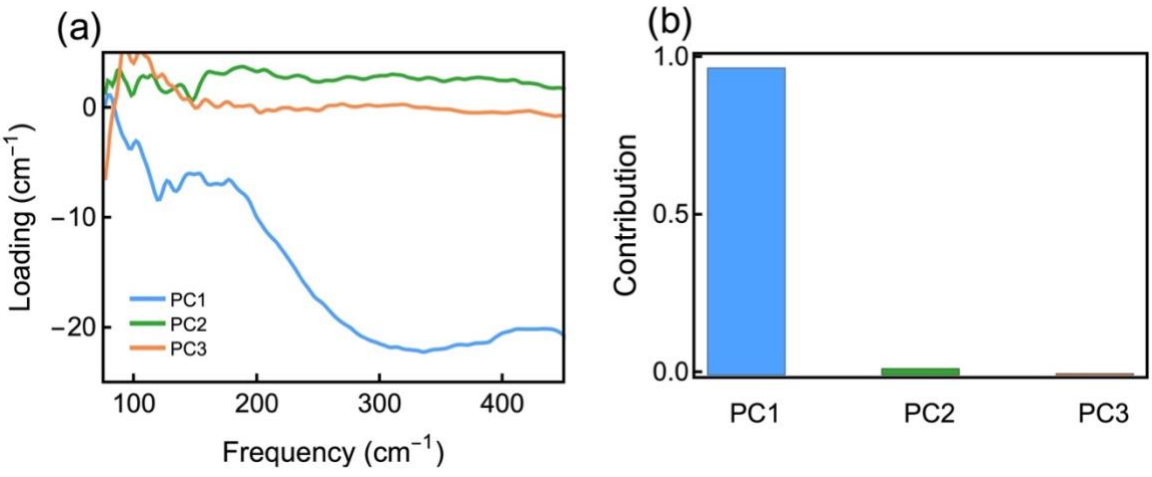

Figure 5H. (a) Representative principal components (PCs) at AS state of DPPC liposome (b) Relative contribution of the first three components.

A representative first three principal components (PC) and their contributions for DPPC liposomes at the AS state is shown in figure 5H. Since the contribution of the first PC is overwhelmingly high (>98%) for all the three lipids and for all the three states, we consider only the first PC for further analysis. We then fit the first PC ($\Delta\alpha^{l}_{PC}(\nu)$) of three distinct states of each liposome using the damping equation 5.1 and the fitted parameters are summarized in figure 5I and table 5e.

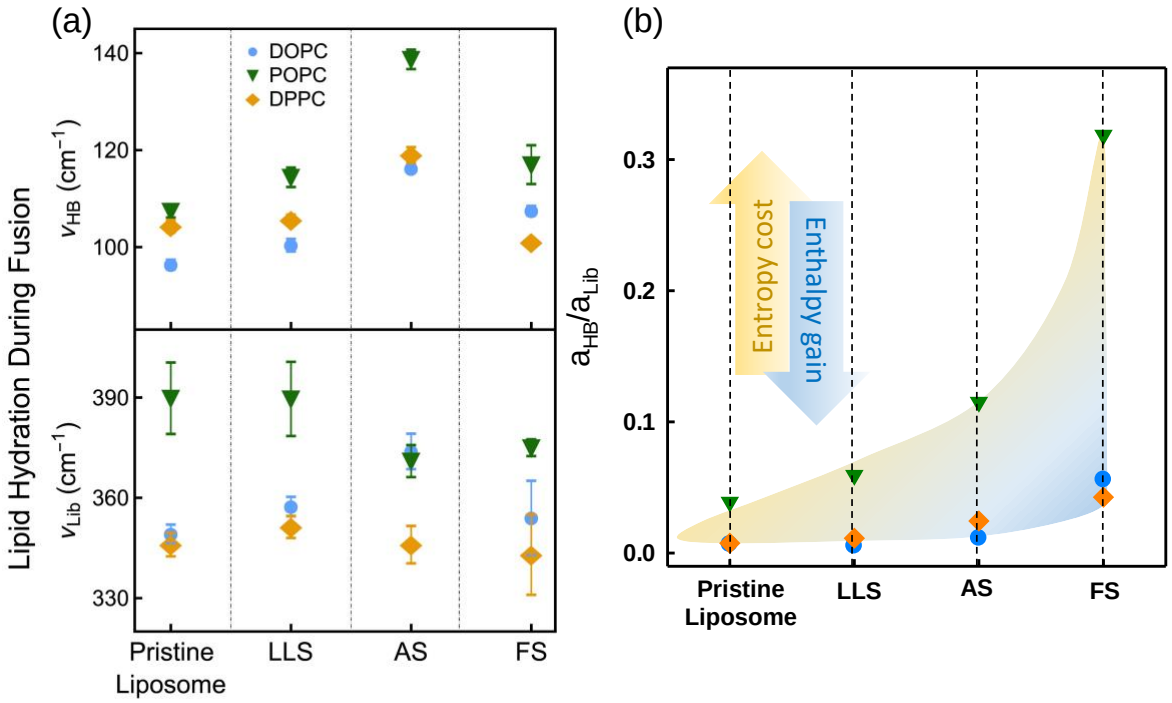

Figure 5I. (a) Peak frequency of intermolecular HB stretching (ν_{HB}) and libration (ν_{Lib}) mode of interfacial water at different states (LLS, AS & FS) during membrane fusion pathway. of three different during the fusion pathway. (b) The ratio of amplitude of HB and libration band of water in the different states of membrane fusion.

Discussion: Our present in-vitro study using model lipid vesicles mimics cellular counterparts and therefore provides insights into the basic structural events necessary for membrane fusion

with a focus on the alteration of the associated hydration dynamics. From the thermodynamic point of view, the change in the membrane mechanical strain, which is a prerequisite for membrane fusion, is closely dependent on the activity of water on both sides of the membrane. It has been predicted that the dynamic equilibrium between the 'hardcore water' and the 'loosely bound water' at the membrane interface dictates its surface pressure; and while estimating such equilibrium, organization of water beyond the first solvation shell should also be taken into consideration.[48] Conventional spectroscopic techniques probe mostly the first solvation shell while THz spectroscopy extracts information beyond the first solvation shell, and therefore is a very suitable tool to investigate membrane fusion.

We choose three lipids which differ in their chain length and saturation, keeping the head group same. DOPC (18:1) and DPPC (16:0) have equal number of C-atoms in both the chains, with the former having one double bond in each of the chains while the latter is fully saturated (scheme 2IV). POPC (16:0-18:1) has different tail lengths (16 and 18) with one double bond in one of the chains. The choice of the lipids is based on the fact that membrane fusion is often assisted with the kink(s) it generates in presence of solutes/proteins, and any asymmetry in the bilayer structure could induce its formation. We, in fact, observe that the lipid with asymmetry (POPC) offers contrasting behaviour in comparison to the other two lipids.

PEG exerts an osmotic stress on membranes as it withdraws water from its surface which in turn creates high membrane tension, and at certain PEG concentration, it exceeds the bilayer tensile strength which causes the vesicle to rupture.[49] In the present investigation we found that liposome aggregates start forming at a low (2-10 wt.%) PEG concentration. We also check the fusion process using a lower molecular weight PEG-200; we observe no structural alteration of pristine liposomes up to ~10 wt.%, and fusion initiates only beyond that concentration. A previous study shows that osmotic pressure of PEG solutions follows a second order polynomial relation with PEG concentration and the values are comparable for PEG 400 and PEG 8000.[47] So, it can be concluded from these results that PEG mediated osmotic stress is not the sole factor that governs membrane fusion.[49] Our measurements have unambiguously shown that lipid layers get dehydrated in presence of PEG 4000, even at a low concentration, and this indeed induces the required membrane stress to fuse.

We now discuss the perturbation in hydration. It is observed that in liposomes, both ν_{HB} and ν_{Lib} are red shifted than bulk water. Since the measured $\Delta\alpha$ profiles probe the surface

hydration explicitly, a red shift designates a lack of cooperativity in the tetrahedral water network at the interface.[45] As the liposomes aggregate, these frequencies suffer a blue shift, the shift being the highest in the *AS* state and for POPC. This blue shift results from the release of trapped water from the membrane interface to the bulk. Note that the peak frequency is comparable to that of bulk water for the AS state in POPC; this suggest the most efficient packing of liposomes with the release of surface water (dehydration) as the aggregated state is formed. Interestingly, in the *FS*, the peak frequencies are lower than that in the *AS*, indicating further rearrangement in surface hydration as the phase changes.

We finally investigate the energetic cost of this aggregation process using a concept of solute hydration model of THz calorimetry. According to this model the free energy change in biomolecular condensation process could be summarized in terms of two contributions: (i) to create a cavity in the water continuum by distorting bulk water network and (ii) to introduce a solute inside the cavity.[50,51] While cavity formation is mostly dominated by an entropic cost, the solute solvation process is enthalpy driven. The difference spectra $\Delta\alpha(\nu)$ manifests the various H-bond modes in the vicinity of solutes, and therefore also corresponds to the solute induce changes in the hydration network associated enthalpy and entropy changes. As discussed earlier, the difference spectra can be deconvoluted into two curves, HB-stretch and libration of the interfacial water. It has been shown that for amphiphilic solutes the amplitude(s) of the HB and Lib bands holds a 1:1 correlation with the specific solvation energetics, and therefore estimating the amplitudes of the $\Delta\alpha(\nu)$ fitted curves enables one to determine hydrophobic and hydrophilic contributions.[50] From the fitted data (table 5f) we estimate and plot the relative amplitude a_{HB}/a_{Lib} for different aggregated states for the different lipids (figure 5Ib). It should be noted here that the $\Delta\alpha(\nu)$ profiles take care of the PEG mediated change of bulk hydration and so also its contribution (if any) towards the corresponding energetics. So the energetic parameters from the analysis can safely be treated as those originating from the PEG-induced fusion process solely. We observe that the ratio increases as the liposomes aggregate, the trend is subtle in case of DOPC and DPPC while in POPC the increase is significant. Since we have performed the experiments at ambient temperature only, we are unable to estimate the entropy and enthalpy changes independently, however, the a_{HB}/a_{Lib} ratio provides with a direct estimate of the relative contribution of entropy and enthalpy to the process involved. It is also important to remember here that the energetics obtained with the analysis is purely those due to solvation change at the interface and does not necessarily correlate linearly with the overall energetic parameters as obtained from

calorimetric experiments. The observed increase in the ratio a_{HB}/a_{Lib} (figure 5Ib) indicates an increase in the solvation entropy as aggregation proceeds. In pristine liposome, the enthalpy of solvation dominates over the cavity formation cost. As the liposomes start aggregating, the entropy cost starts growing, the effect being most prominent in POPC. As discussed earlier, the PEG mediated pressure difference membrane interface leads to the formation of kink(s) and eventually the aggregations. The asymmetry of the POPC molecule eventually makes the entropic cost.

Conclusion: our results provide direct experimental evidence that during PEG mediated membrane fusion, the membrane interface does undergo dehydration, the extent of which is dependent on the lipid structure and on the PEG concentration, as various aggregated phases emerge. We also found that the process of dehydration and fusion is associated with a substantial solvation entropic cost, which is noticeably higher for asymmetric POPC than symmetric DOPC or DPPC. In order to establish whether such a dependency is lipid intrinsic, a detailed systematic study is underway in our lab.

Table 5a. Concentration of PEG 4000 at different state of lipids.

	LLS	**AS**	**FS**
DOPC	$0 \leq [PEG] \leq 0.5$	$1 \leq [PEG] \leq 25$	$25 \leq [PEG]$
POPC	$0 \leq [PEG] \leq 0.5$	$1 \leq [PEG] \leq 25$	$25 \leq [PEG]$
DPPC	$0 \leq [PEG] < 0.5$	$0.5 \leq [PEG] \leq 7$	$10 \leq [PEG]$

Table 5b. Hydrodynamic diameter of liposomes (DOPC,POPC and DPPC) at different concentration of PEG 4000

DOPC		POPC		DPPC	
[PEG 4000] (wt%)	Hyd. Dia (um)	[PEG 4000] (wt%)	Hyd. Dia (um)	[PEG 4000] (wt%)	Hyd. Dia (um)
0	0.1	0	0.1	0	0.1
0.1	0.1	0.1	0.1	0.5	0.1
0.5	0.1	0.5	0.1	1	1.1
1	1.3	1	1.0	3	2.3
3	1.5	2	1.5	7	4.2
5	1.5	3	1.5	10	2.3
7	1.7	5	5.6	15	2.0
10	5.6	10	5.6	20	1.7
12	5.6	12	5.6	25	2.3
15	5.6	15	5.6	30	2.0
20	4.2	20	4.8	32	1.0
25	3.1	25	2.7		
30	2.3	30	2.3		
32	1.7	32	2.3		
35	1.7				

Table 5c. Peak frequency both HB-stretch and librational motion for three liposomes. Data are fitted by using damped harmonic oscillator equation:

DOPC			POPC			DPPC		
PEG (wt%)	ν_{HB} (cm^{-1})	ν_{Lib} (cm^{-1})	**PEG (wt%)**	ν_{HB} (cm^{-1})	ν_{Lib} (cm^{-1})	**PEG (wt%)**	ν_{HB} (cm^{-1})	ν_{Lib} (cm^{-1})
0	96.5±1	349.2±2.8	0	107.4±2.3	389.8±10.7	0	104.3±1.4	346.0±3.5
0.5	100.4±1.3	357.1±2.9	0.5	114.3±2	389.6±19.1	0.5	105.6±1.2	351.3±3.3
3	80.6± 2.5	330.6±2.8	3	119.8±1	376.6±6.3	1	121.3±0.9	348.3±3.9
5	89.2±0.5	326.3±3.2	5	113.7±0.3	368.1±5.9	3	105.8±2.8	338.5±2.6
7	136.3±1.8	303.2±5.5	7	166.1±1.6	362.4±4.5	5	130.2±1.8	362.6±11.8
10	125.7±1.1	276.4±0.8	10	119.5±13	356.3±4.9	7	97.8±6.1	360.3±19.5
15	100.6±9.3	382.3±4.8	15	161.7±6.7	384.7±7.6	10	137.3±2.2	305.9±0.4
20	161.6±3.7	440.8±6.8	20	129.9±3.1	387.4±7.6	15	129.8±2.3	360.9±27.5
25	144.4±1.6	347.9±4.6	25	123.5±1.4	331.6±10.8	25	117.4±2.2	336.5±4.9
30	138.9±1.7	321.1±3.7	30	123.1±1.4	382.5±17.7	30	91.5±0.4	349.4±4.2

Table 5d. Peak frequency both HB-stretch and librational motion for PEG 4000. Data are fitted by using damped harmonic oscillator equation:

PEG (wt%)	ν_{HB} (cm^{-1})	ν_{Lib} (cm^{-1})
0.5	140.0±8.2	372.8±17.4
3	130.5±7.3	375.4±7.8
5	128.7±2.4	361.8±2.7
7	123.6±0.3	371.3±4.9
10	124.2±0.4	370.4±2.7
15	122.6±0.5	371.4±3
20	123.1±0.5	373.3±2.8
25	122.7±5	379.9±3.1
30	123.2±5.1	380.1±0.2

Table 5e. Peak frequency both HB-stretch and librational motion for three liposomes after performing PCA. Data are fitted by using damped harmonic oscillator equation:

	DOPC		**POPC**		**DPPC**	
	ν_{HB} (cm^{-1})	ν_{Lib} (cm^{-1})	ν_{HB} (cm^{-1})	ν_{Lib} (cm^{-1})	ν_{HB} (cm^{-1})	ν_{Lib} (cm^{-1})
Pristine Liposome	96.5±1	349.2±2.8	107.4±2.3	389.8±10.7	104.3±1.4	346.0±3.5
LLS	100.4±1.3	357.1±2.9	114.3±2	389.6±19.1	105.6±1.2	351.3±3.3
AS	116.2±0.6	373.9±5.3	138.7±2	371±4	119±1.6	346±5.6
FS	107.5±1	354±11	117±4	375±2.4	101±0.6	343± 12

Table 5f. Amplitude and relative amplitude of both HB-stretch and librational motion for three liposomes after performing PCA. Data are fitted by using damped harmonic oscillator equation:

	DOPC			**POPC**			**DPPC**		
	A_{HB}	A_{Lib}	A_{HB}/A_{Lib}	A_{HB}	A_{Lib}	A_{HB}/A_{Lib}	A_{HB}	A_{Lib}	A_{HB}/A_{Lib}
Pristine Liposome	-940.7	-141247.4	0.007	-7317.3	-187880.4	0.039	-883.4	-117993.5	0.007
LLS	-679.9	-126642.1	0.005	-10783.5	-181601.6	0.059	-1134.1	-100539.7	0.011
AS	-1629.6	-143177.0	0.011	-27689.6	-240607.0	0.115	-3425.8	-140100.0	0.024
FS	-2715.5	-48590.2	0.056	-8766.6	-27505.5	0.319	-1116.5	-26224.4	0.043

5IV. References:

(1) Jahn, R.; Sudhof, T. C. Membrane Fusion and Exocytosis. *Annu. Rev. Biochem.* **1999**, *68*, 863–911.
(2) Jahn, R.; Lang, T. Membrane Fusion. *Cell* **2003**, *112*, 519–533.
(3) Chernomordik, L.; Kozlov, M. M. Mechanics of Membrane Fusion. *Nat. Struct. Mol. Biol. 15*, 675–683.
(4) Kielian, M.; Rey, F. A. Virus Membrane-Fusion Proteins: More than One Way to Make a Hairpin. *Nat. Rev. Microbiol.* **2006**, *4*, 67–76.
(5) Kozlov, M. M.; Leikin, S. L.; Chernomordik, L. V.; Markin, V. S.; Chizmadzhev, Y. A. Stalk Mechanism of Vesicle Fusion Intermixing of Aqueous Contents. *Eur. Biophys. J.* **1989**, *17*, 121–129.
(6) Aeffner, S.; Reusch, T.; Weinhausen, B.; Salditt, T. Energetics of Stalk Intermediates in Membrane Fusion Are Controlled by Lipid Composition. *Proc. Natl. Acad. Sci. U.S.A.* **2012**, *109*, E1609–E1618.
(7) Skehel, J. J.; Wiley, D. C. Receptor Binding and Membrane Fusion in Virus Entry: The Influenza Hemagglutinin. *Annu. Rev. Biochem.* **2000**, *69*, 531–569.
(8) Lentz, B. R.; Malinin, V.; Haque, M. E.; Evans, K. Protein Machines and Lipid Assemblies: Current Views of Cell Membrane Fusion. *Curr. Opin. Struct. Biol.* **2000**, *10*, 607–615.
(9) Südhof, T. C.; Rothman, J. E. Membrane Fusion: Grappling with SNARE and SM Proteins. *Science* **2009**, *323*, 474–477.
(10) Hua, Y.; Scheller, R. H. Three SNARE Complexes Cooperate to Mediate Membrane Fusion. *Proc. Natl. Acad. Sci. U.S.A.* **2001**, *98*, 8065–8070.
(11) Stroupe, C.; Hickey, C. M.; Mima, J.; Burfeind, A. S.; Wickner, W. Minimal Membrane Dockin Requirements Revealed by Reconstitution of Rab GTPase Dependent Membrane Fusion from Purified Components. *Proc. Natl. Acad. Sci. U.S.A.* **2009**, *106*, 17626–17633.
(12) McNew, J. A.; Weber, T.; Parlati, F.; Johnston, R. J.; Melia, T. J.; Sollner, T. H.; Rothman, J. E. Close Is Not Enougth: SNARE-Dependent Membrane Fusion Requires an Active Mechanism That Transduces Force to Membbrane Anchors. *J. Cell. Biol.* **2000**, *150*, 105–117.
(13) Tahir, M. A.; Guven, Z. P.; Arriaga, L. R.; Alexander-Katz, A. Calcium-Triggered Fusion of Lipid Membranes Is Enabled by Amphiphilic Nanoparticles. *Proc. Natl. Acad. Sci. U.S.A.* **2020**, *117*, 18470–18476.
(14) Shi, S.; Markl, A. M.; Lu, Z.; Liu, R.; Hoernke, M. Interplay of Fusion, Leakage, and Electrostatic Lipid Clustering: Membrane Perturbations by a Hydrophobic Antimicrobial Polycation. *Langmuir* **2022**, *38*, 2379–2391.
(15) MacDonald, R. I. Membrane Fusion Due to Dehydration by Polyethylene Glycol, Dextran, or Sucrose. *Biochem.* **1985**, *24*, 4058–4066.
(16) Lentz, B. R. PEG as a Tool to Gain Insight into Membrane Fusion. *Eur. Biophys. J.* **2007**, *36*, 315–326.

(17) Lentz, B. R.; Lee, J. Poly(Ethylene Glycol) (PEG)-Mediated Fusion between Pure Lipid Bilayers: A Mechanism in Common with Viral Fusion and Secretory Vesicle Release? *Mol. Membr. Biol.* **1999**, *16*, 279–296.
(18) Holland, J. W.; Hui, C.; Cullis, P. R.; Madden, T. D. Poly(Ethylene Glycol)-Lipid Conjugates Regulate the Calcium-Induced Fusion of Liposomes Composed of Phosphatidylethanolamine and Phosphatidylserine. *Biochem.* **1996**, *35*, 2618–2624.
(19) Tyrrell, J.; Weeks, K. M.; Pielak, G. J. Challenge of Mimicking the Influences of the Cellular Environment on RNA Structure by PEG-Induced Macromolecular Crowding. *Biochem.* **2015**, *54*, 6447–6453.
(20) Deshwal, A.; Maiti, S. Macromolecular Crowding Effect on the Activity of Liposome-Bound Alkaline Phosphatase: A Paradoxical Inhibitory Action. *Langmuir* **2021**, *37*, 7273−7284.
(21) Liu, G.; Li, Y.; Yang, L.; Wei, Y.; Wang, X.; Wang, Z.; Tao, L. Cytotoxicity Study of Polyethylene Glycol Derivatives. *RSC Adv.* **2017**, *7*, 18252–18259.
(22) Mostafavi, H.; Thiyagarajan, S.; Stratton, B. S.; Karatekin, E.; Warner, J. M.; Rothman, J. E.; O'Shaughnessy, B. Entropic Forces Drive Self-Organization and Membrane Fusion by SNARE Proteins. *Proc. Natl. Acad. Sci. U.S.A.* **2017**, *114*, 5455–5460.
(23) Gong, B.; Choi, B. K.; Kim, J. Y.; Shetty, D.; Ko, Y. H.; Selvapalam, N.; Lee, N. K.; Kim, K. High Affinity Host−Guest FRET Pair for Single-Vesicle Content-Mixing Assay: Observation of Flickering Fusion Events. *J. Am. Chem. Soc.* **2015**, *137*, 8908–8911.
(24) Stevens, M. J.; Hoh, J. H.; Woolf, T. B. Insights into the Molecular Mechanism of Membrane Fusion from Simulation: Evidence for the Association of Splayed Tails. *Phys. Rev. Lett.* **2003**, *91*, 188102.
(25) Witkowska, A.; Jahn, R. Rapid SNARE-Mediated Fusion of Liposomes and Chromaffin Granules with Giant Unilamellar Vesicles. *BioPhys. J.* **2017**, *113*, 1251–1259.
(26) Perez, M. A.; Beales, P. A. Biomimetic Curvature and Tension-Driven Membrane Fusion Induced by Silica Nanoparticles. *Langmuir* **2021**, *37*, 13917−13931.
(27) Pattnaik, G. P.; Chakraborty, H. Fusogenic Effect of Cholesterol Prevails over the Inhibitory Effect of a Peptide-Based Membrane Fusion Inhibitor. *Langmuir* **2021**, *37*, 3477−3489.
(28) Chakraborty, H.; Tarafdar, P. K.; Lentz, B. R. A Novel Assay for Detecting Fusion Pore Formation: Implications for the Fusion Mechanism. *Biochemistry* **2013**, *52*, 8510−8517.
(29) Meher, G.; Bhattacharjya, S.; Chakraborty, H. Membrane Cholesterol Modulates Oligomeric Status and Peptide- Membrane Interaction of Severe Acute Respiratory Syndrome Coronavirus Fusion Peptide. *J. Phys. Chem. B* **2019**, *123*, 10654−10662.
(30) Schwaab, G.; Sebastiani, F.; Havenith, M. Ion Hydration and Ion Pairing as Probed by THz Spectroscopy. *Angew. Chem. Int. Ed.* **2019**, *58*, 3000–3013.
(31) Schmidt, D. A.; Birer, O.; Funkner, S.; Born, B. P.; Gnanasekaran, R.; Schwaab, G. W.; Leitner, D. M.; Havenith, M. Rattling in the Cage: Ions as Probes of Sub-Picosecond Water Network Dynamics. *J. Am. Chem. Soc.* **2009**, *131*, 18512–18517.
(32) Pyne, P.; Mitra, R. K. Excipients Do Regulate Phase Separation in Lysozyme and Thus Also Its Hydration. *J. Phys. Chem. Lett.* **2022**, *13*, 931–938.
(33) Yamamoto, N.; Andachi, T.; Tamura, A.; Tominaga, K. Temperature and Hydration Dependence of Low-Frequency Spectra of Lipid Bilayers Studied by Terahertz Time-Domain Spectroscopy. *J. Phys. Chem. B* **2015**, *119*, 9359–9368.
(34) Ahlers, J.; Adams, E. M.; Bader, V.; Pezzotti, S.; Winklhofer, K. F.; Tatzelt, J.; Havenith, M. The Key Role of Solvent in Condensation: Mapping Water in Liquid-Liquid Phase-Separated FUS. *Biophys. J.* **2021**, *120*, 1–10.
(35) Pyne, S.; Pyne, P.; Mitra, R. K. Addition of Cholesterol Alters the Hydration at the Surface of Model Lipids: A Spectroscopic Investigation. *Phys. Chem. Chem. Phys.* **2022**, *24*, 20381–20389.
(36) Zhang, W.; Coughlin, M. L.; Metzger, J. M.; Hackel, B. J.; Bates, F. S.; Lodge, T. P. Influence of Cholesterol and Bilayer Curvature on the Interaction of PPO−PEO Block Copolymers with Liposomes. *Langmuir* **2019**, *35*, 7231–7241.
(37) Lee, J.; Lentz, B. R. Evolution of Lipidic Structures during Model Membrane Fusion and the Relation of This Process to Cell Membrane Fusion. *Biochem.* **1997**, *36*, 6251–6259.
(38) Heyden, M.; Sun, J.; Funkner, S.; Mathias, G.; Forbert, H.; Havenith, M.; Marx, D. Dissecting the THz Spectrum of Liquid Water from First Principles via Correlations in Time and Space. *Proc. Natl. Acad. Sci. U.S.A.* **2010**, *107*, 12068–12073.
(39) Pyne, P.; Mitra, R. K. Excipients Do Regulate Phase Separation in Lysozyme and Thus Also Its Hydration. *J. Phys. Chem. Lett.* **2022**, *13*, 931–938.
(40) Born, B.; Kim, S. J.; Ebbinghaus, S.; Gruebele, M.; Havenith, M. The Terahertz Dance of Water with the Proteins: The Effect of Protein Flexibility on the Dynamical Hydration Shell of Ubiquitin. *Faraday Discuss.* **2009**, *141*, 161–173.

(41) Pal, S.; Samanta, N.; Dasmahanta, D.; Mitra, R. K.; Chattyopadhya, A. Effect of Phospholipid Headgroup Charge on the Structure and Dynamics of Water at the Membrane Interface: A Terahertz Spectroscopic Study. *J. Phys. Chem. B* **2018**, *22*, 5066–5074.
(42) Pyne, S.; Pyne, P.; Mitra, R. K. The Inner Hydration in Surfactant/Cholesterol Vesicles Differs from the Outer One: A Spectroscopic Investigation. *ChemPhysChem*. https://doi.org/10.1002/cphc.202200337.
(43) Ahlers, J.; Adams, E. M.; Bader, V.; Pezzotti, S.; Winklhofer, K. F.; Tatzelt, J.; Havenith, M. The Key Role of Solvent in Condensation: Mapping Water in Liquid-Liquid Phase-Separated FUS. *Biophys. J* **2021**, *120*, 1266–1275.
(44) Ebbinghaus, S.; Kim, S. J.; Heyden, M.; Yu, X.; Heugen, U.; Gruebele, M.; Leitner, D. M.; Havenith, M. An Extended Dynamical Hydration Shell around Proteins. *Proc Natl Acad Sci USA* **2007**, *104*, 20749–20752.
(45) Nibali, V. C.; Pezzotti, S.; Sebastiani, F.; Galimberti, D. R.; Schwaab, G.; Heyden, M.; Gaigeot, M. P.; Havenith, M. Wrapping Up Hydrophobic Hydration: Locality Matters. *J. Phys. Chem. Lett.* **2020**, *11*, 4809−4816.
(46) Hu, J.; Yamahara, H.; Liao, Z.; Yano, Y.; Tabata, H. Characterization of Hydrogen Bond Network of Waters around Polyethylene Glycol by Broadband Dielectric Spectroscopy. *Appl. Phys. Lett.* **2022**, *120*, 023702.
(47) Stanley, C. B.; Strey, H. H. Measuring Osmotic Pressure of Poly(Ethylene Glycol) Solutions by Sedimentation Equilibrium Ultracentrifugation. *Macromolecules* **2003**, *36*, 6888–6893.
(48) Disalvo, E. A.; Pinto, O. A.; Martini, M. F.; Bouchet, A. M.; Hollmann, A.; Frias, M. A. Functional Role of Water in Membranes Updated: A Tribute to Träuble. *Biochim. Biophys. Acta* **2015**, *1848*, 1552–1562.
(49) Burgess, S. W.; McIntosh, T. J.; Lentz, B. R. Modulation of Poly(Ethylene Glycol)-Induced Fusion by Membrane Hydration:Importance of Interbilayer Separation. *Biochemistry* **1992**, *31*, 2653–2661.
(50) Pezzotti, S.; Sebastiani, F.; van Dam, E. P.; Ramos, S.; Nibali, V. C.; Schwaab, G.; Havenith, M. Spectroscopic Fingerprints of Cavity Formation and Solute Insertion as a Measure of Hydration Entropic Loss and Enthalpic Gain. *Angew. Chem. Int. Ed.* **2022**, *61*, e202203893.
(51) Pezzotti, S.; Konig, B.; Ramos, S.; Schwaab, G.; Havenith, M. Liquid−Liquid Phase Separation? Ask the Water! *J. Phys. Chem. Lett.* **2023**, *14*, 1556−1563.

Chapter 6

Alteration of lipid hydration in alcoholic environment: THz Spectroscopic investigation

While many simulation results assist that ethanol can modulate the structure of liposomes and promotes the transformation of lipid bilayer to non-bilayer structure, but the role of hydration during such structural alteration has remained almost unaddressed. Here experimentally we explore explicit hydration behaviour of model lipid POPC in presence of alcohols (ethanol and TFE) by using THz-FTIR spectroscopy in the frequency window of 1.5-13.5 THz. Then we check how cholesterol mediated lipid hydration is altered in presence of alcohols. DLS and electron microscopy suggests the deformation of bilayer structure in presence of alcohols. Our hydration results yield that H-bond network gets strengthen at lipid water interface in presence of alcohols and cholesterol does modulates this water structure.

6I. Introduction:

Membrane fluidity plays a vital role to pass the ions, molecules through it to alive the intracellular environments.[1,2] The major factors which alters the membrane bilayer fluidity is the bilayer composition and temperature.[3,4] Cholesterol plays a vital role to maintain the structural integrity and fluidity of animal cell membranes which does reside into the cell membrane.[5] Mammalian cell membrane is highly enriched by cholesterol (~30% of total lipid) and in the red blood cell it could rise up to ~50%.[6,7] Cholesterol exerts a condensing effect into the liquid crystalline phase i.e., it increases the thickness of lipid bilayer and reduces the lateral mobility of lipid membrane.[6]

Ethanol is a small amphiphilic molecule which can also alters the fluidity and structural integrity of lipid membranes.[8] The modulation of function and characteristics of plasma membrane by such pharmaceutically active pathogen molecule is crucial for many biological and biomedical applications including drug delivery, aesthesia, cryo-preservation and permeation enhancement.[9–12] Ethanol has a disordering effect on hydrophobic carbon chain of lipid, increasing the area per head group of lipid and the overall fluidity of the membrane.[13,14] Ethanol has a large number of applications in biotechnology, toxicology and in medical industry as it has the ability to modify lipid's structure.[9,15,16] Very interestingly ethanol is used as a disinfectant to kill the pathogen activity of virus and bacteria; it is hugely used in sanitizers

as it can penetrate and damage the membrane of virus and bacteria and also prevents the transmission of bacterial and viruses' infections.[17,18] Gurtovenko *et al.*[19] studied the effect of ethanol on a model lipid POPC and found that ethanol promotes the transformation of lipid bilayer to non-bilayer structure. Patra *et al.*,[20] using classical MD simulations, reported that ethanol can form hydrogen bonds with the lipid's headgroup and also locates at the lipid head-tail interface. Recently Shobhna *et al.*,[21] using CG-MD simulations, explored the structural perturbation of POPC lipid membrane in presence of ethanol. At low to moderate concentration of ethanol (up to 30%), they found the swelling and aggregation of liposomes and at high ethanol concentration, they even observed the rupturing of bilayer surface. Like ethanol, 2,2,2-trifluoroethanol (TFE) also alters the stability and characteristics of lipid bilayer as well as it modulates the function of membrane proteins.[22,23] Even at high concentration of TFE, it causes the micellar aggregation, reduce acyl chain order and lipid phase transition temperature.[24,25] Zhang *et al.*[26] both experimentally and theoretically studied the effect of different fluoroalcohols (TFE, HFIP, PFTB) on 1,2-dierucoyl-sn-glycero-3-phosphocholin ($DC_{22:1}PC$) lipid bilayer. They found that TFE disrupts bilayer more than PFTB does, and at higher concentration it leads to bilayer disintegration.

While several experimental and theoretical studies reveal the structural perturbation of lipid surface in presence of alcohols but hydration studies have been paid less attention. Questions remain elusive that (i) how the water structure at lipid-water interface is altered in presence of alcohols and (ii) how this phenomenon occurs on cholesterol embedded lipid environment knowing the fact that cholesterol suppress the damaging of lipid membrane caused by ethanol. To search the answer of this questions, we have studied the effect of two alcohols: ethanol and TFE on a model lipid in absence and in presence of cholesterol by using THz spectroscopy. Recently our group has explored the hydration behavior of different charged lipid in presence of cholesterol using far-FTIR (THz) spectroscopy.[27] We observe that the water structure in lipid-water interface becomes weaker and dynamics get accelerated in presence of cholesterol. Now we focus how this water structure is altered in presence of alcohols.

Now a days THz spectroscopy has emerged as a label free, non-invasive powerful technique to measure the collective H-bond network of water molecules associated with biomolecules.[28–31] As it directly probes the fluctuations in the collective dipole moment of water molecules, any change will manifest the hydration of biomolecules.[32–34] Here we use the THz radiation in between 50-450 cm^{-1} and collect the absorption coefficient by using far-FTIR (THz) spectroscopy. We prepare 2-oleoyl-1-palmitoyl-sn-glycero-3-phosphocholine (POPC)

liposome in absence and in presence of cholesterol. We have studied the structural perturbation of liposomes in presence of two alcohols by using dynamic light scattering and field-emission scanning electron microscopic technique. Hydration behavior was probed by using FAR-FTIR spectroscopy. Hydration study yields that water structure at lipid water interface becomes stronger and more restricted in presence of two alcohols and the effect is more prominent in case of TFE.

6II.Materials and Methods:

POPC (2-Oleoyl-1-palmitoyl-sn-glycero-3-phosphocholine) and Cholesterol were procured from Avanti polar lipid with highest purity (>99%) and used without any further purification. Ethanol and chloroform were procured from Merk and 2,2,2-trifluoroethanol was obtained from TCI. Milli-Q water was filtrated with a 0.2 μm filter prior to prepare the PBS. 50 mM PBS (phosphate buffer saline) of pH 7.4 were used for preparing the liposomes. Liposomes preparation technique is described in section 2II.a.iii. All the used instruments are described in section 2.III.

6III. Results and Discussions:

Dynamic Light Scattering measurements: We measure the hydrodynamic diameter (d_H) of liposomes (POPC and cholesterol mediated POPC) by using dynamic light scattering (DLS) technique. Hydrodynamic diameter of POPC liposomes appear at ~106 nm while that for the cholesterol mediated POPC liposomes arises at ~ 122 nm. In our earlier study, we observe that when cholesterol is inserted into liposomes, the d_H of liposome increases.[27] Now we measure the hydrodynamic diameter of liposomes in presence of ethanol and its fluro-derivative 2,2,2-trifluoroethanol (TFE). Figure 6Aa is the representative DLS profiles for POPC liposome with varying the concentration of ethanol (upper panel) and TFE (lower panel). In presence of alcohols, size of the liposomes increases gradually up to 30% (figure 6A(a,c)) and beyond that we observe the appearance of smaller size of particles or small globules at high concentration of TFE (figure 6Aa, lower panel). It has been shown theoretically that high concentration of ethanol causes the destruction of lipid bilayer and transformed it into “inverse micelle” like structures within the bilayer interior.[19] Here we cannot find the smaller globule for ethanol that could be irrecoverable in present size window in DLS technique, but we observe it for TFE. Then we have done same experiments for cholesterol mediated POPC liposomes (figure 6Ab). Interestingly, similar size alteration has been observed for cholesterol mediated POPC liposomes with alcohols content but the values of d_H is distinct (figure 6Ab,d). DLS results confirm us the structural modification of thus prepared two liposomes with alcohol content.

Scanning electron microscopic measurements: To visualize the morphological structure of these two liposomes in presence of alcohols, we use field emission scanning electron microscopic (FESEM) technique. In POPC liposome, we observe the spherical structure of particles (figure 6Aei). For ethanol=60%, we identify the appearance of small particles inside the giant spherical structured liposomes, providing the direct evidence of formation of inverted micelle from lipid bilayer (figure 6Ae(ii-iii)). We also observe similar structural perturbation of liposomes (signature of inverted micelle) at higher concentration of TFE (figure 6Aeiv).

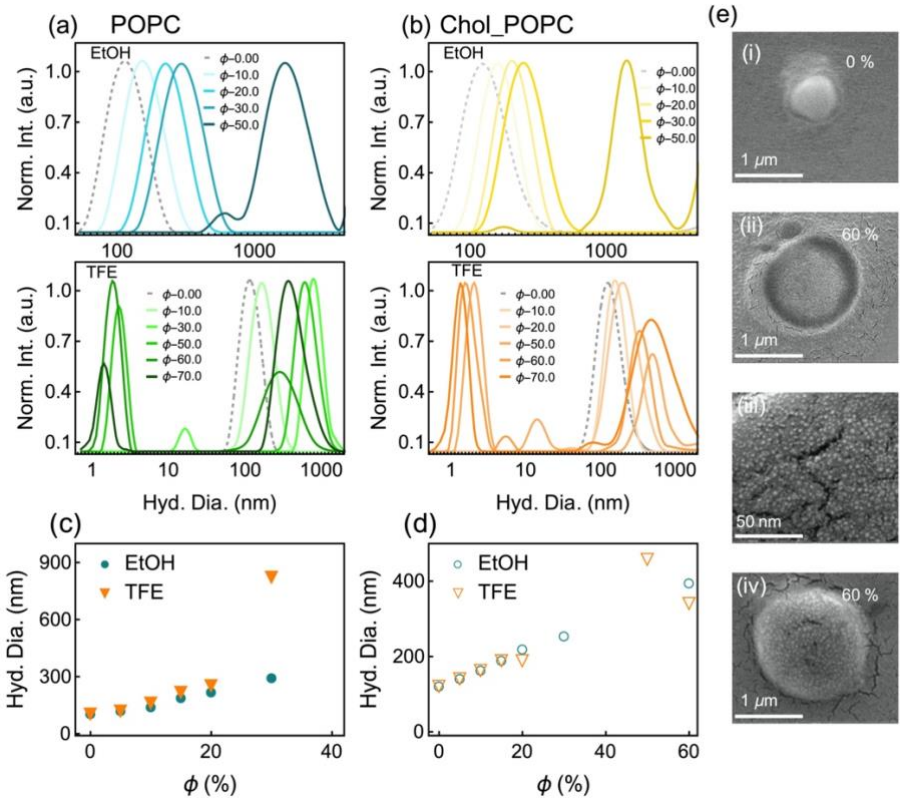

Figure 6A. (a) DLS profile of POPC liposome with the concentration of ethanol (upper panel) and TFE (lower panel). (b) DLS profile of cholesterol mediated POPC liposome with the concentration of ethanol (upper panel) and TFE (lower panel). Hydrodynamic diameter of (c) POPC & (d) cholesterol mediated POPC liposome as a function of two alcohols respectively. (e) SEM images of POPC liposomes at (i) 0% (ii) 60% ethanol; (iii) inverted micelle inside liposome and (iv) 60% TFE.

Steady-state anisotropy measurements:

To visualize the structural perturbation of lipid bilayer in presence of alcohols, we have done the steady-state anisotropy measurements. 1,6-Diphenyl-1,3,5-hexatriene (DPH) is mostly used to probe the fluidity or microviscosity in the acyl chain region of lipid membrane.[35,36] DPH fluorescence anisotropy provides the information of microviscosity or fluidity of bilayer. Here we have used DPH as a fluorophore to determine the structural features of lipid bilayers in presence of alcohols. Figure 6Ba shows the anisotropy values for two liposomes with ethanol contents and the anisotropy values are listed in table 6a. The steady-state anisotropy value of POPC liposome is ~0.1 but in cholesterol loaded liposomes, it becomes ~0.2 which is much more than bare liposomes. Our findings reflect that when cholesterol is incorporated into liposome, the acyl chain of lipid becomes more ordered.[37] As the concentration of ethanol is increased the anisotropy value for both lipid systems decreases gradually (figure 6Ba), indicating an increase in the bilayer fluidity with increasing ethanol concentration. But in presence of TFE, anisotropy value is decreasing up to 30%, then start to increasing for both liposomes.

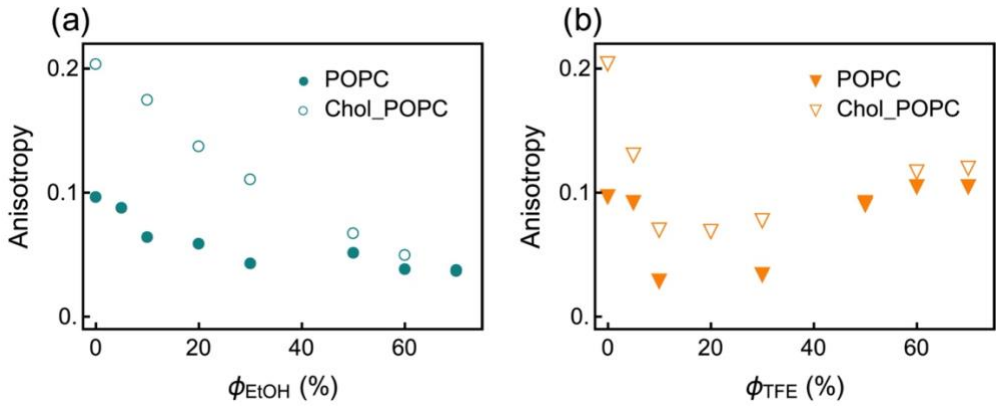

Figure 6B. Steady-state anisotropy value of POPC and cholesterol mediated POPC liposomes in presence of (a) EtOH and (b) TFE.

Far-FTIR (THz) measurements: We now monitor the hydration behaviour of liposomes by using far-IR spectroscopy. We measure the absorbance coefficient of two liposomes in presence of both alcohols in the terahertz frequency region between 50-450 cm^{-1} (1.5-13.5 THz). In this terahertz regime, bulk water exhibits two intense peaks (figure 6Ca): 136 cm^{-1} corresponding to hindered translational motion of water molecules or HB-stretch and another is at ~ 475 cm^{-}

[1] due to the hindered rotational motion of water molecules (librational motion).[38,39] For liposomes, $\alpha(\nu)$ shifts to lower value compare to bulk water as water molecules are replaced by low absorbing lipid molecules, the phenomena named as "THz deficit" (figure 6Cb).[27,29]

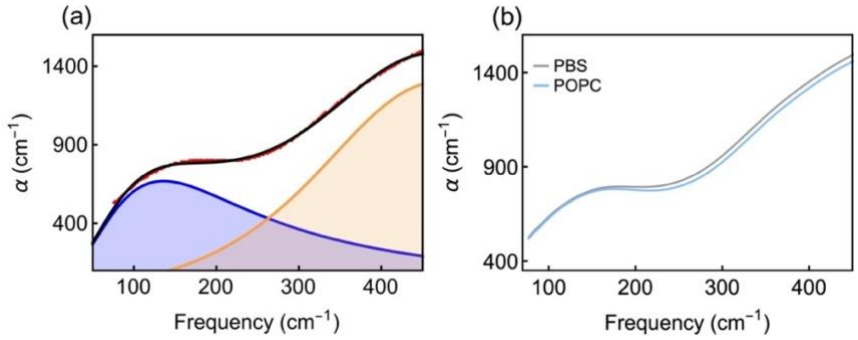

Figure 6C. (a) Representative fitted profile for water. Red curve shows the raw data of water, black line shows the total fitted data. Blue curve indicated HB-stretch and orange curve indicates libration motion of water molecule. (b) absorption coefficient as a function of frequency for bulk water and POPC liposomes (300 μM).

To extract the explicit hydration of liposomes we calculate $\Delta\alpha\ (\nu)$ ($\Delta\alpha(\nu) = \alpha_{liposome}(\nu) - \alpha_{buffer}(\nu)$; difference between absorbance coefficient). We would obtain a finite value of $\Delta\alpha\ (\nu)$ which unambiguously established an altered hydration around liposomes. Now we are focusing on the microscopic picture of water structure around liposome, we fit $\Delta\alpha\ (\nu)$ profile by using a damped harmonic oscillator model[28], assuming the fluctuating dipole moment followed the damped harmonic oscillator motion:

$$\Delta\alpha(\nu) = \sum_{i=1}^{2} \frac{a_i \omega_i \nu^2}{\nu^2\omega_i^2 + \pi^2\left(\nu_i^2 + \frac{\omega_i^2}{4\pi^2} - \nu^2\right)^2} \qquad (6.1)$$

where a_i, ω_i, ν_i are the amplitude, width and the centre frequency of the i^{th} resonance. The unperturbed centre frequency is given as

$$\nu_{0,i} = \sqrt{\nu_i^2 + \frac{\omega_i^2}{4\pi^2}}.$$

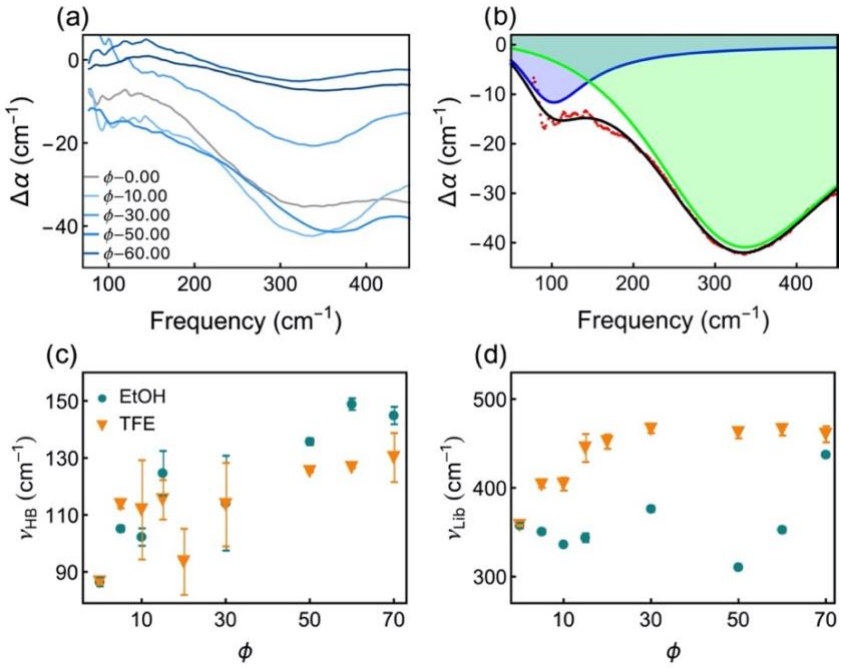

Figure 6D. (a) Representative profiles of change in absorption coefficient ($\Delta\alpha(\nu) = \alpha^{sol}_{liposome}(\nu) - \alpha^{sol}_{ethanol}(\nu)$) as a function of frequency with increasing ethanol concentration. (b) Representative fitting of $\Delta\alpha(\nu)$ profile for POPC liposome (in presence of [ethanol]= 10%) using a damped harmonic oscillator model (equation 6.1). The red broken curve represents the raw data and the black solid line stands for the total fitting. The 1st peak with frequency ν_{HB} (blue line) represents the hydrogen bond stretch while the 2nd peak with frequency ν_{Lib} (green line) presents the librational motion of water molecules. Peak frequency corresponding to (c) HB stretch and (d) librational mode of lipid hydration with the concentration of both EtOH and TFE.

HB-stretch mode (ν_{HB}) for pristine POPC liposome appears at ~ 86 cm^{-1}, which is 50 cm^{-1} red shifted compared to pure bulk water. ν_{HB} for cholesterol mediated liposomes gets ~ 46 cm^{-1} red shifted to be appearing 90 cm^{-1}. Again, librational motion (ν_{lib}) for bare POPC liposome is appeared at ~ 358 cm^{-1}, almost ~117 cm^{-1} red shifted compared to bulk water. But interestingly, lib mode gets blue shifted (50 cm^{-1}) compared to bulk water in cholesterol mediated POPC liposomes. A red (blue) shift of HB-stretch/lib motion indicates the weaker (or stronger)/less (or more) restricted motion of water molecules at lipid-water interface.[40–42] Our experimental results reflect that water structure becomes weaker and follows less restricted motion across lipid-water interface. In presence of cholesterol water structure gets restricted across lipid-water interfaces.

We then monitor how the lipid hydration is modified in presence of ethanol and TFE; we first focus on the bare lipid (POPC) hydration. To extract the explicit lipid hydration we calculate $\Delta\alpha\,(\nu) = \alpha^{sol}_{liposome}(\nu) - \alpha^{sol}_{alcohol}(\nu)$; Representative $\Delta\alpha\,(\nu)$ profiles for POPC liposomes as a function of frequency with increasing ethanol concentration is shown in figure 6Da. For a quantitative insight we fit $\Delta\alpha\,(\nu)$ profiles by using damped harmonic oscillator model (equation 6.1) (figure 6Db at [EtOH]=10%). The results are depicted in figure 6D(c-d) and table 6b. We found that at low concentration of ethanol (5%), ν_{HB} suffers blue shift (~19 cm^{-1}) compare to bare liposomes and ν_{HB} increases successively towards higher frequency with ethanol contents. In presence of TFE, ν_{HB} follows more or less similar nature as like ethanol but the shift is more prominent in presence of ethanol compare to TFE. ν_{lib} appears at ~ 351 cm^{-1} (7 cm^{-1} red shifted) at [ethanol]=5.0%, and follows a "*rise and dip*" pattern with ethanol concentration. Interestingly, ν_{lib} appears at ~ 404 cm^{-1} at [TFE]=5.0%, with further addition of TFE, ν_{lib} is blue shifted and suffers ~ 103 cm^{-1} blue shift at 70%. Our results reflect that water structure at lipid-water interface becomes more restricted in presence of TFE.

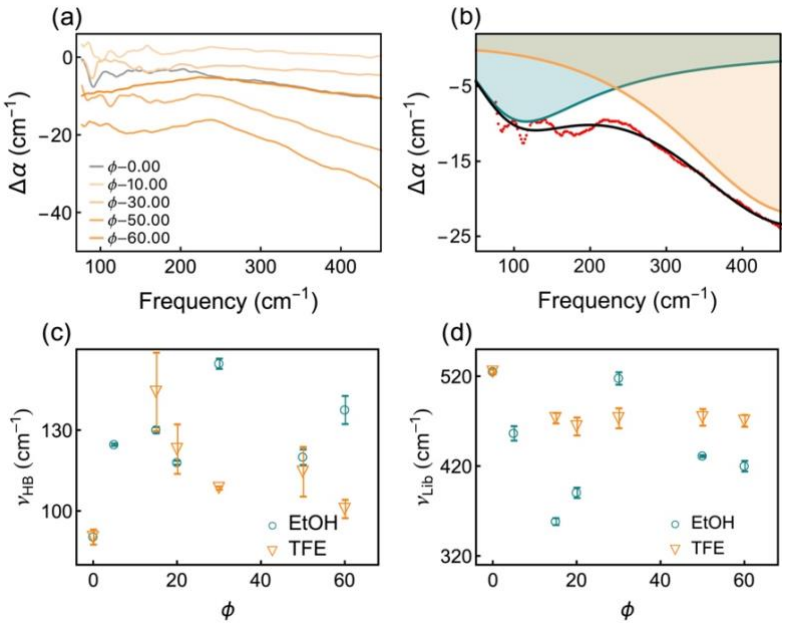

Figure 6E. (a) Representative profiles of change in absorption coefficient $\Delta\alpha(\nu)$ as a function of frequency for cholesterol mediated liposomes with increasing ethanol concentration. (b) Representative fitting of $\Delta\alpha(\nu)$ profile for POPC liposome (in presence of [TFE]= 30%) using a damped harmonic oscillator model (equation 6.1). The red broken curve represents the raw data and the black solid line stands for the total fitting. The 1st peak with frequency ν_{HB} (blue line) represents the hydrogen bond stretch while the 2nd peak with frequency ν_{Lib} (green line) presents the librational motion of water

molecules. Peak frequency corresponding to (c) HB stretch and (d) librational mode of lipid hydration with the concentration of both EtOH and TFE.

We then investigate how the cholesterol mediated lipid hydration is perturbed in presence of ethanol and TFE. Representative $\Delta\alpha\,(\nu)$ profiles for cholesterol mediated liposomes with varying the concentration of alcohols is shown in figure 6Ea. We fit $\Delta\alpha\,(\nu)$ profiles by using same damped harmonic oscillator model (equation 6.1) and results are summarized in figure 6E(c-d) and table 6c. ν_{HB} appears at ~124 cm^{-1} (at [EtOH]=5%), which is 34 cm^{-1} blue shifted and for TFE (15%), ν_{HB} appears at ~ 144 cm^{-1} (figure 6Ec). We observe a non-monotonous behaviour of ν_{HB} with increasing the concentration for both alcohols (figure 6Ec, table 6c). Interestingly, ν_{Lib} follows an oscillatory trend with the concentration of ethanol while ν_{Lib} is ~ 51 cm^{-1} blue shifted at low TFE concentration (TFE 15 %) but at and further addition of TFE, ν_{Lib} does not change appreciably (figure 6Ed, table 6c).

At this point it is important to verify the extent to which the bare ethanol and TFE molecules alter the collective dynamics of bulk water. As a control we study the hydration behaviour of both two alcohols at different concentration. We measure the difference in absorbance coefficient: $\Delta\alpha'(\nu) = \alpha^{sol}_{etoh}(\nu) - \xi_{water}\alpha^{sol}_{water}(\nu) - \xi_{alcohol}\alpha_{alcohol}(\nu)$; where ξ_{water} and ξ_{water} are the correction factors for water and alcohols respectively.

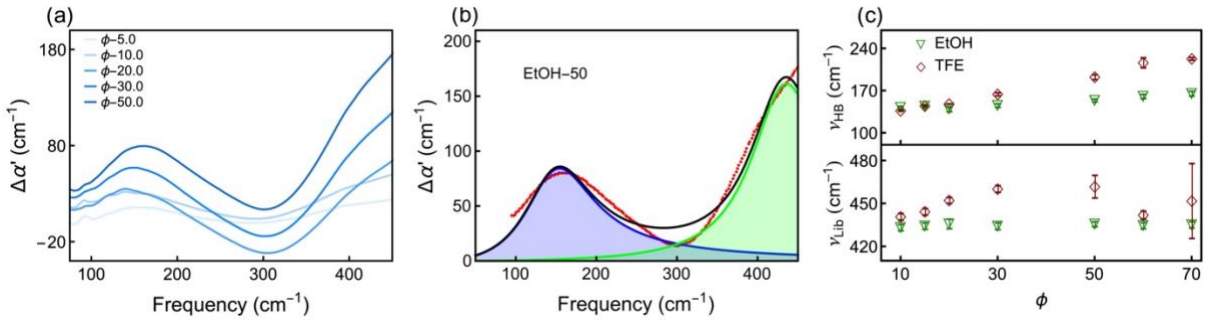

Figure 6F. (a) Representative profiles of change in absorption coefficient ($\Delta\alpha'(\nu)$) as a function of frequency with increasing ethanol concentration. (b) Representative fitting of $\Delta\alpha'(\nu)$ profile for ethanol= 50% using a damped harmonic oscillator model (equation 6.1). The red broken curve represents the raw data and the black solid line stands for the total fitting. The 1st peak with frequency ν_{HB} (blue line) represents the hydrogen bond stretch while the 2nd peak with frequency ν_{Lib} (green line) presents the librational motion of water molecules. Peak frequency corresponding to (c) HB stretch

(upper panel) and librational mode (lower panel) of lipid hydration with the concentration of both EtOH and TFE.

Representative $\Delta\alpha'(\nu)$ profiles at different concentration of ethanol is shown in figure 6Fa. We fit $\Delta\alpha'(\nu)$ profiles by using equation 6.1 and the fitted parameters are presented in table 6d. We observed that with the increasing of alcohol concentration, ν_{HB} shifts to the higher frequency for both EtOH and TFE, but the extend of observed blue shift is much larger for TFE compared to EtOH (figure 6Fc, upper panel). The blue shift of ν_{HB} indicates a strengthening of H-bond network which effect is prominent for more electronegative TFE molecules. For ν_{Lib}, we found a red shift at low concentration of both alcohols compared to water, but the change is nominal with the alcohols content (figure 6Fc, lower panel).

While our results unambiguously established a modification of hydrogen bond network in lipid interface in presence of two alcohols, but both the HB-stretch and librational motion follows a non-regular oscillatory trend in case of specially cholesterol mediated liposomes. At this point, it seems very difficult to reach any alcohols concentration independent definite conclusions.

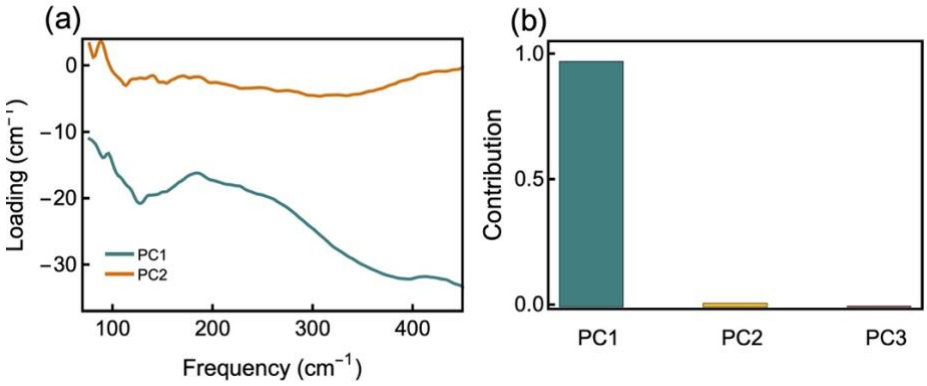

Figure 6G. (a) Representative PCs for cholesterol mediated liposomes in presence of ethanol. (b) Relative contributions of first three components.

We perform principal component analysis on $\Delta\alpha$ of both two liposomes in presence of two alcohols in order to reduce the datasets (see section 2.I.b for PCA analysis details). Representative first two principal components (PCs) for cholesterol mediated POPC liposomes with their contributions are shown in figure 6G. As the first PC carries high contribution (>>98%), we collect the first PC only. For further analysis we fit first PC by using equation 6.1 and collect the peak frequencies which is shown in figure 6H and table 6e. POPC liposomes

suffer ~ 43 cm^{-1} and ~ 38 cm^{-1} blue shift in presence of ethanol and TFE (figure 6Ha) which indicates the stronger HB formation in presence of alcohols in lipid-water interface. Interestingly, for cholesterol mediated POPC liposomes, HB-stretch mode also gets blue shifted (~ 32 cm^{-1} for ethanol and ~ 28 cm^{-1} for TFE) in presence of alcohols but the shifting is less compared to pristine POPC liposomes (figure 6Ha). We found a constructing features of ν_{Lib} for POPC and cholesterol mediated POPC liposomes (figure 6Hb). ν_{Lib} for POPC liposomes remain almost same in presence of ethanol; but in TFE we observe ~ 107 cm^{-1} blue shift which indicates water molecule gets more restricted environment in presence of TFE. For cholesterol mediated POPC liposomes, ν_{Lib} suffers ~103 cm^{-1} and ~ 48 cm^{-1} red shift in presence of ethanol and TFE respectively (figure 6Hb). Water molecules suffer less restricted environment in cholesterol mediated liposomes.

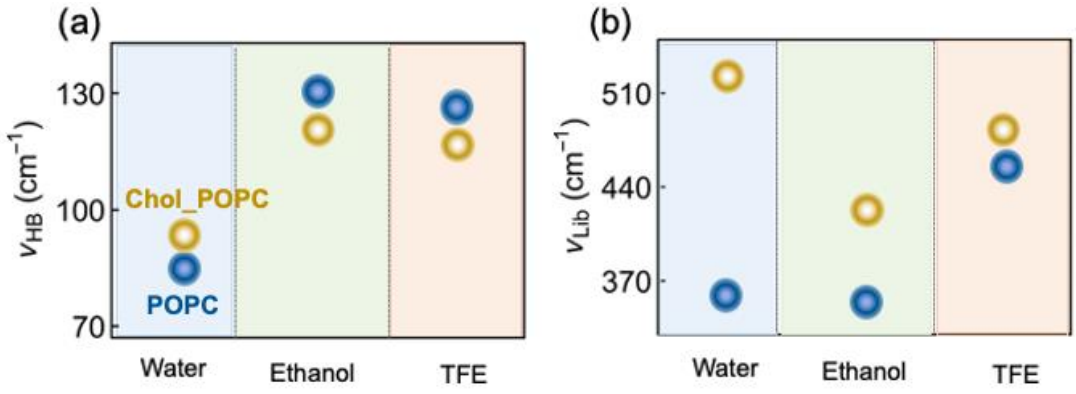

Figure 6H. (a) HB-stretch and (b) lib motion (after performing PCA) of POPC (blue) and cholesterol mediated POPC (yellow) liposomes in two alcohol medium.

Summarize: Ethanol has a disordering effect on hydrophobic carbon chain of lipid, increasing the area per head group of lipid and the overall fluidity of the membrane.[13] It is well known that when ethanol is inserted into liposomes, it binds to the headgroup region of lipid, and after certain concentration even it can penetrate into the lipid bilayer and transform it into non-bilayer structures.[19] DLS and SEM results unambiguously conclude the structural modification of liposomes in presence of both ethanol and TFE. Steady-state anisotropy results suggest the increase in the bilayer fluidity with increasing ethanol concentration. Our study is also intended to explore whether such structural modification imparts on lipid hydration. In presence of both two alcohols, HB-stretch suffers a large blue shift, indicating stronger H-bond formation at lipid water interface in presence of alcohols. Interestingly, H-bond network gets more restricted in presence of more electronegative TFE molecules while it remains unaltered in presence of

ethanol. We observe that addition of cholesterol does modify the lipid hydration. Stronger H-bond formation of cholesterol mediated lipid-water interface is observed in presence of alcohols. Our experimental study unambiguously established the fact that addition of alcohols on model lipid strengthen the H-bond networks at lipid water interface and cholesterol does modulates this H-bond network. Our findings could contribute in the fundamental as well as applied research in pharmaceutics where liposomes is used as a drug delivery agent.

Table 6a. Steady-state anisotropy value of POPC and cholesterol mediated POPC liposomes in presence of ethanol and TFE.

EtOH	**POPC**	**Chol mediated POPC**	**TFE**	**POPC**	**Chol mediated POPC**
0	0.097	0.20	0	0.10	0.20
10	0.065	0.18	5	0.09	0.13
20	0.059	0.14	10	0.03	0.07
30	0.044	0.11	30	0.03	0.08
50	0.052	0.07	50	0.09	0.09
60	0.039	0.05	60	0.11	0.12
70	0.038	0.04	70	0.11	0.12

Table 6b. Peak frequency both HB-stretch and librational motion for POPC liposomes with varying the concentration of ethanol and TFE. Data are fitted by using damped harmonic oscillator equation:

POPC					
EtOH (%)	$\boldsymbol{\nu_{HB}}$ $(\boldsymbol{cm^{-1}})$	$\boldsymbol{\nu_{Lib}}$ $(\boldsymbol{cm^{-1}})$	**TFE (%)**	$\boldsymbol{\nu_{HB}}$ $(\boldsymbol{cm^{-1}})$	$\boldsymbol{\nu_{Lib}}$ $(\boldsymbol{cm^{-1}})$
0	86.7±1.5	358.3±3.2	0	86.7±1.5	358.3±3.2
5	105.4±1.1	351.4±3	5	113.8±1.3	404.1±3.1
10	102.5±3.1	336.9±1.7	10	112.0±17	405.0±7.3
15	124.9±7.8	344.6±4.8	15	115.6±7	445.6±15
30	114.4±16	377.1±3.3	20	93.7±11	452.7±8

50	136.0±1.2	311.4±2	30	113.8±14	466.8±4.3
60	149.1±2.1	353.4±3	50	125.4±0.2	462.9±6.4
70	145.1±3.1	438.2±2.8	60	126.9±0.3	466.3±6.5
			70	130.4±8.6	461.0±9.0

Table 6c. Peak frequency both HB-stretch and librational motion for cholesterol mediated POPC liposomes with varying the concentration of ethanol and TFE. Data are fitted by using damped harmonic oscillator equation:

Chol mediated POPC=0.5					
EtOH (%)	$\boldsymbol{\nu_{HB}}$ $(\boldsymbol{cm^{-1}})$	$\boldsymbol{\nu_{Lib}}$ $(\boldsymbol{cm^{-1}})$	**TFE (%)**	$\boldsymbol{\nu_{HB}}$ $(\boldsymbol{cm^{-1}})$	$\boldsymbol{\nu_{Lib}}$ $(\boldsymbol{cm^{-1}})$
0	90.6±28	525.6±26.8	0	90.6±28	525.6±26.8
5	124.8±0.4	457±15.8	15	144.4±14	474±5.8
15	130.2±1.2	358.9±3.9	20	123.2±9.2	464.7±9.9
20	118.1±0.7	390.9±5.7	30	108.7±0.6	473.9±11
30	154.9±1.9	518.2±69.7	50	114.8±9.2	474.9±9.2
50	120.2±2.9	431.7±1.1	60	101±3.4	471±6.5
60	137.7±5.2	420.5±5.9			

Table 6d. Peak frequency both HB-stretch and librational motion for ethanol and TFE at different concentration. Data are fitted by using damped harmonic oscillator equation:

EtOH (%)	$\boldsymbol{\nu_{HB}}$ $(\boldsymbol{cm^{-1}})$	$\boldsymbol{\nu_{Lib}}$ $(\boldsymbol{cm^{-1}})$	**TFE (%)**	$\boldsymbol{\nu_{HB}}$ $(\boldsymbol{cm^{-1}})$	$\boldsymbol{\nu_{Lib}}$ $(\boldsymbol{cm^{-1}})$
0	136±4.8	475±3.2	0	136±4.8	475±3.2
10	142.7± 2.1	433.4±2.2	10	137.4±0.6	441.0±2.3
15	144.8± 3.1	434.5± 2.2	15	145.1± 0.5	444.5± 2.3
20	140.1± 4.2	436.0± 3.3	20	148.6±0.2	452.5± 2.1
30	146.0± 3	434.4±2.3	30	164.7± 2.5	460.4± 2.3

50	154.4± 2.3	435.9± 1.7	50	193.1± 4.1	462.1± 7.9
60	161.1± 3.5	434.8±2.2	60	216.9± 8.3	442.2± 2.8
70	165.7± 3.9	435.4±2.2	70	223.5± 2.1	452.1± 2.6

Table 6e. Peak frequency both HB-stretch and librational motion (after performin PCA) for water for POPC and cholesterol mediated POPC in presence of ethanol and TFE. Data are fitted by using damped harmonic oscillator equation:

POPC	$\boldsymbol{\nu_{HB}}$ $(\boldsymbol{cm^{-1}})$	$\boldsymbol{\nu_{Lib}}$ $(\boldsymbol{cm^{-1}})$	**Chol.+ POPC**	$\boldsymbol{\nu_{HB}}$ $(\boldsymbol{cm^{-1}})$	$\boldsymbol{\nu_{Lib}}$ $(\boldsymbol{cm^{-1}})$
water	86.7 ±1.5	358.3 ±3.2	water	90.6 ±2.8	525.6± 2.6
Ethanol	129.4± 3.2	355.2± 0.5	Ethanol	122.7 ±1.4	422 ±4.05
TFE	124.8 ±5.9	465.4 ±6.7	TFE	118.9 ±7.4	477.6 ±8.4

6IV. References:

(1) Cordeiro, R. M. Molecular Structure and Permeability at the Interface between Phase-Separated Membrane Domains. *J. Phys. Chem. B* **2018**, *122*, 6954−6965.
(2) Singer, S. J.; Nicolson, G. L. The Fluid Mosaic Model of the Structure of Cell Membranes. *Science* **1972**, *175*, 720–731.
(3) Franks, N.; Lieb, W. Molecular Mechanisms of General Anesthesia. *Nature* **1982**, *300*, 487–493.
(4) Sum, A.; Faller, R.; Pablo, J. de. Molecular Simulation Study of Phospholipid Bilayers and Insights of the Interactions with Disaccharides. *BioPhys. J.* **2003**, *85*, 2830–2844.
(5) Ikonen, E. Cellular Cholesterol Trafficking and Compartmentalization. *Nat. Rev* **2008**, *9*, 125–138.
(6) Mouritsen, O. G.; Zuckermann, M. J. What's So Special About Cholesterol? *Lipids* **2004**, *39*, 1101–1113.
(7) Lipowsky, R.; Sackmann, E. *Structure and Dynamics of Membranes*; Elsevier, 1995.
(8) Eslami, H.; Das, S.; Zhou, T.; Muller-Plathe, F. How Alcoholic Disinfectants Affect Coronavirus Model Membranes: Membrane Fluidity, Permeability, and Disintegration. *J. Phys. Chem. B* **2020**, *124*, 10374–10385.
(9) Bemporad, D.; Luttmann, C.; Essex, J. W. Behaviour of Small Solutes and Large Drugs in a Lipid Bilayer from Computer Simulations. *Biochim. Biophys. Acta, Biomembr.* **2005**, *1718*, 1–21.
(10) Chipot, C.; Comer, J. Subdiffusion in Membrane Permeation of Small Molecules. *Sci. Rep.* **2016**, *6*, 35913.
(11) Patra, M.; Salonen, E.; Terama, E.; Vattulainen, I.; Faller, R.; Lee, B. W.; Holopainen, J.; Karttunen, M. Under the Influence of Alcohol: The Effect of Ethanol and Methanol on Lipid Bilayers. *Biophys. J.* **2006**, *90*, 1121–1135.
(12) Loverde, S. M. Molecular Simulation of the Transport of Drugs across Model Membranes. *J. Phys. Chem. Lett.* **2014**, *5*, 1659–1665.
(13) Barry, J. A.; Gawrisch, K. Direct NMR Evidence for Ethanol Binding to the Lipid-Water Interface of Phospholipid Bilayers. *Biochem.* **1994**, *33*, 8082–8088.
(14) Vierl, U.; Lobbecke, L.; Nagel, N.; Cevc, G. Solute Effects on the Colliodal and Phase Behavior of Lipid Bilayer Membranes: Ethanol-Dipalmitoylphosphatidycholin Mixtures. *BioPhys. J.* **1994**, *67*, 1067–1079.
(15) Lee, B. W.; Faller, R.; Sum, A. K.; Vattulainen, I.; Patra, M.; Karttunen, M. Structural Effects of Small Molecules on Phospholipid Bilayers Investigated by Molecular Simulations. *Fluid Phase Equilib.* **2005**, *228–229*, 135–140.

(16) Chipot, C.; Comer, J. Subdiffusion in Membrane Permeation of Small Molecules. *Sci. Rep.* **2016**, *6*, 35913.
(17) Hirose, R.; Bandou, R.; Ikegaya, H.; Watanabe, N.; Yoshida, T.; Daidoji, T.; Naito, Y.; Itoh, Y.; Nakaya, T. Disinfectant Effectiveness Against SARS-CoV-2 and Influenza Viruses Present on Human Skin: Model-Based Evaluation. *Clin Microbiol Infect* **2021**, *27*, 1042.e1-1042.e4.
(18) Kampf, G. Efficacy of Ethanol Against Viruses in Hand Disinfection. *J. Hosp. Infect.* **2018**, *98*, 331–338.
(19) Gurtovenko, A. A.; Anwar, J. Interaction of Ethanol with Biological Membranes: The Formation of Non Bilayer Structures within the Membrane Interior and Their Significance. *J. Phys. Chem. B* **2009**, *113*, 1983–1992.
(20) Patra, M.; Salonen, E.; Terama, E.; Vattulainen, I.; Faller, R.; Lee, B. W.; Holopainen, J.; Karttunen, M. Under the Influence of Alcohol: The Effect of Ethanol and Methanol on Lipid Bilayers. *BioPhys. J.* **2006**, *90*, 1121–1135.
(21) Shobhna; Kashyap, H. K. Deciphering Ethanol-Driven Swelling, Rupturing, Aggregation, and Fusion of Lipid Vesicles Using Coarse-Grained Molecular Dynamics Simulations. *Langmuir* **2022**, *38*, 2445–2459.
(22) Imai, S.; Osawa, M.; Mita, K.; Toyonga, S.; Machiyama, A.; Ueda, T.; Takeuchi, K.; Oiki, S.; Shimada, I. Functional Equilibrium of the KcsA Structure Revealed by NMR. *J. Biol. Chem.* **2012**, *287*, 39634–39641.
(23) Weight, F. F.; Li, C.; Peoples, R. W. Alcohol Action on Membrane Ion Channels Gated by Extracellular ATP (P2X Receptors). *Neurochem Int.* **1999**, *35*, 143–152.
(24) Laan, E. van den B. der; Chupin, V.; Killian, J. A.; Kruijff, B. D. Small Alcohols Destabilize the KcsA Tetramer via Their Effect on the Membrane Lateral Pressure. *Biochemistry* **2004**, *43*, 5937–5942.
(25) Ennaceur, S. M.; Sanderson, J. M. Micellar Aggregates Formed Following the Addition of Hexafluoroisopropanol to Phospholipid Membranes. *Langmuir* **2005**, *21*, 552–561.
(26) Zhang, M.; Peyear, T.; Patmanidis, I.; Greathouse, D. V.; Marrink, S. J.; Andersen, O. S.; Ingolfsson, H. I. Fluorinated Alcohols' Effects on Lipid Bilayer Properties. *BioPhys. J.* **2018**, *115*, 679–689.
(27) Pyne, S.; Pyne, P.; Mitra, R. K. Addition of Cholesterol Alters the Hydration at the Surface of Model Lipids: A Spectroscopic Investigation. *Phys. Chem. Chem. Phys.* **2022**, *24*, 20381–20389.
(28) Schwaab, G.; Sebastiani, F.; Havenith, M. Ion Hydration and Ion Pairing as Probed by THz Spectroscopy. *Angew. Chem. Int. Ed.* **2019**, *58*, 3000–3013.
(29) Schmidt, D. A.; Birer, O.; Funkner, S.; Born, B. P.; Gnanasekaran, R.; Schwaab, G. W.; Leitner, D. M.; Havenith, M. Rattling in the Cage: Ions as Probes of Sub-Picosecond Water Network Dynamics. *J. Am. Chem. Soc.* **2009**, *131*, 18512–18517.
(30) Samanta, N.; Luong, T. Q.; Das Mahanta, D.; Mitra, R. K.; Havenith, M. Effect of Short Chain Poly(Ethylene Glycol)s on the Hydration Structure and Dynamics around Human Serum Albumin. *Langmuir* **2016**, *32*, 831−837.
(31) Pyne, P.; Mitra, R. K. Excipients Do Regulate Phase Separation in Lysozyme and Thus Also Its Hydration. *J. Phys. Chem. Lett.* **2022**, *13*, 931−938.
(32) Born, B.; Kim, S. J.; Ebbinghaus, S.; Gruebele, M.; Havenith, M. The Terahertz Dance of Water with the Proteins: The Effect of Protein Flexibility on the Dynamical Hydration Shell of Ubiquitin. *Faraday Discuss.* **2009**, *141*, 161–173.
(33) Yamamoto, N.; Andachi, T.; Tamura, A.; Tominaga, K. Temperature and Hydration Dependence of Low-Frequency Spectra of Lipid Bilayers Studied by Terahertz Time-Domain Spectroscopy. *J. Phys. Chem. B* **2015**, *119*, 9359–9368.
(34) Ahlers, J.; Adams, E. M.; Bader, V.; Pezzotti, S.; Winklhofer, K. F.; Tatzelt, J.; Havenith, M. The Key Role of Solvent in Condensation: Mapping Water in Liquid-Liquid Phase-Separated FUS. *Biophys. J.* **2021**, *120*, 1–10.
(35) Poojari, C.; Wilkosz, N.; Lira, R. B.; Dimova, R.; Jurkiewicz, P.; Petka, R.; Kepczynski, M.; Rog, T. Behavior of the DPH Fluorescence Probe in Membranes Perturbed by Drugs. *Chem Phys Lipids* **2019**, *223*, 104784.
(36) Kepczynski, M.; Nawalany, K.; Kumorek, M.; Kobierska, A.; Jachimska, B.; Nowakowska, M. Which Physical and Structural Factors of Liposome Carriers Control Their Drug-Loading Efficiency? *Chem. Phys. Lipids* **2008**, *155*, 7–15.
(37) Gidwani, A.; Holowka, D.; Baird, B. Fluorescence Anisotropy Measurements of Lipid Order in Plasma Membranes and Lipid Rafts from RBL-2H3 Mast Cells. *Biochem.* **2001**, *40*, 12422–12429.
(38) Heyden, M.; Sun, J.; Funkner, S.; Mathias, G.; Forbert, H.; Havenith, M.; Marx, D. Dissecting the THz Spectrum of Liquid Water from First Principles via Correlations in Time and Space. *Proc. Natl. Acad. Sci. U.S.A.* **2010**, *107*, 12068–12073.
(39) Pyne, P.; Mitra, R. K. Excipients Do Regulate Phase Separation in Lysozyme and Thus Also Its Hydration. *J. Phys. Chem. Lett.* **2022**, *13*, 931–938.
(40) Ahlers, J.; Adams, E. M.; Bader, V.; Pezzotti, S.; Winklhofer, K. F.; Tatzelt, J.; Havenith, M. The Key Role of Solvent in Condensation: Mapping Water in Liquid-Liquid Phase-Separated FUS. *Biophys. J* **2021**, *120*, 1266–1275.

(41) Li, X.; Liu, L.; Schlegel, H. B. On the Physical Origin of Blue-Shifted Hydrogen Bonds. *J Am Chem Soc* **2002**, *124*, 9639–9647.
(42) Nibali, V. C.; Pezzotti, S.; Sebastiani, F.; Galimberti, D. R.; Schwaab, G.; Heyden, M.; Gaigeot, M. P.; Havenith, M. Wrapping Up Hydrophobic Hydration: Locality Matters. *J Phys Chem Lett* **2020**, *11*, 4809–4816.

Chapter 7

Summary and Future Perspective

7I. Summary:

In the present thesis our main goal is to explore the physical response (both structure and dynamics) of water at the interface of liposomes at different conformations. For that we choose lipid as a biomolecule. We have started with the vesicle as it mimics the lipid cellular environments. We have used SDS (-ve), CTAB (+ve) and Brij 30 (neutral) surfactant to prepare three different charged surfactant/cholesterol based vesicles by using sonication technique. Both dynamic light scattering (DLS) and atomic force microscopy (AFM) technique affirms us the formation of vesicles in presence of cholesterol in micellar environments. We calculate the surface charge density of the charged vesicles using zeta potential measurements and observe cholesterol molecules perturb the charge distribution. We measure the solvation of both micelle and vesicles by using THz (FAR-IR) spectroscopy and observe that solvation nature gets alter as micelles are converted into the vesicles. In vesicles, a new core of *inner hydration* develops. We have aimed to investigate how this inner hydration differs from the outer hydration. We obtain the exclusive information of the inner solvation of the vesicles and observe that for both charged vesicles (SDS and CTAB) inner solvation offers more labile binding with the interface compare to overall hydration and interestingly for neutral Brij 30 vesicles stronger hydrogen binding of water at the inner surface.

In our next study we aim to explore the hydration behaviour of phospholipids with varying the charge in presence of cholesterol. We have used DOPC (1,2-Dioleoyl-sn-glycero-3-phosphocholine) as a zwitterionic and DOPG (1,2-Dioleoyl-sn-glycero-3-phospho-rac-(1-glycerol) sodium salt) as a negatively charged lipids. We prepare DOPC, DOPG and DOPC/DOPG (1:1, mol/mol) liposomes in absence and in presence of cholesterol by using film-hydration sonication technique. Both DLS and AFM techniques establish the formation of liposomes in absence and presence of cholesterol. Then we extract the hydration information of liposomes by using FAR-IR technique and observe that interfacial hydration is lipid charge dependent and addition of cholesterol does modify it. Our results (from Principal component analysis (PCA)) unambiguously conclude that cholesterol induces weaker hydrogen bond and faster hydrogen bond vibration/stretching dynamics at lipid interface.

We then investigate the hydration behavior of three lipids when they undergo the fusogenic transition by using THz FTIR spectroscopy (1.5-13.5 THz frequency domain). We have chosen three zwitterionic lipids: 1,2-Dioleoyl-sn-glycero-3-phosphocholine (DOPC), 2-Oleoyl-1-palmitoyl-sn-glycero-3-phosphocholine (POPC) and 1,2-Dipalmitoyl-sn-glycero-3-phosphocholine (DPPC) with different aliphatic tail and PEG (average molecular weight 4000) as a fusogenic molecule. We use dynamic light scattering and electron microscopy to monitor the lipid fusion process and the results confirm the formation of different intermediate steps of the liposomes during the fusion process: bilayer aggregation, destabilization and finally lipid fusion. THz-FTIR results conclude that liposomes get dehydrated in presence of PEG during the fusion pathway. Hydration measurements yield that stronger H bond is formed in the aggregated state of the lipid interface compared to that of the pristine liposome for all the liposomes irrespective of the constituting lipid molecules.

We also monitor the hydration behaviour of liposomes in presence of two alcohols (ethanol and 2,2,2-trifluoroethanol) by using THz FTIR spectroscopy. Here POPC is used as a model lipid. Our DLS and SEM results reflect that alcohols promote the transformation of bilayer structure into a non-bilayer structure and formation of small globules inside lipid bilayer interior. Our hydration results reflect the strengthening of H-bond network at the lipid water interface in presence of alcohols.

The key finding of the thesis is:

- As the micelles are converted into vesicles new inner solvation appears and the solvation nature of inner interface is surprisingly differing from the overall solvation. The solvation nature (both inner and overall) is surfactant charge dependent.
- When cholesterol is incorporated into the lipid, the water structure at lipid interface becomes weaker and the vibration/stretching dynamics becomes faster.
- Liposome follows different intermediate steps (bilayer aggregation, destabilization and finally lipid fusion) during fusion in presence of PEG (a fusogenic molecule) and liposomes get dehydrated during fusion pathway. Stogner H-bond is formed in the aggregated state compare to pristine liposomes.
- Alcohols disrupt the bilayer structure of lipid-membranes and H-bond networks at lipid water interface becomes stronger in presence of alcohols.

7II. Future Perspective:

The main focus of the thesis is to explore the hydration behaviour of vesicles/liposomes in presence of different biomolecules. Here we have characterized different charged vesicles and liposomes and investigate their interfacial water structure. This finding could contribute in the fundamental as well as applied research towards developing liposomes as a delivery agents in medicine industries and in pharmacology. We have investigated interfacial hydration behaviour of cholesterol loaded liposomes which could improve the strategies for controlling cholesterol-related pathologies. Our findings would encourage the understanding in different biological phenomenon like lipid-protein interaction, ligand-membrane interaction, ion transport, ion-membrane interaction etc.

In this thesis we explored the hydration behaviour of liposomes in presence of cholesterol (animal sterol); Our future plan will be to explore the hydration behaviour of ergosterol (sterol in fungal membrane) and stigmasterol (sterol in plant cell membrane) in cell membrane as sterols are important for the structural and dynamical properties of cell membranes.[1,2] DPPC will be used as a model lipid and liposomes will be prepared by using film hydration technique. Dynamics light scattering and scanning electron microscopic techniques will be used to characterize the liposomes. 1,6-Diphenyl-1,3,5-hexatriene (DPH) Anisotropy measurements will give us the information of fluidity and rigidity of lipid bilayer in presence of sterol as DPH is mostly used to probe the fluidity or microviscosity in the acyl chain region of lipid membrane.[3,4] Finally THz spectroscopy will be used to monitor the structural and dynamical response of water at the hydration cell of lipid membranes.

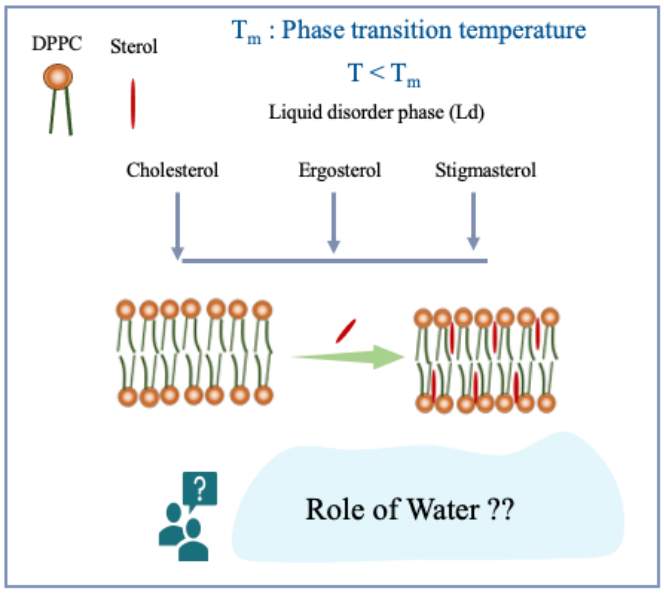

7III. References:

(1) Ikonen, E. Cellular Cholesterol Trafficking and Compartmentalization. *Nat. Rev* **2008**, *9*, 125–138.
(2) Lipowsky, R.; Sackmann, E. *Structure and Dynamics of Membranes*; Elsevier, 1995.
(3) Poojari, C.; Wilkosz, N.; Lira, R. B.; Dimova, R.; Jurkiewicz, P.; Petka, R.; Kepczynski, M.; Rog, T. Behavior of the DPH Fluorescence Probe in Membranes Perturbed by Drugs. *Chem Phys Lipids* **2019**, *223*, 104784.
(4) Kepczynski, M.; Nawalany, K.; Kumorek, M.; Kobierska, A.; Jachimska, B.; Nowakowska, M. Which Physical and Structural Factors of Liposome Carriers Control Their Drug-Loading Efficiency? *Chem. Phys. Lipids* **2008**, *155*, 7–15.